University of Nottingham

School of Civil Engineering

NONLINEAR VIBRATIONS OF CRACKED REINFORCED CONCRETE BEAMS

BY CHUAN MING TAN, BENG(HONS)

Thesis submitted to The University of Nottingham
for the degree of Doctor of Philosophy

April 2003

"A scientist can discover a new star, but he cannot make one. He would have to ask an engineer to do that."

- Gordon L. Glegg, 1969.

DECLARATION

I declare that, except where cited in the text, all work contained within thesis is my own original work, under the direction of my supervisors and the UK Highways Agency. The work presented herein was performed at the University of Nottingham between September 1999 and March 2003.

The thesis has not been submitted to any institution other than the University of Nottingham for the degree of Doctor of Philosophy.

ABSTRACT

Although a great deal of work in investigating the possibility of using linear vibration techniques to detect damage in bridges has been carried out over the past 25 years, there are still some major concerns, such as poor sensitivity of modal parameters to damage, requirement of baseline data, need of measuring excitation force as well as environmental effects. Nonlinearity in the vibration characteristics when the structure is damaged further complicates the problem and causes doubts on the feasibility of applying these techniques on actual structures. Understanding of the nonlinear behaviour is therefore crucial. The aim of the work presented herein is to improve the current understanding of the nonlinear vibration characteristics of reinforced concrete beams and to assess its importance to the subject of structural health monitoring of bridges.

These non-linear vibration characteristics were studied by conducting harmonic excitation vibration tests on reinforced concrete beams at various damage levels. In order to detect and characterise the nonlinear behaviour, both linear and nonlinear system identification techniques were used. Results indicated that the responses of the tested beams showed marked softening behaviour and that this non-linear vibration behaviour varied with increasing damage. The restoring force surface technique was applied to the test data and results suggested that cracks in reinforced concrete beams never fully closed in the vibration cycle.

Existing phenomenological models suggested by other researchers were investigated and compared with the experimental results. The study confirmed that a bilinear crack model would not be sufficient to replicate the observed vibrating cracked reinforced concrete beams' behaviour. Based on these phenomenological models, an empirical model was derived. Using the

empirical crack model proposed, the author suggested a means of estimating the ratio of cracked and uncracked stiffness of a vibrating cracked reinforced concrete beam. The author further suggested a possible routine for structural health monitoring for reinforced concrete beam and stressed that it could be extended for more complicated structures, like bridges.

To improve understanding of the nonlinearities in the vibration characteristics, a damage mechanics model of cracked reinforced concrete beam was suggested. Based on strain softening behaviour of concrete material under tensile force, the model is capable of including damage in the form of a moment rotation relationship over the cracked region. Results from the vibration analysis of the model were compared with experimental data.

LIST OF CONTENTS

LIST OF FIGURES

LIST OF TABLES

NOMENCLATURE

$\phi''(x)$ – *mode shape*

$\ddot{u}(t)$ – *acceleration*

$u(t)$ – *displacement*

$\ddot{u}_i$ – *instantaneous acceleration*

$\dot{u}_i$ – *instantaneous velocity*

$f(u,\dot{u})$ – *internal restoring force of a system*

$\overline{m}$ – *mass of beam element*

$\dot{u}(t)$ – *velocity*

$[C]$ – *damping matrix of a system*

$[k]$ – *stiffness matrix of a beam element*

$[K]$ – *stiffness matrix of a system*

$[k_{crk}]$ – *stiffness matrix of rotational spring*

$[m]$ – *mass matrix of a beam element*

$[M]$ – *mass matrix of a system*

$\{\ddot{u}\}$ – *vector of nodal accelerations*

$\{P\}$ – *applied load/moment vector of a system*

$\{u\}$ – *vector of nodal displacements and rotations*

A – *cross-sectional area*

$A(t)$ – *instantaneous amplitude*

a_0, a_1 – *proportionality constants*

A_s – *area of steel reinforcement*

b – *breadth of concrete section*

c – *damping*

C_1, C_2 – *parameters used in Cormelissen et. al. concrete model*

d – *depth to reinforcement of concrete section*

E – *Young's modulus*

E_c – *Young's modulus of concrete*

E_s – *Young's modulus of steel reinforcement*

$E_{unloading}$ – *unloading gradient*

f – *frequency in Hz*

$F\{x(t)\}$ – *Fourier Transform of x(t)*

F_{com} – *total compressive force*

F_{crk} –*load at which first crack appears*

f_{ct} – *maximum tensile stress of concrete*

f_{cu} – *cube strength of concrete*

f_D – *frequency shifted by Doppler's effect*

F_{du} – *ultimate force due to dowel action*

f_e – *total external force*

$f_i(u_{exact})$ – *total internal force at exact displacement/rotation* u_{exact}

f_{norm} – *normalised force*

F_{ten} – *total tensile force*

$F_{ten,c}$ – *tensile force from concrete*

$F_{ten,s}$ –*tensile force from steel reinforcement*

f_y, f_{sy} – *yield stress of steel reinforcement*

g – *acceleration due to gravity*

h – *overall depth of concrete section*

$h(\tau)$ – *impulse function*

$H[x(t)]$ – *Hilbert Transform of x(t)*

h_c – *thickness of equivalent elastic layer*

$H_n(\omega)$ – *frequency response function of order n*

I – *second moment of area*

k – *stiffness*

k_0, k_i – *undamaged stiffness*

k_c – *ratio of equivalent elastic layer to beam depth*

$k_c(\theta)$ – *stiffness interpolated linearly from figure 7.14*

$k_{\Delta c}$ – *difference between undamaged and fully open crack stiffness*

L, l – *length of beam*

m – *modal mass*

M – *total bending moment*

M_c –*bending moment from concrete*

M_{crk} – *moment at which first crack appears*

M_s – *bending moment from steel reinforcement*

$p(t)$ – *force in function*

p_i – *instantaneous force*

r^* – *approximated residual force*

t, τ – *time*

u^* – *known approximation of* u_{exact}

u_o – *mid-span deflection due to self-weight*

v – *elongation*

V – *shear force*

v – *velocity of measured surface*

v_c – *strain of concrete*

v_i – *ith translational degree of freedom*

v_{norm} – *normalised strain*

v_s – *strain of steel reinforcement*

v_x – *strain of concrete at extreme end*

w_c – *maximum crack width*

x – *depth to neutral axis of concrete section*

$x(t)$ – *generalised input in time domain*

$X(\omega)$ – *generalised input in frequency domain*

x_i – *instantaneous displacement*

$y(i)$ – *depth to stripe i of concrete section*

$y(t)$ – *generalised output in time domain*

$Y(\omega)$ – *generalised output in frequency domain*

α, β – *parameters describing stiffness changes*

γ_m – *partial safety factor*

δ, w – *crack opening displacement*

δu – *unknown error of* u^*

θ – *rotation*

θ_i – i^{th} *rotational degree of freedom*

λ – *wavelength of laser beam*

$\mu(i)$ – *moment at stripe i*

σ_c – *stress of concrete*

σ_s – *stress of steel reinforcement*

ε_r – *error*

μ – *ratio of cracked to uncracked stiffness*

ρ – *density of concrete*

ω – *frequency in rad/sec*

ω_n – *natural frequency in rad/sec*

ξ – *damping ratio*

ABBREVIATIONS

BCM – *Blunt Crack Model*

COMAC – *Co-Ordinate Modal Assurance Criterion*

DBFO – *Design, Build, Finance and Operate*

DFT – *Discrete Fourier Transform*

FCM – *Fictitious Crack Model*

FE – *Finite Element*

FFT – *Fast Fourier Transform*

FRF – *Frequency Response Function*

HA – *UK Highways Agency*

hcp – *Hydrated Cement Paste*

MAC – *Modal Assurance Criterion*

MDOF – *Multiple Degrees Of Freedom*

RC – *Reinforced Concrete*

RMS – *Root Mean Square*

SDOF – *Single Degree Of Freedom*

ACKNOWLEDGEMENTS

The help and guidance of the following, without whom this thesis would not have been produced, is gratefully acknowledged.

The author would like to thank Dr John S Owen of the University of Nottingham and Prof Ban Seng Choo of Napier University for their guidance, support and supervision in seeing the project through to completion.

The help of Mr Steven Pearson, Dr Daniel Ridley-Ellis and Mr Zhongsheng Wang for provision of their precious advice, knowledge and encouragement is greatly appreciated.

The support of Mr David Allinson, Mr Bal Loyla, Mr Geoff Mitchell, Mr Nigel Rook and Mr Mel Ridal is gratefully acknowledged for their relentless assistance during the laboratory testing.

The author would also like to thank the UK Highways Agency for financial support of the research through a studentship provided to the author. Additional financial support was provided by the International Office, University of Nottingham, UK.

This work represents more than an academic achievement and could not have been accomplished without the continued encouragement of my family. Thank you.

CHAPTER 1

INTRODUCTION

1.1 BACKGROUND

In the UK, the Highways Agency is responsible for maintaining over 10,000 bridges, of which over 50% are of reinforced concrete construction, 28% are of prestressed concrete construction and a further 13% are steel-concrete composite structures. In order to maintain these bridges in a serviceable state, structural condition assessments are carried out at regular intervals. Structural condition assessment is defined as the process by which the state of a structure is determined (Doebling et al., 1999). It usually refers to quantifying the integrity of the structure, its ability to adequately sustain its original design loading, and its ability to continue fulfilling the above in the future.

Current approaches adopted by the Highways Agency are visual inspections and localised experimental testing such as radar survey, material sampling, acoustic and ultrasonic methods (BD 21/93, BD 63/94, BD 44/95). These are not only labour intensive, expensive and time consuming, but also depend greatly on the skill and judgement of the responsible engineer. Furthermore, they tend to be overly conservative (Eccles, 1999). The increase

of maximum weight of service goods vehicles in 1999, the 15-year bridge rehabilitation project and the introduction of DBFO (Design, Build, Finance and Operate) contracts have further increased the pressure for more reliable and cost effective methods to be developed than those currently available.

In response to the above need, the Highways Agency carried out a fundamental re-evaluation of the current Pass/Fail type of assessment and proposed the alternative Pass/Monitor/Fail assessment methodology (Das et al., 1995). A Pass/Monitor/Fail assessment is designed to accommodate bridges that fail a traditional assessment by a small margin and do not show significant deterioration. In these borderline cases it is more appropriate to carry out a period of structural health monitoring. Structural health monitoring can be seen as the ongoing implementation of structural condition assessment to continually acquire new information about the state of the structure. This approach has potential to significantly increase the life of the bridge.

Ideally, a robust health monitoring scheme will be able to identify at an early stage the onset of damage or deterioration, locate its position within the sensor resolution being used, provide some estimate of the severity of damage, and predict the remaining useful life of structure. The method should also be well suited to automation. The Highways Agency considers a feasible condition monitoring method could be based on modal analysis and has therefore funded research in this area. This is the second phase of a larger project on the use of dynamic testing for bridge assessment and structural health monitoring.

1.2 ROLE OF EXPERIMENTAL MODAL ANALYSIS

Over the past twenty-five years there have been many studies into the application of modal and dynamic testing for the detection of damage or deterioration in bridges. The key principle underlying this technique is that

damage to a bridge - such as cracking or even the loss of one or more components - will result in a loss of stiffness, which is then detected as a change in modal properties (i.e. natural frequencies, mode shapes and modal damping). An overall reduction in stiffness will result in a reduced natural frequency whereas a change in distribution of stiffness through localised damage will result in a change in mode shape. The use of modal testing to detect these changes in stiffness has two distinct advantages over other forms of non-destructive testing. First, the modal characteristics provide a global picture of the structural system. Second, it is simple to monitor changes in these modal properties using relatively few sensors strategically placed on the bridge.

The work to investigate the possibility of using vibration techniques to detect damage in bridges has ranged from looking at changes in natural frequencies and mode shapes due to damage to using finite element (FE) models to assess changes in modal properties. The FE models are updated using measured data, usually modal properties (Friswell et al., 1994) or frequency response functions (Waters and Lieven, 1996). Each of these enables an accurate representation of the structure to be devised. With these computer models, the condition of the actual structures can be predicted.

However, there remain a few concerns regarding the feasibility of using vibration techniques to detect damage in bridges. Firstly, a baseline set of modal parameters is required for the undamaged bridge so that changes in these parameters due to damage can be readily detected. Such baseline data are normally unavailable for bridges. It is also a well known fact that it is difficult to accurately establish insitu, the mode shapes and modal damping for bridges (Salawu and Williams, 1995a). A further problem is that environmental factors such as temperature and humidity tend to affect the modal properties significantly (Abdel Wahab and De Roeck, 1997). More importantly, much of the research in this area assumed that the vibration is linear, i.e. the modal properties do not vary with amplitude of excitation. It is suggested, mainly in mechanical and aeronautical engineering, that a damaged structure tends to

behave nonlinearly (Doebling et al., 1996). This nonlinear behaviour tends to become more significant if the material is inhomogeneous, such as reinforced concrete (Eccles, 1999). It is unwise to use linear techniques on nonlinear structures without great care.

In contrast to the large amount of effort spent on developing methods of detecting damage based on linear vibration, there has been very little research on the feasibility of using nonlinear vibration properties to assess the condition of structures. Much of this research has concentrated on isolated cracks in homogeneous media, such as fatigue cracks in steel beams. There has also been progress in detecting damage in aeroplane wings (Tsyfansky and Beresnevich, 2000) and mechanical applications (Vanhoenacker et al., 2000). However, this research is not applicable to the case of reinforced concrete structures. This is because concrete is an inhomogeneous material that is subject to microcrack initiation and propagation at load levels far below the actual failure load (Neville, 1990). This often leads to a distributed pattern of cracking much of which is not discernable during visual inspections. The influence of both visible cracks and microcracking on the vibration characteristics of reinforced concrete beams cannot be properly examined without considering nonlinear behaviour.

1.3 AIM AND OBJECTIVES

The aim of the work presented herein is to improve the current understanding of the nonlinear vibration characteristics of reinforced concrete beams and to assess its importance to the subject of structural health monitoring of bridges. To achieve this, the following objectives are targeted:

- confirm the presence of nonlinear behaviour in the vibration characteristics of damaged reinforced concrete beams and thereafter characterise it

- improve understanding of possible crack mechanisms that result in amplitude dependent natural frequencies
- obtain an empirical model that replicates the behaviour
- discuss feasibility of using the nonlinearity for structural health monitoring
- create a theoretical model that will facilitate an improved understanding of possible sources of nonlinear mechanisms

1.4 METHODOLOGY

To achieve the objectives defined in section 1.3, the work reported within this thesis was carried out in the following stages. First, tests were conducted on reinforced concrete beams at increasing levels of damage caused by overloading. The test data enabled the author to confirm the presence of nonlinear vibration behaviour. Of the numerous existing techniques, the most appropriate nonlinear system identification technique was adopted to systematically characterise the detected nonlinearities. These experimental results were then compared with existing phenomenological models (i.e. models that seek to replicate the observed phenomena rather than the physics of the system) suggested by other researchers. Based on these phenomenological models, an empirical model, potentially capable of detecting and identifying the severity of damage, was obtained. With a model capable of replicating the vibration characteristics of reinforced concrete beams the next logical step to improve understanding of the observed nonlinear behaviour is to find the potential sources of it. This is achieved by assessing different potential nonlinear mechanisms and based on these, a theoretical crack model was derived. Finally, the theoretical crack model was incorporated into a beam model and the results of simulations were compared with the experimental behaviour.

1.5 ORGANISATION OF THESIS

The work presented within this thesis is divided into eight chapters. Following the present introductory chapter, the next chapter contains a review of the available literature in the field of structural health monitoring and damage detection, paying particular attention to civil engineering structures and nonlinear vibration characteristics. Chapter three presents the design of the experimental work. Results and implications from the experimental work can be found in chapter four. Chapter five focuses on the numerical aspect of the work including comparing the existing phenomenological models and deriving an empirical model for the vibration characteristics of the reinforced concrete beams described in chapter four. Chapter five also proposes a possible health monitoring routine. Chapter six concentrates on identifying the possible cause of the nonlinear behaviour and presents a discussion of the theoretical aspects of the nonlinear behaviour. In chapter seven, the author derives an analytical crack model based on the discussions in chapter six. A reinforced concrete beam model is also presented in chapter seven. Lastly, chapter eight summarises the work and provides suggestions for future research.

CHAPTER 2

REVIEW OF LITERATURE

2.1 INTRODUCTION

Health monitoring, as determined by changes in the dynamic properties or response of structures, is a subject that has received considerable attention in recent years. A system of classification for health monitoring and damage detection methods, as presented by Rytter(1993), defines four levels of damage identification, as follows:

- Level 1: Determination that damage is present in the structure
- Level 2: Determination of the geometric location of the damage
- Level 3: Quantification of the severity of the damage
- Level 4: Prediction of the remaining service life of the structure

This review principally considers literature relevant to Level 1, Level 2, or Level 3 methods because these levels are most often related directly to structural dynamics testing and modelling issues. Level 4 is generally related to the field of fracture mechanics, fatigue life analysis, or structure design assessment.

Many different issues are critical to the success of using the vibration characteristics of a structure for health monitoring and damage detection. Among the important issues are excitation and measurement considerations, including the selection of the type and location of sensors, and the type and location of the excitations. In this chapter, these peripheral issues will not be directly addressed. Discussion will be limited to the methods that use changes in modal properties (i.e. modal frequencies, modal damping ratios and mode shapes) to detect changes in structural properties, and the application of these methods to civil engineering problems, paying particular attention to bridges.

This chapter is organised as follows: First, there is a brief introduction to basic linear modal analysis theory. Next, key papers on damage detection based on linear vibration theory are discussed. This is then followed by a review of relevant literature concerned with nonlinearities in the vibration responses. Finally, brief discussions and conclusions drawn from the reviewed literature are presented.

2.2 MODAL ANALYSIS AND STRUCTURAL HEALTH MONITORING

Two approaches, analytical and experimental, are used in studying the vibrations of a system, as shown in figure 2.1. For analytical work, one usually has prior knowledge of the structure geometry, boundary conditions and material characteristics. The mass, stiffness and damping distribution of the structure are therefore usually well known and are sufficient to enable the dynamic properties (natural frequencies, damping and mode shapes) of the structure to be determined.

The experimental approach is the reverse of the analytical approach. It starts from measurements of dynamic input forces and output responses on the structure of interest. These measurements are most often transformed into frequency response functions (FRF), i.e. the relationship between output and

input as a function of frequency. FRF can be expressed in terms of modal parameters. Hence, the second step of an experimental modal analysis consists of estimating these parameters from the measured FRFs. Once again, with these parameters, the dynamic behaviour of the structure of interest is represented.

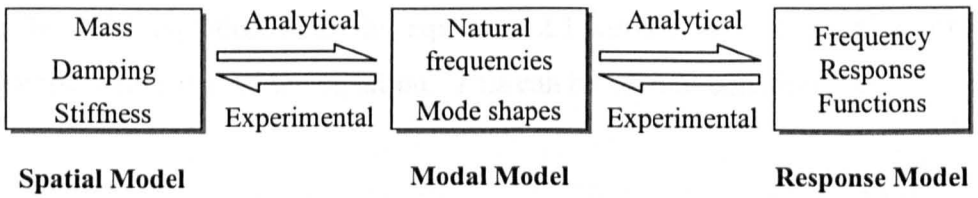

Figure 2.1: Two approaches for modal analysis. (Heylen et al., 1998)

In modal analysis theory, it is always assumed that the structural behaviour is linear, that is, the output of any combination of inputs is equal to the same combination of the respective outputs. The dynamics can be presented by a set of linear, second order differential equations. It is also assumed that the response is time invariant, i.e. the structure dynamic characteristics do not change with time. This means that the coefficients of the differential equations remain constant.

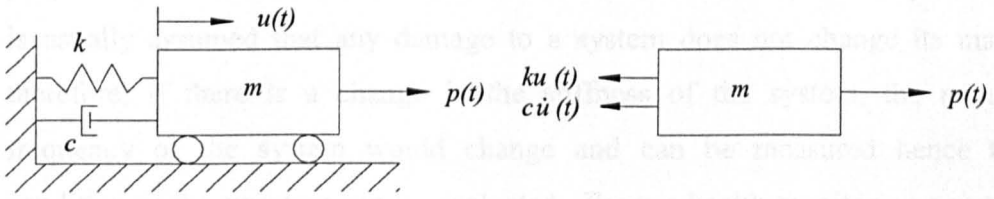

Figure 2.2: Schematic diagram of a SDOF dynamical model.

Figure 2.2 shows a schematic diagram of a single degree of freedom (SDOF) system in which $p(t)$ represents the excitation force, $ku(t)$ is a force due to the structure's stiffness and $c\dot{u}(t)$ represents a resistant force due to viscous damping in the system. The application of Newton's second law of

motion produces equation 2.1, which is the fundamental equation of motion for any system, including SDOF systems.

$$m\ddot{u}(t)+c\dot{u}(t)+ku(t)=p(t) \tag{2.1}$$

The free vibration state of the system described by the 2nd order differential equation seen in equation 2.1 relates to the solution of the homogeneous part of the equation. This can be seen in equation 2.2.

$$m\ddot{u}(t)+ku(t)=0 \tag{2.2}$$

The damping term has been omitted to clarify the link between the stiffness and the mass terms and the dynamic response. If the solution for $u(t)$ is assumed to be a harmonic function then the natural frequency of the SDOF system can be shown to be,

$$f=\frac{1}{2\pi}\sqrt{\frac{k}{m}} \tag{2.3}$$

In equation 2.3, there is a clear link between the system's structural properties, stiffness, k, and mass, m, and the natural frequency of the system. It is usually assumed that any damage to a system does not change its mass; therefore, if there is a change in the stiffness of the system, the natural frequency of the system would change and can be measured hence the condition of the structure can be evaluated. From a health monitoring point of view any significant change in natural frequency is then used to launch a further investigation. This is the basis of using dynamic testing for structural health monitoring.

2.3 LINEAR MODAL METHODS

2.3.1 PREVIOUS LITERATURE SURVEYS

A detailed survey of both the available technical literature and transcripts of interviews of selected recognised experts in the field of damage identification (using modal analysis procedures) was carried out in 1995 and presented by Doebling et al. (1996). The survey focused on damage detection and health monitoring of structural and mechanical systems mainly from the changes in their vibration characteristics. Mottershead and Friswell (1993) present another survey of the literature related to dynamic finite element model updating, which has been used extensively for structural damage detection. Their review contains a long list of references on the topic of model updating. Salawu (1997a) also presented a survey of literature on detection of structural damage, paying particular attention to changes in frequency. Several doctoral theses that addressed damage detection and related issues have recently been published (Rytter, 1993, Hemez, 1993, Doebling, 1995, Eccles, 1999 and Nield, 2001). Each of which provides interesting updates on recent development in the current field.

2.3.2 NATURAL FREQUENCIES

Damage detection by measuring natural frequencies is by far the most popular method among researchers. It is thought to be probably the most useful damage detection method (based on dynamic testing) as taking measurements is normally quick and often reliable (Salawu, 1997a).

Cawley and Adams (1979) is a landmark paper in the field of damage identification and structural health monitoring. They proposed the idea of using vibration measurements to detect damage and provided a formulation to detect damage in composite materials from frequency shifts, which forms the basis of using modal analysis for damage identification (Owen and Choo,

1998). They first computed the ratio between frequency shifts for different modes for damaged and undamaged cases from experimental results. A grid of possible damage points was considered, and an error term constructed that related the measured frequency shifts to those predicted by a computer model based on a local stiffness reduction. A number of mode pairs were considered for each potential damage location, and the pair giving the lowest error indicated the location of the damage. The formulation, however, did not account for possible multiple-damage locations. Another drawback of this method was the need to model all possible damage mechanisms at all possible sites, and hence considerable computing time was required subsequent to physical measurements (Salawu, 1997a).

Based on the idea of using frequency shifts as a method of damage detection, as suggested by Cawley and Adams (1979), much research has since been carried out and different ways of improving the applicability of their original concept suggested. Creed (1987) is one of the first who attempted to apply dynamic testing on a motorway bridge. Based on the data, he suggested that a 5% drop of natural frequencies would be a good damage threshold. He also found that the mode shapes are too unreliable and can only be used as an identifier of which mode was associated with each natural frequency. His experimental results also indicated that modal parameters are generally insensitive to structural damage.

Uzgider et al. (1993) later proposed a damage location method that used measured natural frequencies to identify bending stiffness. They first selected the vibration modes whose parameters had significant influence and utilised the natural frequencies of these selected modes to identify the bending stiffness. The presence of structural damage was indicated by the relative magnitudes of the differences between identified parameters and prior estimates. The success of this method however depends on accurate prior estimates and identification of suitable stiffness parameters.

Brincker et al. (1995) furthered the investigation by using a statistical analysis method to detect damage in two concrete beams with different reinforcement ratios, based on the changes in the measured vibration frequencies. They scaled the observed change in modal frequency by an estimated standard deviation of the frequencies and weighted accordingly based on the confidence level (the higher the confidence level, the lower the standard deviation). The authors also defined a "unified significance indicator" by summing the frequency and damping significance indicator over several measured modes. The significance indicator proved to be a sensitive indicator of structural damage on that particular test set-up, but it was not capable of providing an estimate of damage location.

Salawu and Williams (1995a, 1995b) later proposed a global damage integrity index that is based on a weighted ratio of the damaged natural frequency to the undamaged natural frequency. The weighting factors were used to reflect the relative sensitivity of each mode to the damage event. When damage is indicated, local integrity indices are calculated to locate the defective areas. The local integrity index is calculated from the global integrity index by further weighting the global index by the square of the ratio of damaged mode amplitude to the undamaged mode amplitude for a particular measurement point. Salawu (1997b) also conducted tests on a concrete bridge before and after the support bearings had been replaced. He reported there is only an average change of 1.7% in frequency for the first six modes of vibration.

Eccles (1999) was interested in the trend of the natural frequency drops for concrete structures with increasing damage. By applying damage to concrete beams, the natural frequencies dropped initially by about 12% with 15% of damage, but stayed almost even (2.5% drop) for greater damage (between 20%-80%) and dropped again at severely damaged states. This tri-linear relationship was later confirmed by Pearson (2002) and Rohrmann et. al. (2001).

2.3.3 MODE SHAPES

Some researchers believe it is far better to detect damage using mode shapes than measuring natural frequencies. They consider that by looking into the changes of mode shapes, damage can not only be detected, but also located.

Mode shapes are normally compared using Modal Assurance Criterion (MAC) and Co-Ordinate Modal Assurance Criterion (COMAC). These are techniques of correlating two different sets of mode shapes of a structure at the same mode, but at different state, normally the undamaged and damaged state. Using these techniques, Salawu and Williams (1995a, 1995b) tested a reinforced concrete bridge and showed that the MAC and COMAC values can detect and locate the damage to some extent. They also compared the results using relative changes in mode shapes and changes in mode shape curvature to detect damage. They demonstrated that the relative difference measure does not typically give a good indicator of damage using experimental data. They also pointed out that the most important factor was the selection of the modes used in the analysis. Similar work has been conducted by Ko et al. (1994) on steel framed structures. Although positive results were obtained, they reported that indication of damage was masked by modes that were not sensitive to that particular damage.

Pandey et al. (1991) suggested that using mode shape curvature is a better way to obtain spatial information about vibration changes. It was thought that small changes of mode shape induced by damage should be more obvious when looking at the curvature rather than the whole mode shape. They found that modal curvature was a far more sensitive damage indicator than the MAC and COMAC method. By using this proposed method, Zhang and Aktan (1995) recommended that changes in curvatures of the uniform load surface (deformed shape of the structure when subjected to a uniform load), calculated using the uniform load flexibilities, could be a sensitive indicator of local damage. They stated that changes in the uniform load surface were appropriate to identify uniform deterioration. Maeck et. al. (2000) further suggested that curvatures, calculated directly from experimental mode shapes could be used to

derive stiffness directly. Although this technique was only true for statically determinate systems, it had the advantage that no prior numerical model was needed. The mode shapes, however, had to be identified with a sufficient degree of accuracy to be able to obtain good curvature estimation. This will be discussed later in this chapter.

In contrast, Das et. al. (1997) raised doubts on the use of mode shapes as damage indicators. By performing tests on reinforced concrete beams damaged by bending, they concluded that mode shape measurements were only useful when damage is localised, i.e. at the onset of first cracking and at the point when steel yields. They also suggested that this was due to the fact that when damage became more uniform the mode shape returned to a shape similar to its undamaged state. This view was supported by Raghavendrachar and Aktan (1992) who stated that only higher modes would be possible to indicate local damage but these higher modes would be difficult to identify experimentally in an aged bridge. Pearson et. al. (2001) also agreed on the difficulty of using mode shape measurements for damage detection. By conducting tests on quarter-scale reinforced concrete bridge decks, they found that localised damage can lead to changes in vibration modes and this made it difficult to compare mode shapes. Another key problem of using mode shape measurements as damage indicators is that a large number of measurement points are needed to obtain results with confidence (Modena et. al., 1999, Pearson, 2002). This is normally not practical in field tests of civil engineering structures, such as bridges.

2.3.4 MODAL DAMPING

Although some work has been carried out, attempts at using damping ratios as damage indicators have been generally unsuccessful. Salawu and Williams (1995b) tested a reinforced concrete bridge and found that damping ratios do not have a consistent trend with increasing damage. Similar findings were obtained by Salane and Baldwin (1990) and they suggested that damping

ratios are unsuitable indicators as they do not behave monotonically with damage. This finding was later affirmed by many other researchers, including Casas and Aparicio (1994) and Chowdhury et. al. (2000).

2.3.5 FINITE ELEMENT MODELS AND MODEL UPDATING

Due to recent advances in digital computer processing power, a great deal of effort has been invested in the development of sophisticated finite element (FE) models for the analysis of engineering structures. Predictions made using these models have often been called into question as they are often in conflict with test results. This is because the more complex the model, the greater is the need to include local phenomena and calibrate it against test results. Model updating is concerned with the correction of the finite element models by processing records of dynamic response from test structures (Friswell, 1995).

Several studies have been carried out based on the FE approach for structural health monitoring. Using only frequency information, Cawley and Adams (1979) were one of the first to carry out work in this field. They examined a metal sheet containing a saw cut to represent damage and achieve reasonable results. The authors first presumed that the prior model of the structure is highly accurate. Using this model, they computed frequency shifts for both the undamaged structure and then all the considered types of damage. By measuring the frequency changes in the real structure, the location of the damage could then be estimated. This approach has since been investigated and developed greatly in the aeronautical and mechanical engineering field.(Friswell et. al., 1994, Hearn and Testa, 1991).

The use of FE models in the civil engineering field is somewhat limited compared to the mechanical and aerospace disciplines. Though there is some success in research on applying this technique on bridges (Thyagarajan et. al., 1998, Messina et. al., 1996), most researchers (Salawu, 1997a, Owen and Choo, 1998) have doubts over the capability of FE models to predict the

damage behaviour of civil engineering structures as accurately as for mechanical and aeronautical engineering applications. This is due to the fact that civil engineering structures tend to be much larger in size, more variable and less well controlled than in the field of mechanical and manufacturing engineering.

2.3.6 PATTERN RECOGNITION

Recently, there is growing research interest in using the statistical pattern recognition paradigm for structural health monitoring. Instead of relying on conventional modal parameters extracted from experiments with inherent uncertainties, statistical analysis procedures are used to compare and quantify changes in the whole vibration response, i.e. FRF or time history, of a structure (Sohn et al., 2000). Control charts are often used in these cases to provide a statistical framework. The key advantage of this method is its simplicity and the ability to implement this damage detection technique on civil engineering structures with minimal interaction with users. Much of this work, with some success, has been carried out in Europe (Kulla, 2001, Owen et al., 2001, Pearson, 2003) and the USA (Farrar et al., 2001, and Sohn and Farrar, 2000). Although research in this area is still in the early ages, one problem with this paradigm is the large amount of test data needed in order to produce a statistical framework with sufficient accuracy.

2.3.7 LIMITATIONS OF LINEAR MODAL ANALYSIS

Many researchers have doubts about the sensitivity of modal parameters to light damage on a structure. This is demonstrated by Farrar et. al. (1994) during the tests conducted on the I-40 bridge. When the cross-sectional stiffness at the centre of a main plate girder had been reduced by 96.4%, reducing the bending stiffness of the overall bridge cross-section by 21%, no significant reductions in the modal frequencies were observed. Similarly in

Eccles' (1999) experimental work, resonant frequencies were observed to increase slightly for some modes after damage had been introduced. These low frequency shifts have potentially significant practical limitations for applications in large civil engineering structures as it requires either very precise measurements or large levels of damage.

Together with this, the frequency generally cannot provide spatial information about structural changes (Salawu, 1997a). This is due to the fact that modal frequencies are global properties of the structure and therefore it is not clear that shifts in this parameter can be used to identify more than the mere existence of damage. An exception to this limitation occurs at higher order modal frequencies, where the modes are associated with local responses. However, this usually can only be analysed using the Volterra series (discussed in section 2.4.1.4), which are notorious for their complexity (Worden and Tomlinson, 2001). On the other hand, spatial information can potentially be obtained using mode shapes measurement (Salawu, 1995b). However, an acceptable accuracy of measurement of mode shapes tends to require large numbers and locations of sensors, which normally is not practical in field tests of civil engineering structures such as bridges.

Another issue to consider is the dependence upon measuring the excitation force. Almost all of the literature reviewed here has used either impact or harmonic excitation. Both impact and harmonic excitation requires test structures to be isolated from other sources of vibration. However, structural health monitoring of bridges is a long-term monitoring process measuring the structures' vibration characteristics. Authorities would almost certainly prefer minimal disruption from traffic flow and it is also financially unviable to close a bridge down during the whole monitoring process. The use of impact hammer or electromagnetic shaker on the bridge is therefore not feasible for actual monitoring. The ability to use vibrations induced by ambient environment, such as traffic, for the monitoring process is therefore very important and needs further research. However, it is the most difficult excitation method to interpret. As the input excitation is unknown it is often

assumed to be white noise (Felber et. al, 1993, Kramer et. al., 1999), which is not always accurate. There are also doubts on whether ambient excitation will be sufficiently large to allow the modal properties to be measured (Ward, 1984). Although some work has been done, more research on this area would be merited.

Further investigations are also required to establish the relationship between modal properties and environmental conditions. Some research has been carried out to investigate the effect of temperature on natural frequencies. Abdel Wahab and De Roeck (1997) measured the natural frequency of a prestressed bridge when the ambient temperature was 0°C and the again when it was 15°C. The resulting change in natural frequency due to the increase of temperature was a decrease of about 4%. Similar results were obtained by Roberts (1995) and Creed (1987). It is therefore suggested that temperature has a potentially significant influence on the results. This has later been confirmed by Purkiss et al. (1994a, 1994b) analysing the effect of ambient conditions of the dynamic response of four prestressed concrete bridge decks. By measuring the site's air temperature, soffit temperature, humidity, mean air pressure and rainfall on the day preceding the test, they found that soffit temperature is by far the most influential and showed a gradual decrease in natural frequency with increasing soffit temperature.

Another issue of primary importance is the dependence on prior analytical models or/and test data. Almost all of the works reviewed here presume access either to a detailed FE model or a set of undamaged data of the structure. The lack of availability of these baselines, which is normally the case for bridges, often makes the method impractical. While it is doubtful that all dependence on prior models and data can be eliminated (Doebling et al., 1996), steps should be taken to at least minimise the use of the baselines. Nevertheless, an assessment of deterioration between the current and a future condition should be possible by assuming the current condition as a baseline (Salawu, 1997b). This would however require a very good knowledge of the current defects of the structure.

2.4 NONLINEAR MODAL METHODS

Nonlinear behaviour has been regularly observed in damaged structures (Okauchi et al., 1997, Wenzel and Pichler, 1998, Eccles, 1999 and Vanhoenacker et al., 2000). This is not surprising as all structures encountered in practice are nonlinear to some degree. The nonlinearity depends upon many factors including boundary conditions, material properties, excitation levels and type, loading conditions, clearance and previous history. Therefore, it can be seen that the basic modal analysis and system identification methods, discussed in the previous sections, could not be applied due to the fact that this classical theory is based on the assumption that the system investigated is linear.

System identification for nonlinear structures is an area still lacking uniqueness of approach (Tomlinson, 1988). Nonlinearity is often difficult to produce experimentally in a controlled fashion and is often just as problematic numerically. To investigate the use of this nonlinear behaviour as a tool for structural health monitoring, the following steps need to be taken. Firstly, the nonlinearity needs to be identified and understood. This can be done using nonlinear system identification techniques. Then, a model that reproduces this nonlinear behaviour should be obtained or derived. Finally, based on the characteristics of the nonlinear behaviour that are most sensitive to damage, a method for damage identification is then proposed.

Extensive research has been carried out on the use of different nonlinear system identification techniques. However, very little research has been carried out on modelling and the use of nonlinear behaviour as a tool of damage detection and structural health monitoring. The following is a brief summary of some of the more popular nonlinear system identification techniques, followed by a discussion of some of the key papers on cracked beam modelling. Investigation on the use of nonlinearities for structural health monitoring can be found in the next section.

2.4.1 NONLINEAR SYSTEM IDENTIFICATION TECHNIQUES

Characterisation of nonlinearities, as presented by Adams and Allemang (1998), can be divided into three different levels:

- Level 1: Detection of the presence of nonlinearity
- Level 2: Classification of the type of nonlinearity
- Level 3: Location of the source of nonlinearity

The nonlinear system identification techniques discussed below are mainly Level 1 and 2. Locating the source of nonlinearity (Level 3) is a very challenging process and is normally not possible to obtain directly without prior knowledge of the system. Trial and error methods are often utilised to locate the nonlinearity in a particular model structure (Adams and Allemeng, 1998).

2.4.1.1 Nyquist Plot

Arguably the easiest way of detecting nonlinearities is by visually inspecting FRFs for distortions. Nyquist plots (i.e. imaginary versus real part of the FRFs) offer the quickest and most effective way of inspecting the FRFs for distortions. If FRF characteristics in the Nyquist plane differ significantly from a circular or near-circular locus in the vicinity of the resonances then nonlinearity is suspected. The main problem for this technique is that it is not suitable for all types of nonlinearity. For example, polynomial or piecewise response nonlinearities under low levels of excitation appear as circular loci in a Nyquist plot (Worden and Tomlinson, 2001). Furthermore, this technique is very much a Level 1 technique due to the classification of the type of nonlinearity being almost impossible.

2.4.1.2 Hilbert Transform

The Hilbert transform technique is based on the idea that the actual time response of a system is just one of many possible responses that could have been produced by a phase shifted version of the input. By shifting the phase of the time response, the Hilbert transform creates a generalised analytic signal. Instantaneous amplitudes and frequencies are calculated by taking the magnitude of the analytic signal and derivative of the instantaneous phase of the signal. With these, a plot between amplitude and frequency, normally known as the backbone curve, can be obtained. A brief account of the more important formulae is presented below. By shifting all frequency components in a signal by $\pm\pi/2$ radians, the Hilbert transform of a time history, $x(t)$, can be written as:

$$H[x(t)] = \frac{1}{\pi}\int_{-\infty}^{\infty}\frac{x(\tau)}{\tau - t}d\tau = \frac{-1}{\pi t}x(t) \tag{2.5}$$

where the generalised analytic signal, $y(t)$ can then be written as

$$y(t) = x(t) + jH[x(t)] \tag{2.6}$$

Finally, the instantaneous amplitude, $A(t)$ and frequency, $\omega(t)$ are computed directly using the formulae below:

$$\begin{aligned} A(t) &= |y(t)| = \sqrt{x^2(t) + H^2[x(t)]} \\ \omega(t) &= \frac{d}{dt}\left(\arctan\frac{H[x(t)]}{x(t)}\right) \end{aligned} \tag{2.7}$$

The problems with the Hilbert transform techniques are that they are very subjective and do not work well with many closely-spaced modes of vibration. The fact that extensive filtering and smoothing are required to obtain

satisfactory data also shows that this technique is highly vulnerable to noise in the raw data (Bendat and Piersol, 1986).

2.4.1.3 Wavelet Transform

Fourier transforms, used in linear modal analysis to transform data from the time domain to the frequency domain, are expressed as the summation of an infinite number of sine and cosine terms (details are discussed in appendix C). The problem with the Fourier transform for a nonlinear test system is the inability to locate and analyse short portions of a signal, due to the fact that the entire time record is processed at each frequency. In other words, the Fourier transform has only frequency resolution and no time resolution. Wavelet transforms use the same type of operation as the Fourier transforms except that Wavelet transforms use a localised basis function that decays quickly to locate parts of a signal that occur over short time intervals. This property of Wavelet transforms enables them to analyse non-stationary systems. As in the technique used with Hilbert transform, the backbone curve is the main product of this technique.

Although this technique has been widely applied in the fields of telecommunication technology and image compression (Wells Jr., 1994), it is still relatively rare in the field of structural system identification. One of the main reasons is that the parameters used in the Wavelet transform, such as ridges and skeletons, do not have a physical meaning for the system (Staszewski and Chance, 1997).

2.4.1.4 Volterra Series

The Volterra series method is a powerful system identification method that derives higher order FRFs of a system. The main difference between the first and higher order FRFs is that the higher order FRFs keep track of the

harmonics produced by nonlinear systems under sinusoidal excitation, whereas the first order FRFs do not (Adams and Allemang, 1998). This nonlinear system identification technique is based on Duhamel's integral of linear vibration:

$$y(t) = \int_{-\infty}^{\infty} h(\tau)x(t-\tau)d\tau \tag{2.8}$$

The Volterra series assumes that the output of a system can be expressed as an infinite series and that an equivalent Duhamel's integral can be formed using the terms in the series (Worden and Manson, 1997, Worden, 1998). The impulse response function in the Duhamel's integral is replaced by a function of terms in the series and expressed in the following form:

$$y(t) = y_1(t) + y_2(t) + y_3(t) + \ldots + y_n(t) + \ldots \tag{2.9}$$

where

$$y_n(t) = \int_{-\infty}^{+\infty} \ldots \int_{-\infty}^{+\infty} h_n(\tau_1,\ldots,\tau_n)x(t-\tau_1)\ldots x(t-\tau_n)d\tau_i \ldots d\tau_n \tag{2.10}$$

The functions h_n are referred to as the Volterra kernels. As in linear modal analysis theory, there exists a dual frequency-domain representation for nonlinear systems based on the higher-order FRFs, $H_n(\omega_1, \ldots, \omega_n)$, $n = 1, \ldots, \infty$ which are defined as the multi-dimensional Fourier transforms of the kernels

$$H_n(\omega_1,\ldots,\omega_n) = \int_{-\infty}^{+\infty} \ldots \int_{-\infty}^{+\infty} h_n(\tau_1,\ldots,\tau_n)e^{-i(\omega_1\tau_1+\ldots+\omega_n\tau_n)}d\tau_1\ldots d\tau_n \tag{2.11}$$

The problems with this method are that higher order FRFs are difficult to compute and measure. It is also difficult to interpret for MDOF (Multiple Degree Of Freedom) systems' experimental data. More importantly, Volterra

series only converge for polynomial nonlinearities and are therefore unable to deal with any non-polynomial nonlinearities (Tomlinson, 1988).

2.4.1.5 Restoring Force Method

The restoring force method (also known as force-state mapping method) enables quick visualisation of nonlinearities in a SDOF system. Introduced by Masri and Caughey (1979) and further improved by Worden (1989), it is based on Newton's second law for a SDOF system:

$$m\ddot{u}(t) + f(u,\dot{u}) = p(t) \tag{2.12}$$

where $f(u,\dot{u})$ is the internal restoring force of the system expressed as a function of the system displacement and velocity. This can be treated as a surface over the phase plane. If the force $p(t)$ and velocity $\dot{u}(t)$ are sampled simultaneously at regular intervals, then at each sampling instant the value of the displacement and acceleration can respectively be obtained by integrating and differentiating the velocity data. Hence, using:

$$f_i = p_i - m\ddot{u}_i \tag{2.13}$$

where p_i is the i^{th} sampled value of the input etc., a sequence of triplets $(u_i, \dot{u}_i, f_i)$ can be obtained. Each triplet specifies a point in the phase plane and the height of the restoring force surface above that point. A continuous representation of the force surface can then be constructed and the intersection of this surface with the plane through $\dot{u} = 0$ will provide the relationship between restoring force and displacement for the system.

This method can also be extended to MDOF systems by using the modal vectors of the system in combination with an expression for the restoring force

in modal coordinates. A detailed explanation of this method is presented in chapter 5.

2.4.2 CRACKED BEAM MODELLING

Many investigations into the dynamic properties of a cracked structure focus on the modelling of the cracks themselves. The existence of a crack reduces the stiffness of the structure and consequently reduces its natural frequencies. This indicates that by measuring changes in the modal parameters the location of a crack can be identified. Despite the growing research efforts, a rigorous cracked beam vibration theory has yet to be developed (Dimarogonas, 1996). Models of cracked beams in the field generally include either a crack that is permanently open, i.e. open crack model, or a crack which opens and closes during vibration, i.e. breathing crack model. More recently, many researchers have attempted to model cracked beams with a nonlinear crack (a crack that considers transition intervals between open and closed). Key papers reviewed here are divided into sections dependent on differing types of crack models.

2.4.2.1 Open Crack Models

Much of the research has been done for mechanical and aeronautical engineering fields, and the cracks investigated were usually caused by fatigue loading. Single, discrete cracks can form in ductile materials as a result of cyclic loading at levels below the structure's ultimate capacity. Looking at the dynamic behaviour of the cracked structure, the crack effectively creates a local discontinuity in the structure and this discontinuity has to be accounted for when the mode shapes are integrated to calculate the modal mass and stiffness.

In the 1940's, researchers, the majority of which being mechanical engineers began to develop methods of modelling the effects of cracks. These studies mainly focused on the simply supported or cantilever beams with the crack modelled as a simple notch. The effect of a notch on the structure flexibility was simulated by a spring, or reduced section, with magnitudes, which were estimated by experimentation (Kirmsher, 1944 and Thomson, 1943). This method of modelling a crack is effectively an open crack model. This idea was extended in the 1950s by Irwin (1957) and Bueckner (1958) who relate local flexibility to the crack stiffness stress intensity factor. Stress intensity factor is the one-parameter representation of the mechanical load level, on material near the edge of the crack, for each mode of crack opening, provided that certain length requirements are met. The stress intensity factor concept provides a basis for quantifying the resistance of materials to the onset of growth of a pre-existing crack, as well as for predicting the initiation of fracture in a cracked, nominally elastic structure in the field of fracture mechanics (Freund, 1998).

A similar approach was adopted by Rizos et. al. (1990). In modelling a beam with an open crack, they used two undamaged beams connected by a spring. They used the general form of the mode shapes of the two undamaged beams, along with the boundary conditions at the crack location, to develop equations for the displacement at either side of the crack. The method was extended to a crack in a beam with variable cross-section (Nandwana and Maiti, 1997) and a beam with multiple cracks (Shifrin and Ruotolo, 1999). Several variations of the approach were suggested by Chaudhari and Maiti (1999), Mahmoud et. al. (1990) and Narkis (1994).

However, the open crack model is considered unrealistic as most cracks open and close during oscillations. The reduced stiffness, modelled at the crack location, remains constant irrespective of the magnitude of the load applied whilst the beam oscillates. Gudmundson (1982) demonstrated that the model predicted a significantly larger reduction of modal frequencies from the experimental specimen. Similar results were seen by other researchers

(Brandon and Richards, 1989, Ismail et al., 1990, and Cheng et al., 1999). This indicates that crack detection by an open crack model would underestimate the crack severity if the crack were actually growing under fatigue loading conditions (Ruotolo et al., 1996a and Lamonaca, 1997).

2.4.2.2 Breathing Crack Models

Knowing that it is unrealistic to consider a crack to be always open in a vibrating structure, researchers suggested that the cracked zone should be attributed with a compressive capacity when the two surfaces bear directly against each other. The recognition of this compressive capacity brought about the proposition of a 'breathing' crack model. A breathing crack model shows a crack which opens and closes as the stress around the crack location alternates between tension and compression. This model is based on the assumption that the dynamic loads are sufficient to close the crack during part of the oscillation cycle. A stepped change in the stiffness term was introduced in the early models of breathing crack, bringing nonlinearity into the model.

Brandon and Richards (1989) suggested that the compressive and tensile parts of the motion of the crack should be treated separately. The reason for this was that when the crack was in compression, the cracked beam should act as an undamaged beam, whilst in tension, the crack causes a reduction in stiffness near the crack. Based on this stiffness discontinuity, Friswell (1992) later produced an equivalent SDOF bi-linear model of a cracked beam vibrating in its fundamental mode. Rather than stress distribution, Friswell assumed flexural rigidity along the beam was locally reduced.

A more complicated model, incorporating various features such as dry friction at the crack interface, was then proposed by Abraham and Brandon (1995). By using the sub-structuring approach, the model comprises two linear states, (1) open-crack and (2) closed-crack, with a short interval of transition corresponding to closure or opening of the crack. The model comprises a

Fourier development of flexibility matrix presented previously by Papadopoulos and Dimarogonas (1988). Lagrange multipliers were used to enforce the continuity conditions at the crack section, which avoids the interference or overlapping of cracked surfaces.

Actis and Dimarogonas (1989) developed a FE model for a beam with a bilinear crack model. They developed a model to determine whether the crack is open or closed by looking at the sign of the bending moment at the crack location. They made the approximation that the mode shape does not change as a result of the crack. They also presented results showing the harmonic generated from the opening and closing of the crack. A similar approach was used by Qian et al. (1990), where they formulated different EI values for positive and negative curvature to represent crack opening and closure. Rotational inertia and shear effects were not included in both of the formulations and the models assumed that complete opening and closing always occurred at the zero bending moment or curvature.

Instead of using FE models, Shen and Chu(1992) developed a closed-form solution for the vibration of a beam with a bilinear crack model subjected to low-frequency harmonic force. The crack was determined to be open or closed based on the sign of the axial strain at the crack location. They presented results that indicated the possibility of identifying damage based on the frequency and magnitude of harmonic vibrations.

A big drawback of modelling cracks in a bilinear fashion is that a bilinear stiffness system will not produce a nonlinear behaviour (Tan et al., 2000, 2001). In fact, a bilinear system (with state changes at origin) is a special type of nonlinear system that produces a linear response (Bendat, 1998). Therefore, unless the self-weight of the structure is incorporated in the model, a bilinear crack model would not be able to reproduce the nonlinear behaviour observed by a number of researchers (Eccles, 1997, Van dan Abeele, 1999 and Owen et al. 2002).

2.4.2.3 *Nonlinear Crack Models*

Instead of modelling the crack bilinearly, Brandon and Mathias (1995) suggested that the transition interval as the crack closes and opens should be taken into account. They suggested that the response of a cracked beam can be modelled as a sequence of four stages: (1) crack in tension, (2) transition interval as crack closes, (3) crack in compression and (4) transition interval as crack opens. They also suggested that the transitions would cause more nonlinearity. This was demonstrated by Clark et al. (1984) during studies on the effect of crack closure on the accuracy of different non-destructive testing predictions of crack size. By using four-point bending specimens and measuring the crack opening, they obtained the relationship of opening-closing displacement versus applied load, shown in figure 2.3. The result highlights that the bilinear crack model is inaccurate and attention should be paid to the transitions between open crack state and closed crack state when modelling crack vibration.

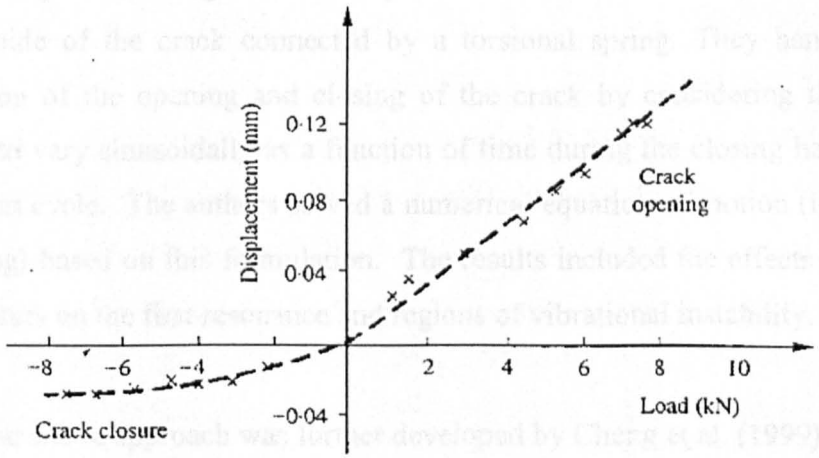

Figure 2.3: Clark's relation for opening-closing displacement versus applied load. (Clark et al., 1984)

In order to study the nonlinearity behaviour, Brandon and Sudraud (1998) demonstrated that the response behaviour of a cracked vibrating beam contained regions of topological instability, indicated by a period of doubling behaviour. However, it was not possible to induce a further bifurcation

response. They also indicated that the response behaviour below the boundary of topological instability contained non-linear characteristics such as harmonics of the forcing frequency.

Instead of investigating the transitions between crack open and crack closed, Zhang and Testa (1999) explored the nonlinearity induced by crack closure. They demonstrated that experimental study of crack closure and its effect on the vibration of a simple beam showed that both frequency and damping changes due to the crack were influenced significantly. These results would be of value in the further development of models to detect crack damage in structures as well as in modelling of crack closure and the mechanism of damping at a crack.

With the view to investigate the behaviour of the beam during the transition interval, Kwarczuk and Ostacowicz (1992) developed a model for transverse vibration of a Bernoulli-Euler beam (explained in appendix A) with an opening and closing crack. They modelled the beam as two sections on either side of the crack connected by a torsional spring. They handled the transition of the opening and closing of the crack by considering the crack length to vary sinusoidally as a function of time during the closing half of the vibration cycle. The authors solved a numerical equation of motion (including damping) based on this formulation. The results included the effects of crack parameters on the first resonance and regions of vibrational instability.

The above approach was further developed by Cheng et al. (1999). Cheng et al. related the stiffness of the structure with crack breathing frequency, which is also equal to the excitation frequency, sinusoidally, in the whole vibration cycle. By expressing k_0 and $k_{\Delta C}$ as the undamaged stiffness and the difference between undamaged stiffness and fully open crack stiffness, they expressed the equation of motion of the crack model as:

$$m\ddot{u} + c\dot{u} + \left[k_0 + k_{\Delta C}\left(1 + \cos(\omega_1 t)\right)\right]u = f(t) \tag{2.14}$$

Owen et al. (1999) and Eccles (1999) have also done some similar preliminary work on crack modelling. As opposed to relating the stiffness change to a time parameter, the authors relate the stiffness changes in their breathing crack models to the displacement of a vibrating beam. Note that the specimens investigated by both Owen et. al and Eccles et. al. were reinforced concrete and a series of evenly-spaced cracks was formed in the specimens. Details of these three nonlinear crack models will be further discussed in chapter 4.

2.4.3 NONLINEAR VIBRATIONS OF CRACKED REINFORCED CONCRETE BEAM

Eccles (1999) has also shown that the natural frequency of a cracked reinforced concrete beam is related to the oscillation magnitude. He first found that the cracked reinforced concrete beams produced different response frequencies for different impact magnitude and went on to demonstrate that the same relationship exists within individual time histories as the response magnitude decayed. These findings indicated that the specimens tested do not obey the law of superposition and therefore the effect of nonlinearity comes into account. This was then further investigated by a visiting researcher to the University of Nottingham, Marina Lute, from Romania, who with the collaboration of the author carried out stepped sine sweep tests on three reinforced concrete beams (Tan et al., 2000). The results show clear softening spring behaviour, as the natural frequency decreases with increasing dynamic excitation. The details and results of the tests can be found in chapter four.

The softening spring behaviour found in a cracked reinforced concrete beam was also suggested by Van Den Abeele and De Visscher (2000) as they obtained similar results. They carried out a complete experimental modal analysis at different levels of damage on a reinforced concrete beam and analysed it both linearly and nonlinearly. Although Van Den Abeele et al. also obtained a softening spring behaviour from the response, the aim of their

research was to compare the linear and nonlinear system identification techniques and was therefore focused less on crack modelling itself.

With reference to Eccles's work, Goldsmith (1999) conducted a pilot research project at the University of Oxford. Nield et. al. (2001, 2002) continued with this work and suggested a time-stepping model capable of including damage in the form of rotation relationship over a cracked region. The model was validated for linear vibrations against theoretical values and the representation of a nonlinear mechanism using the model was compared with experimental data. Nield also conducted tests using vibrating wire strain gauges to investigate the moment-rotation behaviour over the cracked region of reinforced concrete beams. He discussed several possible nonlinear crack mechanisms but no firm conclusions were drawn (Nield, 2001).

In addition to work carried out by Owen et al., Eccles, and Ruotolo et al. (1996a, 1996b, 1997) the behaviour of beams with multiple cracks have also been investigated. FE models of a clamped-free beam with two cracks or with multiple cracks were made. A good correlation between the experimental results and the FE models was shown as the models predicted the frequency variation accurately.

2.4.4 Damage Detection Using Nonlinear Vibrations

As discussed in the previous chapter, very little research has been carried out in investigating the feasibility of using the nonlinear characteristics as a means of damage detection and structural health monitoring.

It is believed that nonlinear dynamic behaviour leads to the presence of super-harmonics in the response spectrum (Pugno et al., 2000). A super-harmonic is a harmonic at a frequency that is an integer multiple of one of the modal frequencies. It results from the motion not being perfectly sinusoidal but taking the form of a distorted sinusoid at the same frequency. This was

demonstrated by Tsyfansky and Beresnevich (2000). They conducted forced vibration tests on aircraft wings and used the change of super-harmonics to detect cracks. Some success was obtained but the method was only valid if the fatigue crack present in the aircraft wing opens and closes during the excitation.

Techniques based on measuring the higher order FRFs of the structure were suggested by some researchers (Storer and Tomlinson, 1993, Crespo et al., 1996). The analysis of the higher order FRFs showed that they are highly dependent upon the size and the position of the crack, i.e. damage, and thus can be used as damage indicators. The correlation of the shape and the value of these functions with the crack size and position may form the basis for a relatively sensitive structural damage identification procedure. The main problem for these techniques is the fact that it is very difficult to measure higher order FRFs with acceptable accuracy.

Vanhoenacker et. al. (2000) suggested the use of odd-odd multisine excitations to characterise damage in structures. Odd-odd multisine excitation is a specifically designed broadband periodic signal in which the frequencies at spectral lines 1,5,9,13,..., $4k+1$ are excited, while the intermediate lines contain no energy. From the energy levels at intermediate lines in the response signal, information about the even and odd order nonlinearities of the system can then be extracted. A variation on this technique has also been suggested (Vanlanduit et al., 2000). The drawback of this method is that the measurement time to obtain a certain frequency resolution is four times larger than a fully excited frequency grid. More importantly, this technique predominantly assumes polynomial nonlinearities and therefore is not suitable for other types of nonlinearity.

Johnson et al. (2000) suggested a method of exciting a sample with continuous waves of two separate frequencies simultaneously, and then inspecting the harmonics of the two waves, their sum and their difference of the frequencies (side bands). It is based on the fact that undamaged materials

are essentially linear in their response to the two waves, whereas the same material, when damaged, becomes highly nonlinear, manifested by harmonics and side band generation. This method can be quickly applied and is ideally suited to applications where the question of damage versus undamaged must be quickly addressed (Donskoy et al., 2000). However, this method is very much a quick check on the presence, but not the degree and type, of nonlinearity.

2.5 SUMMARY AND DISCUSSIONS

From the survey of literature, it is clear that a great deal of work investigating the possibility of using linear vibration techniques to detect damage in bridges has been carried out over the past 25 years. Although there have been some promising results, it is also clear that there are still some major drawbacks, such as poor sensitivity of the modal parameters to damage, requirement in obtaining baseline data, the need for measuring excitation force as well as environmental effects. The existence of nonlinearity in the vibration characteristics of a damaged structure further complicated the problem and caused doubts on the feasibility of applying these techniques to actual structures. Understanding of the nonlinear behaviour is therefore crucial. To facilitate this, nonlinear system identification techniques are needed, although this area still lacks uniqueness of approach. Modelling of cracked beams to replicate the behaviour will assist in gaining a better understanding of the source of nonlinearity. However, a rigorous cracked beam vibration theory has yet to be developed. Due to the reporting of different findings indicating that nonlinearities are somewhat more sensitive then linear modal parameters, researchers have also suggested that there is a possibility of using this nonlinear behaviour as a tool for health monitoring and damage detection.

This area of research on the use of nonlinear behaviour as a damage indicator is relatively new and therefore very little research has actually been carried out. There is a general lack of consensus amongst researchers, of the suitable approaches and parameters to be measured. Furthermore, almost all

the suggested techniques have been designed specifically for use within aeronautical and mechanical engineering applications. It would therefore appear sensible to extend this area of research to the field of civil engineering.

In conclusion, the findings from the literature survey justified the aim and objectives set in the introductory chapter.

CHAPTER 3

EXPERIMENTAL DESIGN

3.1 INTRODUCTION

From the literature reviewed in the previous chapter, it is clear that vibration measurements show potential in structural health monitoring. However, it is also evident that nonlinearity is an important issue to be addressed, especially for civil engineering applications. This is because the sensitivity of modal parameters to damage within civil engineering structures, like bridges, is low. With such a low sensitivity, any nonlinearity that presents in the vibration data can significantly change the results of the condition monitoring, the consequences of which, could be serious. It is therefore very important to fully understand the issue of nonlinearity.

A sensible place to begin the investigation is to confirm the presence of nonlinearity in cracked reinforced concrete structures. Therefore, preliminary experimental work was carried out by performing a modal analysis test on reinforced concrete beams in a conventional manner, i.e. linearly, but with the emphasis on detecting the presence of nonlinear behaviour. After obtaining confirmation of the presence of, and gaining knowledge of the characteristics of the nonlinear behaviour of the reinforced concrete specimens, a series of

experimental investigations was then performed. These focused primarily on characterising the nonlinearity using a nonlinear system identification technique.

Following this introduction, the aim and objectives of the experiment are established. The methodology used to achieve the aim and objectives is then discussed. This is followed by discussions of the differing issues to be considered in the experimental design. Details of the experimental set-up are presented in the final section. Experimental results can be found in the following chapter.

3.2 AIM AND OBJECTIVES

The aim of the experimental investigation was to improve understanding of the existence and source of nonlinearity in the vibration characteristics of cracked reinforced concrete beams. To achieve this, the following objectives were set:

- Confirm the presence of nonlinearity
- Identify the nonlinear behaviour
- Assess the changes of nonlinear behaviour with increasing damage
- Characterise the type of nonlinearity

3.3 METHODOLOGY

In order to achieve the above-mentioned aim and objectives, the following methodology was employed:

- Carry out a preliminary experimental investigation to replicate Eccles' work and confirm the presence of nonlinear behaviour. (Details of the preliminary investigation can be found in section 4.2.)

- Apply the nonlinear system identification technique to identify and characterise the behaviour

- Repeat the test at different damage levels to provide details of variation of nonlinearity with increasing damage.

With the methodology laid out, it was possible to design an experiment to study the vibration of reinforced concrete beams at different damage states. There were many issues to be considered in the experimental design, but the more important were; the excitation method, the excitation signal, the transducer, the nonlinear system identification technique, the design of specimens and the test set-up. Each issue is discussed in detail in the following sections. Some of the issues are inter-related, for example, certain nonlinear system identification techniques require a specific excitation signal. It should be noted therefore, that cross-referencing is inevitably frequent in the following discussions.

3.4 EXCITATION METHOD CONSIDERATIONS

It is important that the excitation method adopted in the test was best suited to achieve the objectives stated above. Ideally, the frequencies and

amplitude of the adopted excitation method could be controlled in a precise manner. This is essential for the studies of nonlinearity. It was also necessary that the input excitation was known and the repeatability high. Preferably, the excitation method could be easily adopted for field-testing, especially for bridges.

There are , generally, two viable ways to excite a test structure, namely impact excitation and forced vibration. The advantages and limitations are discussed as follows:

3.4.1 IMPACT EXCITATION

Impact excitation is arguably the easiest to perform on laboratory test structures and is usually carried out using an instrumented hammer. An instrumented hammer is a device that introduces an excitation force pulse to the test structure with the impact force measured by a built-in force transducer. The hardness of the tip is directly related to the frequency range of the input pulse force. For a hard tip impacting a hard surface, the force pulse distributes energy to a wider range of spectrum, when compared with a soft tip. It is, however, reasonably difficult to control as it is almost impossible to ensure that each impact is the same as the previous one, regarding the position, magnitude and orientation relative to the normal of the surface. For nonlinearity detection, different magnitudes of excitation are needed and to achieve this an instrumented hammer is used to hit the specimen with varying force, usually exerted by the user. In practical terms therefore, it is difficult to vary the magnitude of excitation precisely to detect nonlinearity.

3.4.2 FORCED VIBRATION

Forced vibration tests normally comprise exciting a test structure using an electromagnetic actuator. The electromagnetic actuator consists of a magnet, a

moving block, and a coil, positioned inside the magnet. When an electric current from a signal generator passes through the coil, located inside the actuator, a force, proportional to the current and the magnetic flux density, is generated, which drives the moving block. An electromagnetic actuator has a wide frequency, amplitude and dynamic range. It can also be carried out over a broad band of frequencies, at one frequency or at a gradually changing frequency.

The main advantage of using forced vibration is that it allows users to have good control over the input signals, i.e. frequencies, magnitudes, waveforms, range etc. Other benefits include known input excitation and high repeatability. Depending on the excitation signal chosen, forced vibration is by far the best method of excitation for studies of nonlinearity. Forced vibration, however, is not considered to be the most practical method for field-testing, especially for bridges. A very large actuator is needed to produce a signal with reasonable amplitude and therefore the cost of testing would be increased. Closure of the bridge is inevitable for the test to be carried out, as vehicles on the bridge would produce significant noise. Although forced vibration has been used on test structures, it is generally considered to be unrealistic.

3.4.3 SELECTION OF EXCITATION METHOD

Given that the objectives of the test were to identify and characterise the nonlinearity found in the vibration, it was decided that forced vibration using an electromagnetic actuator was the most sensible choice of excitation for this test. This is because good control of the input excitation is essential in studies of nonlinearity.

3.5 EXCITATION SIGNAL CONSIDERATIONS

The choice of excitation signal is crucial to conduct accurate vibration analysis. Although theoretically the FRF data should not depend on the excitations and responses, in practice the accuracy and quality of FRF data does depend on the choice of excitation among many other factors. As some excitation signals are better suited for one task, it is important that the chosen excitation signal suits the test objectives, in this case, nonlinearity detection and characterisation. A description of some of the more readily available excitation signals follows:

3.5.1 SINUSOIDAL EXCITATIONS

Sinusoidal excitations are the most traditionally used for vibration analysis, of which swept sine excitation is arguably the most popular. Swept sine excitation consists of a sine signal, which slowly and continuously varies in frequency. The low rate of change allows users to assume the measurement of virtually steady state response characteristics. Although the process is extremely time-consuming, a high degree of control in the frequency and amplitude of the excitation signal ensures that the swept sine excitation is arguably the best suited for characterising nonlinearities.

3.5.2 RANDOM EXCITATION

The force signal for random excitation is a non-periodic stochastic signal with Gaussian probability distribution. It contains all frequencies within the frequency range. For a structure that behaves nonlinearly, random excitation has the tendency to linearise the behaviour from the measurement data. The other problem for random excitation is that leakage occurs since neither the force signal nor the response are periodic with infinite time history.

3.5.3 PSEUDO RANDOM EXCITATION

Pseudo random excitation has the force of an ergodic, stationary random signal, which consists of discrete frequencies formed by integer multiples of the frequency resolution used by the Fourier transforms. It is a periodic signal with random amplitude and phase distribution and the response will therefore be periodic with respect to the sample period. As a result of this periodicity of the signals, no leakage problem exists. However, pseudo random excitation normally requires a signal dedicated hardware and it requires longer time for any transient response to the initiation of the signal to decay.

3.5.4 CHIRP EXCITATION

A Chirp excitation is a very rapid sine sweep, where the frequency is swept up and down in one observation period of the data acquisition. The procedure repeats this sweeping in such a way that it becomes a periodic function. This signal is actually a special case of a pseudo random signal and therefore has similar characteristics. Sufficient time is needed to allow for transient responses to decay and nonlinear distortions can occur in the measurement results.

An improved version of Chirp excitation, known as burst Chirp signal, consists of a short section of an underlying Chirp signal followed by a period of zero output, resulting in a response which shows a transient build-up followed by a decay. Burst Chirp is also considered suitable for characterising nonlinear systems due to the ease of amplitude and frequency control. However, special equipment is normally required for signal generation.

3.5.5 SELECTION OF EXCITATION SIGNAL

In spite of the time-consuming process, swept sine excitation is chosen as the excitation signal because of the suitability of the excitation signal for

characterising nonlinearity. Hardware restrictions prevent the consideration of using Chirp excitation as an excitation signal.

3.6 SELECTION OF TRANSDUCERS

3.6.1 ACCELEROMETERS

Accelerometers are the most common transducer for vibration analysis. They measure acceleration of a test structure and output the signal in the form of a voltage. Accelerometers are simple mass-spring-damper systems. The most common type is the piezoelectric accelerometer, as illustrated in figure 3.1. It is based on the phenomenon that straining certain types of crystal produces a small electric charge. By using a seismic mass to generate a force in a crystal, an accelerometer produces a signal proportional to the acceleration in a frequency band well below its proper resonance.

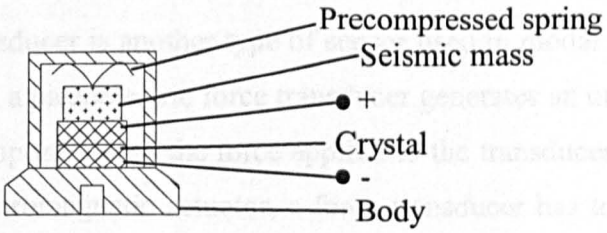

Figure 3.1: Diagram of a piezoelectric accelerometer

3.6.2 LASER VIBROMETERS

The laser vibrometer is a device which is capable of detecting the instantaneous velocity of the surface of a structure. During the process, a laser beam from the vibrometer (generally helium neon laser) is directed onto the vibrating surface and reflected. The reflected light is combined with the

internal reference beam. When the surface moves, the path difference between the reference and reflected beams varies. This results in an intensity modulation of the recombined beam due to interference phenomena. This can be seen as the effect of the recombination of a reference beam with a signal beam, the frequency of which is shifted by the Doppler effect by an amount of $f_d=2v/\lambda$ (with λ, the wavelength of the laser beam and v, the velocity of the surface). Since a one to one correspondence exists between the Doppler frequency f_d and the frequency of the intensity modulation, it contains the information about the surface velocity. More electronic processing allows determination of the direction of the velocity and generation of a voltage signal proportional to the surface velocity. The main requirements in the use of the laser vibrometer is that there must be a line of sight to the target measurement point and a surface which is capable of reflecting the laser beam adequately. The main advantage of using a laser vibrometer is that it provides contactless motion measurements.

3.6.3 FORCE TRANSDUCER

A force transducer is another type of sensor used in modal analysis. Like an accelerometer, a piezoelectric force transducer generates an output charge or voltage that is proportional to the force applied to the transducer. For a modal test using an electromagnetic actuator, a force transducer has to be connected between the surface structure and the shaker.

The main consideration in selecting a force transducer is to understand how it interacts with the excitation device to which it connects. When the force transducer is used with a shaker, the presence of its mass may cause distortion to the force signal measured at structural resonance. However, this distortion is dependent on the mass difference between the transducer and the test structure. For this case, since the test specimen is sufficiently large compared with the chosen force transducer (>1000 times), the issue of distortion of the force signal is not considered an issue.

3.6.4 SELECTION OF TRANSDUCERS

With good experimental practice, there is no major difference in using accelerometers and laser vibrometer in terms of quality. However, as will be discussed in the next section, the choice of restoring force surface method as the nonlinear system identification technique requires displacement, velocity and acceleration at the same instance. In order to obtain velocity and displacement data, two levels of integrations would be needed if raw data is in the form of acceleration, i.e. accelerometers. On the other hand, data from a vibrometer (in the form of velocity) would only require one level of integration and differentiation. As numerical integration of discrete time series can introduce more integration errors (see Chapter 4), it is therefore considered that laser vibrometer would be the more sensible option.

Furthermore, at the time of testing there were two other modal analysis tests planned (by other researchers), and the full set of accelerometers would therefore not be readily available for a long period of time. However, as most other similar tests were carried out using accelerometers as response measurement, both accelerometers and the laser vibrometer were used on one of the specimens to ensure compatibility.

3.7 SELECTION OF NONLINEAR SYSTEM IDENTIFICATION METHODS

A brief list of different nonlinear system identification methods is discussed in Section 2.4.1. It was decided that the following methods would be used to detect and characterise the nonlinearity:

3.7.1 SWEPT SINE

Swept sine excitation was chosen as the excitation signal for this test (see section 3.5). Using the sine sweep excitation signal, two checks can be applied to investigate nonlinearity: (1) tuning direction, and (2) magnitude variation.

The first check was based on the fact that for a system to be linear, the shape of the FRF would be independent of tuning direction (Weiland and Linke, 1996). It was decided that this would be a good characteristic to be utilised as a tool for nonlinearity detection. A sine sweep was repeated using both increasing and decreasing frequencies over a range around the natural frequencies. If a system is linear, both the resulting FRFs should coincide; a sway in the FRFs would indicate the possible presence of nonlinear behaviour (see figure 3.2).

The second check to be carried out was by exciting the test specimen with different amplitudes of swept sine signals. Again, if a system is linear, the FRF will be independent of the magnitude of excitation. A lean to the left by the spectrum of output would indicate a system having a softening behaviour and hardening behaviour would be shown by a lean to the right (see figure 3.3). For this test, ten different amplitudes of excitation were used to investigate the magnitude variation.

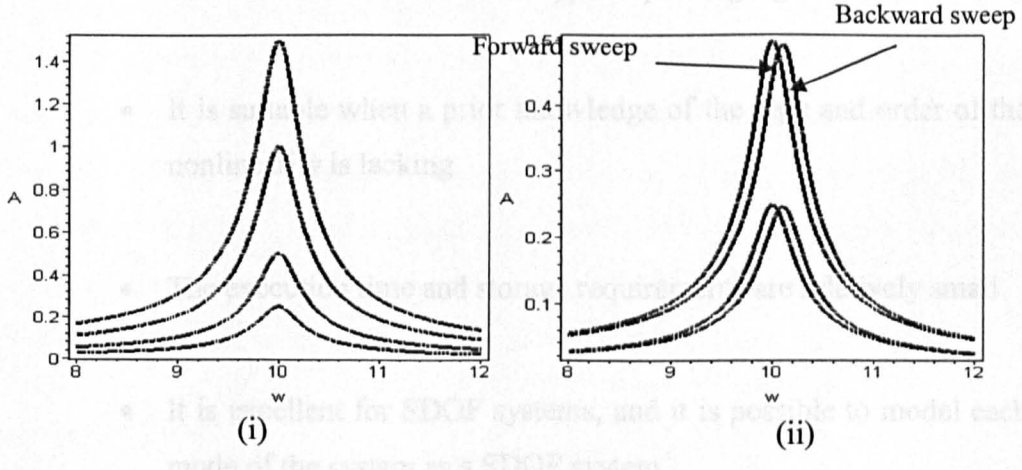

Figure 3.2: Response from (i) a linear system and (ii) a weakly nonlinear system with different tuning directions

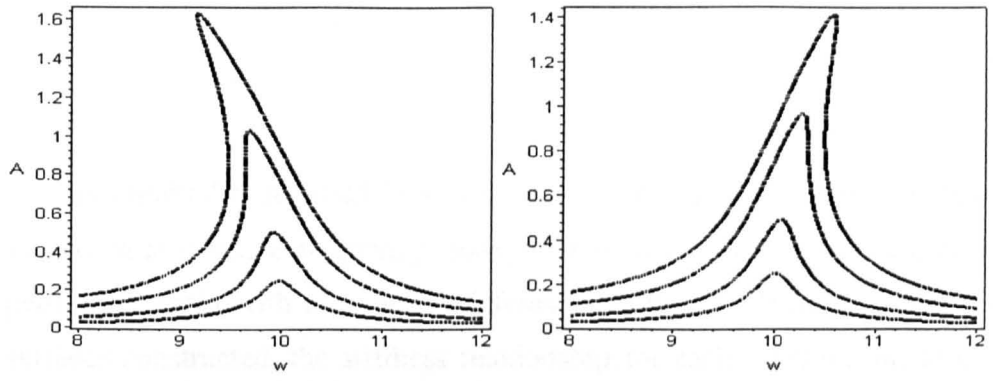

(i) (ii)

Figure 3.3: Response from (i) a softening behaviour and (iv) a hardening behaviour

3.7.2 RESTORING FORCE SURFACE METHOD

It was decided that the Restoring Force Surface Method should be the main nonlinear system identification technique to be adopted. This was due to the following reasons:

- It is applicable to linear, nonlinear non-hysteretic and self-excited systems with limit cycles
- There is no restriction on the type of probing signal used
- It is suitable when a prior knowledge of the type and order of the nonlinearity is lacking
- The execution time and storage requirements are relatively small
- It is excellent for SDOF systems, and it is possible to model each mode of the system as a SDOF system.

- It provides a visual representation of the internal forces of the system.

To obtain data required for constructing restoring force surfaces, harmonic excitation at a single frequency close to each of the natural frequencies was performed again with a range of different amplitudes. With restoring force surfaces constructed, the stiffness relationship for each vibration mode could be established.

3.8 SPECIMEN DESIGN CONSIDERATIONS

3.8.1 USE OF LASER VIBROMETER

Vibration data of the specimens was to be collected using a laser Doppler vibrometer, and it was a requirement that the laser vibrometer be positioned directly above the specimen. It was also important that the positions of interest were within the coverage of the camera of the laser vibrometer, the maximum angle of coverage of the camera being 20 degrees from the vertical axis. However, it was recommended that the angle of coverage be kept within 10 degrees to ensure optimum accuracy. Therefore, for the laser vibrometer to cover a bigger area, it would need to be positioned at a greater height. The maximum height for this is about 5m from the surface of the specimen. Due to the cost of the equipment, it needed to be taken down over night and at weekends. The ease of taking down and setting up was therefore an important factor. Due to these restrictions, and to allow the laser vibrometer to cover the whole of the beam, the length was therefore restricted to 2m.

3.8.2 SUPPORT CONDITION

Two different types of support condition were utilised. The beam would be simply supported at both ends when tested statically, i.e. overloaded to cause damage. During the dynamic test, the beam would ideally be in a free-free condition. The reason for this is that a free-free condition cuts noise and interference by other objects to a minimal level in the vibration data. To achieve this desired support condition, two cables were used to lift the beam specimen whilst the dynamic test was being carried out. The attachment positions of the cables to the beam were carefully considered and it was decided that the two nodes of the first mode of vibration of the specimen would be ideal, as this would cause a minimal effect on the first mode of vibration of the beam. To further minimise the effect of the cables, both cables should be attached to the specimen at its neutral axis, as this should reduce the effect of tensile forces applied from the cables to the surfaces of the specimen. However, as the damaging processes would alter the specimen's neutral axis positions it was unrealistic to alter the attachment positions accordingly. It was therefore decided to position the attachment points at a location halfway from the top surface of the specimen.

3.8.3 EASE OF TESTING

Ideally the beam specimen would have a fundamental frequency similar to that of a typical bridge. However, typical fundamental frequencies of reinforced concrete bridges are reported to be between 1.5Hz and 12.5Hz (Billing, 1984). In order for the beam specimen to possess such a low fundamental frequency, an extremely long and slender beam design would be required causing handling difficulties. And if such a slender beam specimen were used, the ratio of aggregate to beam size would be extremely large. This untypical ratio could easily cause a different kind of nonlinearity. It was therefore decided that it was more important to reproduce the nonlinearity realistically than reproducing a representative fundamental frequency by having a typical cross sectional area of beam.

3.8.4 SPECIMEN SPECIFICATION

Six reinforced concrete beams, purposely designed to fail in tension, having a length of 1.7m and cross section measuring 200mm X 100mm. The tension reinforcement comprised two 12mm diameter high yield steel bars with nominal top reinforcement of two 6mm diameter high yield steel bars. The shear links were made from 6mm diameter mild steel bars at 100mm centres. A concrete mix of 4:3:1 (aggregate(10mm):sand:cement) with 0.69 water cement ratio was used. The concrete mix gave a slump of 35mm and saturated density was averaged at 2385kgm^{-3}. Cube compressive tests were carried out at 7 days and 28 days after casting, giving an average cube strength of 28.0Nmm^{-2} and 36.8Nmm^{-2} respectively.

The natural frequencies of the first four bending modes of the specimen, assumed free-free supported, were calculated as 272Hz, 749Hz, 1469Hz and 2428Hz. The moment capacity of the specimen was 16.4kNm, corresponding to a point load of 40.5kN, applied at the centre-span. The shear capacity of the specimen was estimated as 82.5kN. The full dimensions of the beams and the concrete mix details are summarised in table 3.1.

Table 3.1: Test specimen specifications

Beam Dimensions (mm)		**Static Properties**		
length	1700	failure moment		16.4kNm
span	1650	failure load		40.5kN
depth	200	maximum shear force		82.5kN
width	100	**Reinforcement Dimensions**		
Natural Frequencies (Hz)			**bottom**	**top**
First	272	type	deformed	deformed
Second	749	effective depth	180mm	18mm
Third	1469	diameter	10mm	6mm
Fourth	2428	number of bars	3	2
Concrete Mix		yield strength	410MPa	410MPa
design cube strength	35MPa	**Shear stirrup**		
water	0.69	type		deformed
fine aggregate	3	orientation		vertical
course aggregate	4	spacing		100mm
cement	1	bar diameter		8mm

3.9 TEST METHODOLOGY

The testing program for each specimen was cyclical. Each of the undamaged beams were tested dynamically to determine their natural frequencies and mode shapes and to establish any non-linear behaviour. The beams were then loaded in three-point bending to introduce damage in the form of cracks. At each load increment the static load was removed and the dynamic tests repeated to ascertain whether there were any significant changes in natural frequency or non-linearity. The load was then re-applied and incremented before being removed so that the dynamic tests could be conducted again. The same test procedure was followed for each specimen tested. Key points of the procedure are set out in figure 3.4.

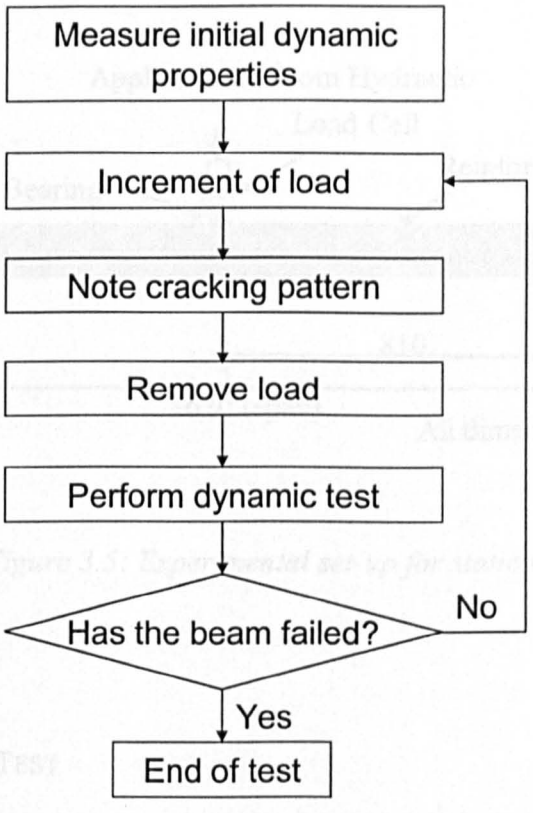

Figure 3.4: Adopted testing procedure.

3.9.1 LOADING

Three-point loading was used to introduce damage to the beam. After each load increment the cracking patterns were noted. This process was repeated until the beam had failed, typified by the yielding of the reinforcement. The load step increment was judgmental, with each increment being halted either when the extent of the cracking had grown appreciably or when the load had increased by 5kN, whichever was reached first.

All of the beams were loaded using the same procedure; the load was applied using a hydraulic jack and measured using a 100kN load cell. Central displacement of the beam was measured during the loading process using a dial gauge. The experimental set-up can be seen in figure 3.5

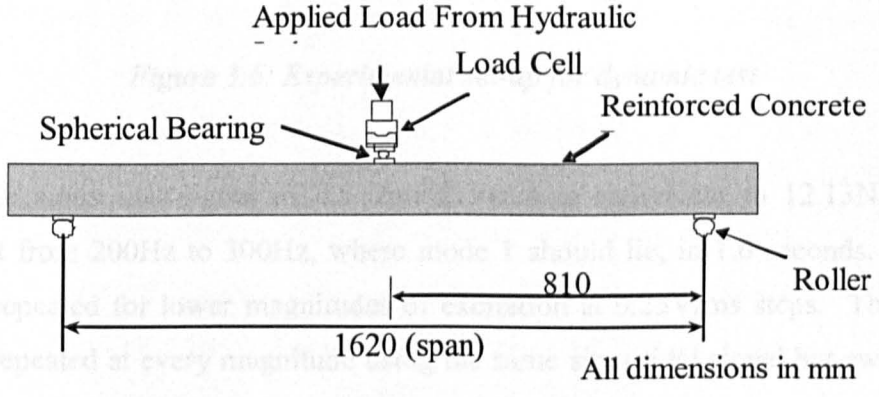

Figure 3.5: Experimental set-up for static test

3.9.2 DYNAMIC TEST

For the dynamic investigations the beams were supported by cables in a quasi free-free configuration (figure 3.6). The responses of points along the axis of the specimen were obtained using a scanning laser Doppler vibrometer. An excitation signal was generated by a signal generator box, model TGA 1230, made by Thurlby Thandar Instruments. As discussed before, sine sweep

tests at different amplitude and tuning direction and harmonic excitation at single frequency were used in the experiment.

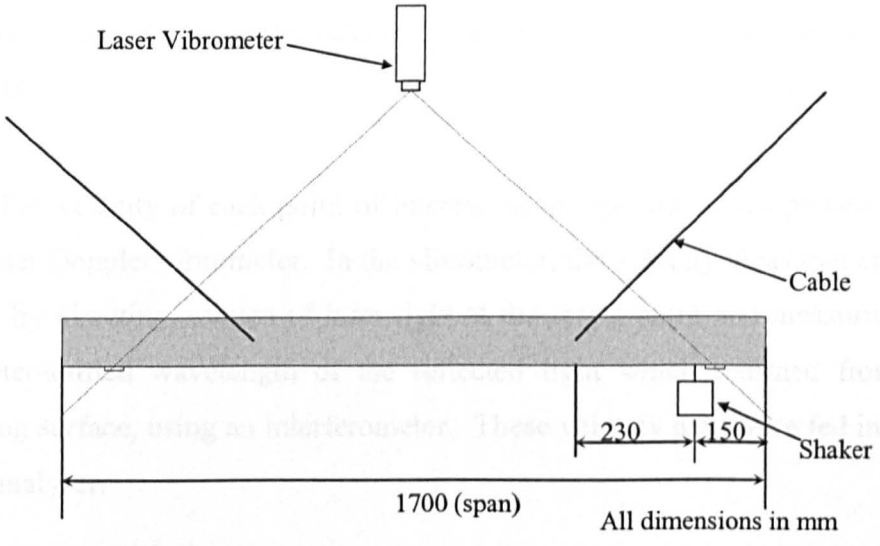

Figure 3.6: Experimental set-up for dynamic test

A sinusoidal signal of 2.5Vrms (1Vrms is equivalent to 12.13N) was swept from 200Hz to 300Hz, where mode 1 should lie, in 1.6 seconds. This was repeated for lower magnitudes of excitation at 0.25Vrms steps. The test was repeated at every magnitude using the same sinusoidal signal but swept in the reverse direction, i.e. from 300Hz to 200Hz. The whole process was then repeated for mode 2, between 550Hz and 650Hz. After the sine sweep test, a harmonic excitation at a single frequency was carried out with a frequency 1Hz lower than the observed resonance frequency.

An excitation signal from the signal generator box was then amplified and transmitted to an excitation mechanism consisting of a 14.1 kg electromagnetic actuator, model V406, made by Ling Dynamic Systems. Vibration was generated based on the excitation signal to provide excitation to the test specimen. Input force by the actuator to the test specimen was measured using a force transducer model M221B02, made by PCB Piezotronics and with a sensitivity of 52.9 $mVlb^{-1}F^{-1}$, attached to the actuator and test specimen by rubber stingers. The point of excitation was located 150mm from the end of

the beam. The selection of the point of excitation was to ensure that all first four bending modes could be excited. This was done by selecting a location which was not the node of the bending mode of interest. Measurements obtained from the force transducer were fed to the data analyser for later processing.

The velocity of each point of interest on the specimen was picked up by the laser Doppler vibrometer. In the vibrometer, the velocity measurement was made by directing a beam of laser light at the target point and measuring the Doppler-shifted wavelength of the reflected light which returned from the moving surface, using an interferometer. These velocity data were fed into the data analyser.

The signals from all the transducers were passed to an Analogue/Digital conversion board in a vibrometer controller before being passed to a personal computer for further processing. The data acquisition and spectrum analyser software used in the experiment was a VibSoft Analyzer, produced by Polytec. In the personal computer, the digitised data was filtered using a built-in 1.2 kHz low-pass filter. Data from swept sine test was transformed to spectrum based using Fast Fourier Transform packages provided by VibSoft Analyzer, with a frequency resolution of 0.625Hz. A general layout of the experimental setup can be seen in figure 3.7.

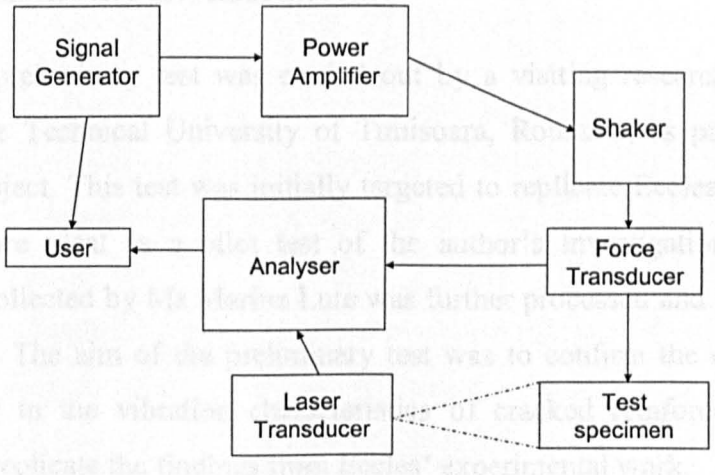

Figure 3.7: General layout of experimental set-up

CHAPTER 4

EXPERIMENTAL RESULTS

4.1 INTRODUCTION

Having discussed the experimental design in the previous chapter, the results from the tests are presented in this chapter. Results from the main investigations have been divided into three major categories, namely the static analysis, the linear dynamic analysis and the nonlinear dynamic analysis. Test results from each of the categories are discussed in detail in this chapter. Before that, results of the preliminary investigation are presented.

4.2 PRELIMINARY INVESTIGATION

This preliminary test was carried out by a visiting researcher; Marina Lute, of the Technical University of Timisoara, Romania, as part of a EU Tempus project. This test was initially targeted to replicate Eccles' work, and was therefore ideal as a pilot test of the author's investigation, and data originally collected by Ms Marina Lute was further processed and analysed by the author. The aim of the preliminary test was to confirm the existence of nonlinearity in the vibration characteristics of cracked reinforced concrete beams and replicate the findings from Eccles' experimental work.

4.2.1 TEST SPECIMENS

Three reinforced concrete beams – length 3m, height 210mm and width 135mm – were cast using grade 35 concrete. Reinforcement consisted of three T10 deformed bars in the tension zone; two R6 deformed bars in the compression zone and R6 shear links at 125mm centres. It should be noted that the dimensions of the specimens were selected to be identical to Eccles' experimental work for better comparison purposes. The first four theoretical natural frequencies for the specimens on free-free boundary conditions were 105Hz, 289Hz, 566Hz and 936Hz.

4.2.2 TEST SET-UP

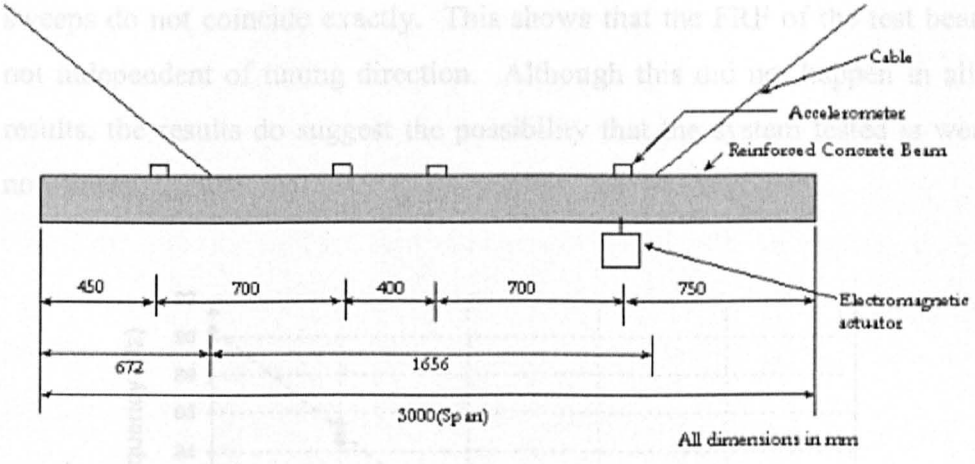

Figure 4.1: Experimental set-up for preliminary test

A set of laboratory tests was carried out on a near free-free supported reinforced concrete beam, excited by an electrodynamic actuator. Each beam was tested in its undamaged state to determine the mode shapes and natural frequencies of its first four vibration modes. The beams were then incrementally loaded in four-point bending until yielding of the reinforcement occurred. At each load increment, the static load was removed and the dynamic behaviour of the beam investigated using a stepped sine sweep excitation around each natural frequency. This sine sweep was repeated using both increasing and decreasing frequencies, and three different amplitudes of

excitation. The location of the excitation and the accelerometers used to measure the response are shown in figure 4.1.

4.2.3 RESULTS

When plotted against load level, fundamental frequencies show a tri-linear relationship as shown in figure 4.2. This is thought to be due to the crack development pattern. A further explanation of this can be found in Section 4.4.2. The result is consistent with Eccles' work, in which fundamental frequencies vary in a tri-linear fashion with increasing damage. Figure 4.3 shows typical results from a sweep test for one of the modes of the test beams and it can be seen that the results of the forward and backward sweeps do not coincide exactly. This shows that the FRF of the test beam is not independent of tuning direction. Although this did not happen in all the results, the results do suggest the possibility that the system tested is weakly non-linear.

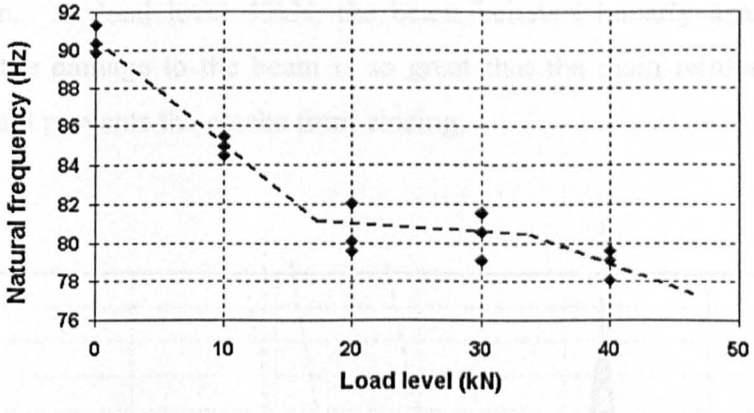

Figure 4.2: Variations of natural frequencies with increasing load levels for all beams

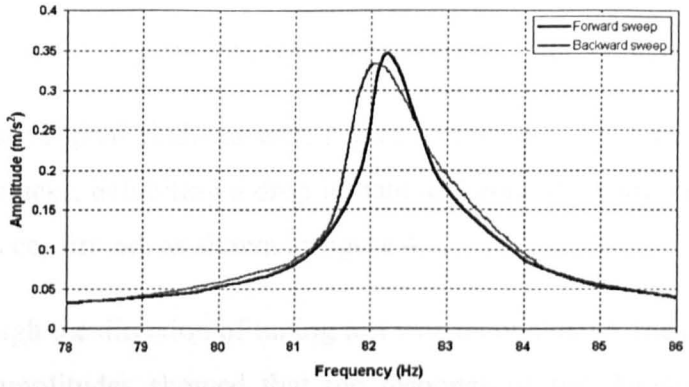

Figure 4.3: Frequency response function for beam 2 mode 1 at 20kN

Figure 4.4 is a typical set of data obtained from the first mode of the beam at different static load increments. When the beam is undamaged, it is clear that the beam behaves in a linear manner and the natural frequency does not change with excitation amplitude. Increasing the static load level causes damage to the beam and a clear drop in natural frequency can be seen at load levels 10kN, 20kN and 30kN. The results also show a clear softening spring behaviour, as the natural frequency decreases with increasing dynamic excitation. At load level 40kN, the beam behaves linearly again. This is because the damage to the beam is so great that the main reinforcement has yielded and prevents the cracks from closing.

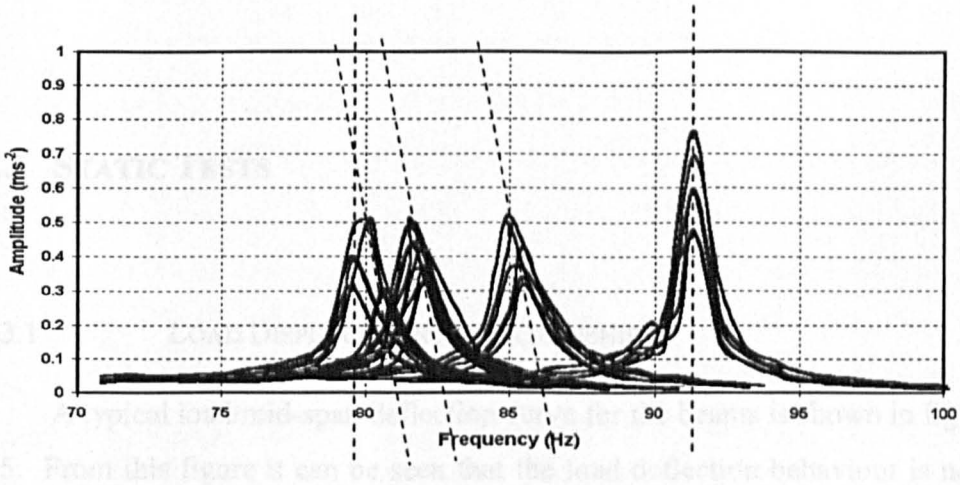

Figure 4.4: Variations of amplitude with frequency for all damage levels for beam 1

4.2.4 FINDINGS AND DISCUSSIONS

The main findings of the preliminary test are:

Eccles' original findings with regard to reinforced concrete beams with distributed cracks, exhibiting a drop in natural frequency with increasing crack height, were confirmed, as shown in figure 4.2.

Although the direction of tuning test was inconclusive, the swept sine test at various amplitudes showed that the response of the damaged reinforced concrete beam was magnitude dependent. This indicated that damaged reinforced concrete beams exhibit a weak non-linear behaviour, with the characteristics of a softening spring, i.e. natural frequency decreases with increasing dynamic excitation.

The results also showed that the degree of nonlinearity appeared to contain a pattern of changes with increasing damage. Both undamaged and badly damaged beams tended to show a much lower degree of nonlinearity than beams which were only lightly damaged.

These initial tests showed encouraging findings and it was therefore sensible to take the investigation a step further to understand more about the nonlinearity found in the vibration characteristics. Results of the main investigation can be found in the following sections.

4.3 STATIC TESTS

4.3.1 LOAD DISPLACEMENT RELATIONSHIPS

A typical load/mid-span deflection curve for the beams is shown in figure 4.5. From this figure it can be seen that the load deflection behaviour is non-linear for the first static load increment. However, for subsequent load increments the relationship is linear up to the previous load level, after which the system becomes non-linear. One could note that there is a significant drop

of stiffness above 40kN, as the reinforcing steels yield. It is also clear that the static stiffness of the linear region becomes less with each load increment. Another point to be noted is that there is a considerable amount of residual displacement after each unloading phase. The residual displacement shows that there is a change in the equilibrium position of the beam during vibration for each damage state.

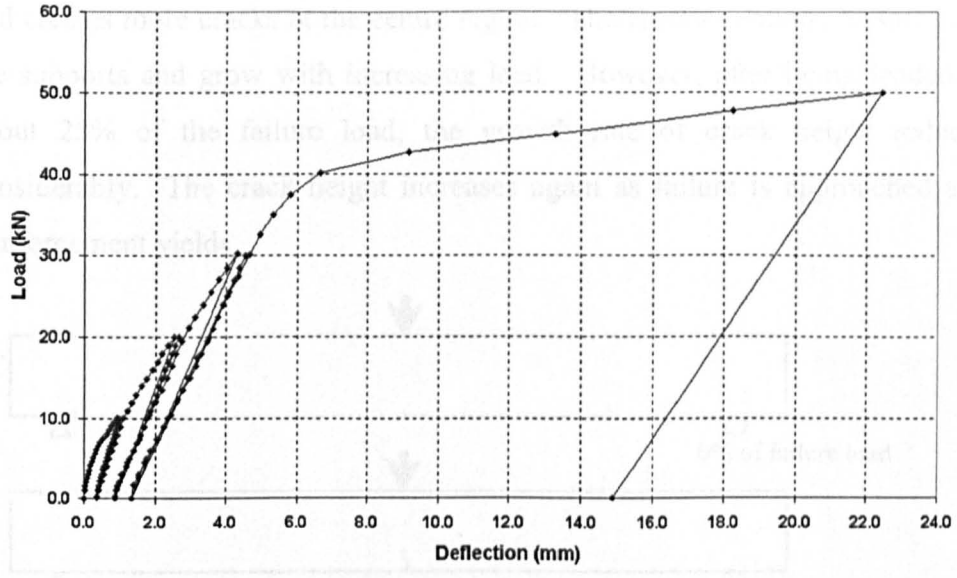

Figure 4.5: Static load deflection curve for beam 2

4.3.2 CRACK DEVELOPMENT

Crack heights have been measured throughout the static test; with both maximum and average crack heights being recorded. Maximum crack height is measured by taking the height of the longest cracks, which is almost always the height of the crack at the mid-span. Average crack height is measured by dividing the beams into 10 zones of 150mm width with 100mm from each end of the beam not being taken into consideration. The mean of maximum crack heights from each zone gives the value of average crack height. One should note that most zones have one principal crack but for some zones, there are two principal cracks. This is due to the fact that the spacing of shear links is 100mm c/c and it is expected that one principal crack would appear at each

shear link. It is therefore more realistic to divide the beams into zones of 100mm.

A typical crack development pattern is shown in figure 4.6. The first cracks, on all the beams tested, appear at 6-8kN. One can see that when the beam is loaded to around 15% of failure load, a single crack develops at the mid-span of the beam. A further increase of load lengthens the centre crack and creates more cracks at the centre region. The cracks continue to spread to the supports and grow with increasing load. However, after being loaded to about 25% of the failure load, the growth rate of crack height reduces considerably. The crack height increases again as failure is approached and reinforcement yields.

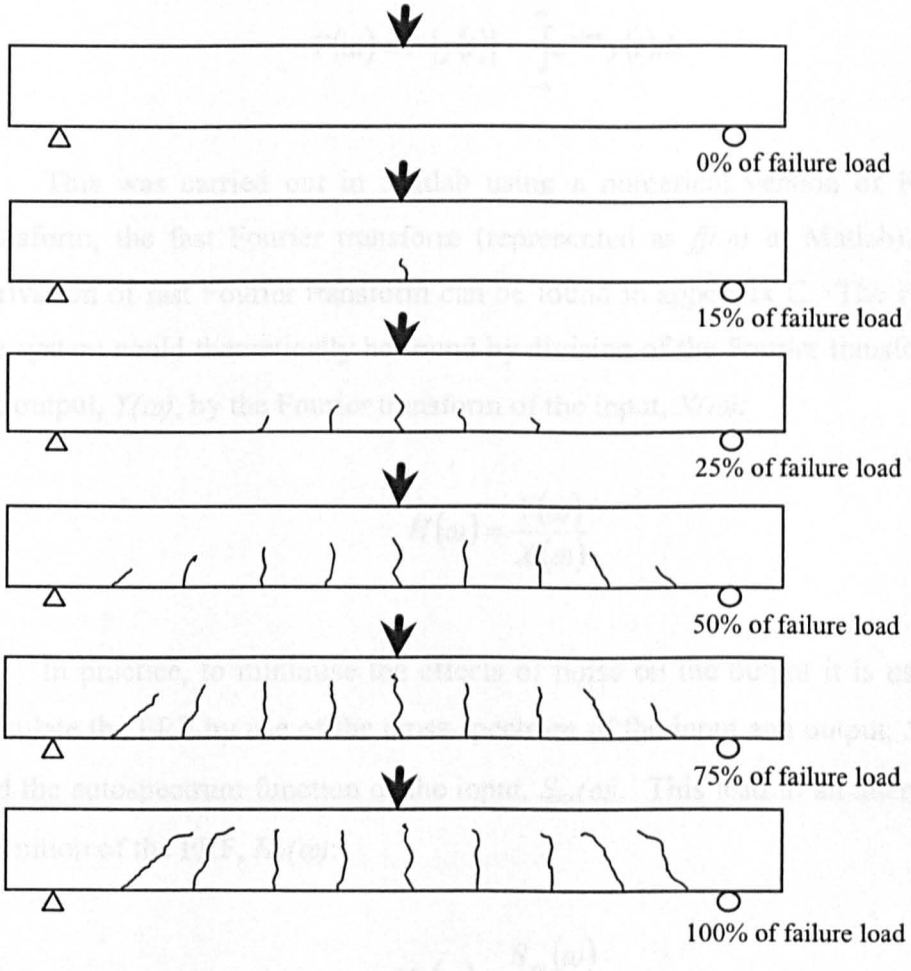

Figure 4.6: Development of cracks for reinforced concrete beam 4

4.4 LINEAR DYNAMIC ANALYSIS

4.4.1 DATA PROCESSING

The data processing procedure for linear analysis is relatively simple. Collected time histories of input, $x(t)$, and output data, $y(t)$, are converted into frequency domain, $X(\omega)$ and $Y(\omega)$, using Fourier transforms:

$$X(\omega) = F\{x(t)\} = \int_{-\infty}^{\infty} e^{-i\omega t} x(t) dt \tag{4.1}$$

$$Y(\omega) = F\{y(t)\} = \int_{-\infty}^{\infty} e^{-i\omega t} y(t) dt \tag{4.2}$$

This was carried out in Matlab using a numerical version of Fourier transform, the fast Fourier transform (represented as *fft.m* in Matlab). The derivation of fast Fourier transform can be found in appendix C. The FRF of the system could theoretically be found by division of the Fourier transform of the output, $Y(\omega)$, by the Fourier transform of the input, $X(\omega)$:

$$H(\omega) = \frac{Y(\omega)}{X(\omega)} \tag{4.3}$$

In practice, to minimise the effects of noise on the output it is usual to calculate the FRF by use of the cross-spectrum of the input and output, $S_{xy}(\omega)$, and the autospectrum function of the input, $S_{xx}(\omega)$. This lead to an alternative definition of the FRF, $H_1(\omega)$:

$$H_1(\omega) = \frac{S_{xy}(\omega)}{S_{xx}(\omega)} \tag{4.4}$$

$$S_{xx}(\omega) = \frac{1}{N_x^2}\left[\sum_{n=0}^{N_x-1} x(t)_n e^{-\frac{i2\pi mn}{N_x}}\right]^2 \quad \text{..... for } m = 0,1,...,N_x - 1 \qquad (4.5)$$

$$S_{xy}(\omega) = \frac{1}{N_x N_y}\left[\sum_{n=0}^{N_x-1} x(t)_n e^{-\frac{i2\pi mn}{N_x}}\right]\left[\sum_{n=0}^{N_y-1} y(t)_n e^{-\frac{i2\pi mn}{N_y}}\right] \qquad (4.6)$$

$$\text{..... for } m = 0,1,...,N-1$$

where $x(t)_n$ and $y(t)_n$ are the measured data of N samples of input and output respectively. Based on these, FRFs were plotted and modal properties (natural frequencies and mode shapes) were then extracted using the peak-picking method. Again, this was carried out in Matlab.

4.4.2 CHANGE OF FUNDAMENTAL FREQUENCIES

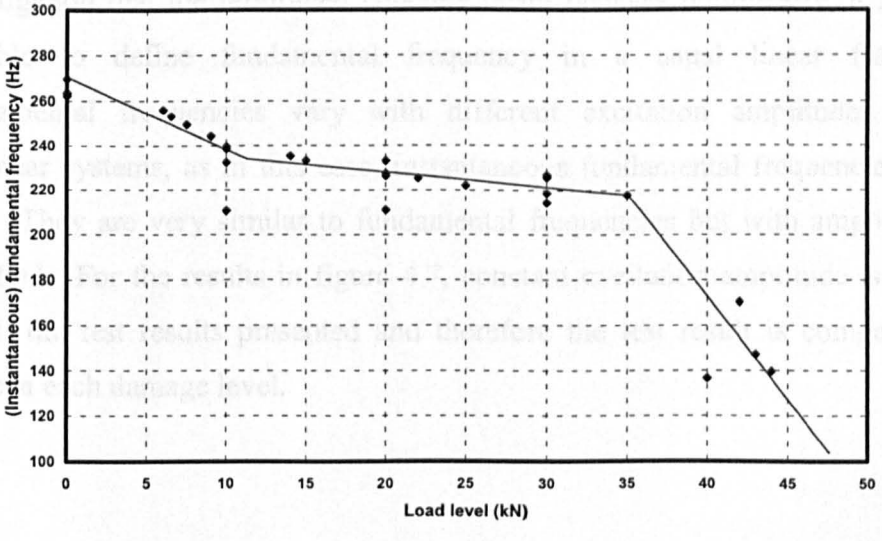

Figure 4.7: Variations of fundamental frequencies with increasing damage levels for beam 1-4

Figure 4.7 shows a variation of fundamental frequencies with increasing damage for four of the beams tested. It is clear that there is a tri-linear relationship, for which the fundamental frequencies drop initially until around 15% damage and stay relatively unchanged to around 85% before the

fundamental frequencies drop again. This is in good agreement with findings by Eccles (1999) (see figure 4.8) and Rohrmann et. al. (2001).

This phenomenon can be explained with the help of a crack development diagram (see figure 4.6). At low load levels (up to around 15%), cracks developed radically mainly in the mid-span. This rapid development of cracks reduces the effective cross-sectional area of the beam and hence the fundamental frequency. With further increases of load levels, cracks started to spread along the beam but with very small increases in maximum crack heights. The overall stiffnesses of the beam stay relatively constant and so were the fundamental frequencies at these load levels (15%-85%). A further increase of load level (>85%) causes reinforcements to yield and therefore further reduces the overall stiffness of the beam and hence fundamental frequencies.

It should be noted that as it was confirmed in the preliminary investigation that the reinforced concrete beam behaves nonlinearly, it is not possible to define fundamental frequency in a usual linear fashion. Fundamental frequencies vary with different excitation amplitudes. In nonlinear systems, as in this case, instantaneous fundamental frequencies are used. They are very similar to fundamental frequencies but with amplitudes specified. For the results in figure 4.7, constant excitation amplitude is used for all the test results presented and therefore the test result is comparable between each damage level.

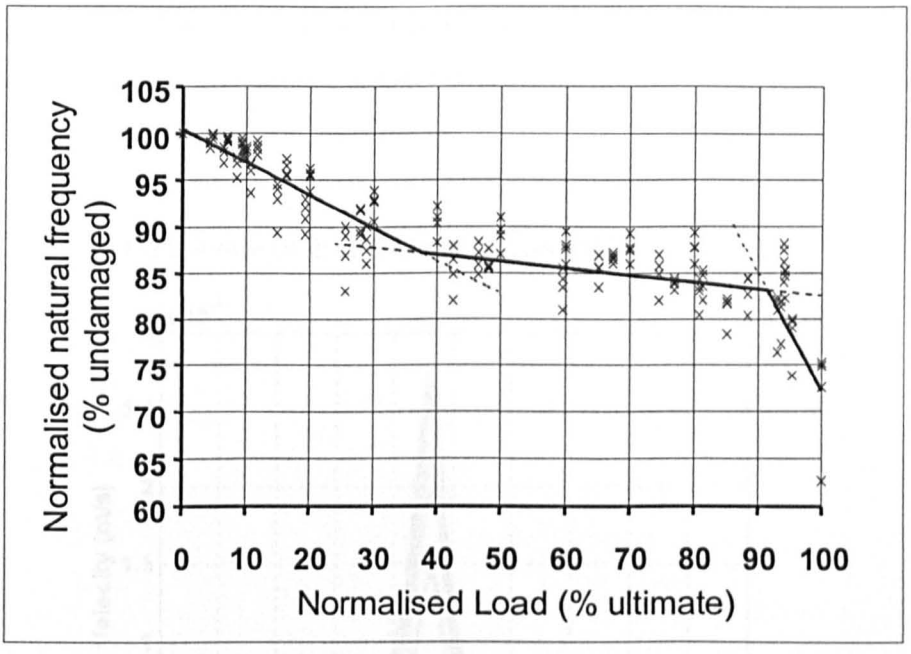

Figure 4.8: Variations of fundamental frequencies with increasing damage levels for reinforced concrete beams (data from Eccles, 1999)

4.4.3 INFLUENCE OF TUNING DIRECTION

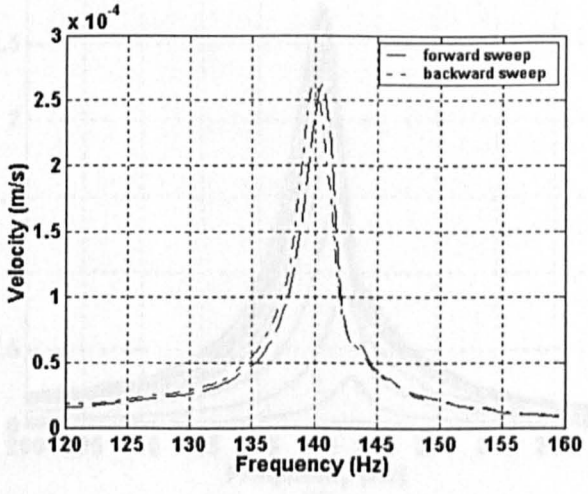

Figure 4.9: Influence of tuning direction on damaged beam

As mentioned in the preliminary investigation, comparing the results of sweep tests with forward and backward direction is one method of detecting non-linearity in weakly non-linear systems. For the beam tests described here most of the results show little difference between forward and backward sweeps, suggesting that the beams are essentially linear. However, in some

cases there is a difference between the two sets of results (figure 4.9). The results are generally considered inconclusive.

4.4.4 INFLUENCE OF EXCITATION MAGNITUDE

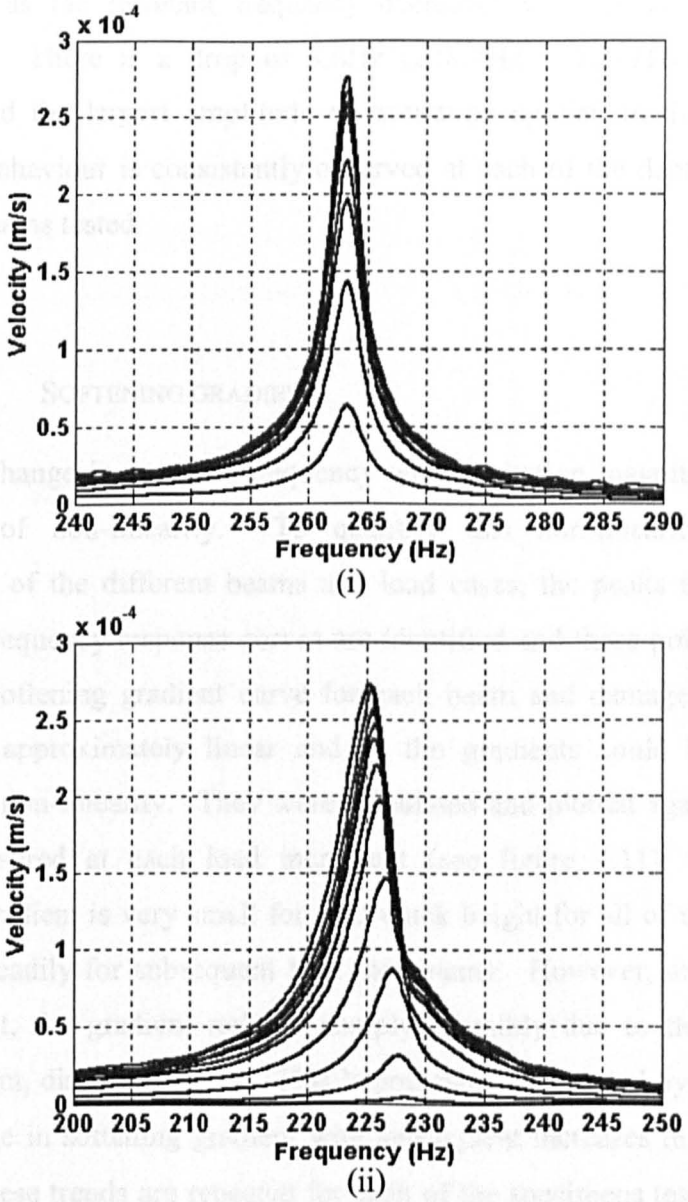

Figure 4.10: Influence of excitation magnitude on frequency response curves for (i) undamaged and (ii) damaged beams

Figure 4.10(i) shows a typical set of frequency response curves for an undamaged reinforced concrete beam. These results show that the resonant frequency is almost independent of the magnitude of excitation, having a value of 263.2Hz at all amplitudes of excitation except at the lowest where it rises to

263.4Hz. This small change is probably due to the presence of microcracking even before any load is applied, although the beam is effectively behaving as linear. In contrast, the corresponding curves for a damaged beam (figure 4.10(ii)) not only show a global reduction in natural frequency due to the reduced stiffness of the cracked section, but also show marked softening spring behaviour, as the resonant frequency decreases with increasing excitation magnitude. There is a drop of 3.6Hz (228.7Hz – 225.1Hz) between the smallest and the largest amplitude of excitation applied in this case. This softening behaviour is consistently observed at each of the damage levels for all of the beams tested.

4.4.5 SOFTENING GRADIENT

The change in resonant frequency with excitation magnitude is a clear indication of non-linearity. To quantify this non-linearity and allow comparison of the different beams and load cases, the peaks in each of the measured frequency response curves are identified and these points connected to form a softening gradient curve for each beam and damage case. These curves are approximately linear and so the gradients could be used as a measure of non-linearity. They were calculated and plotted against the crack height measured at each load increment (see figure 4.11). Clearly, the softening gradient is very small for zero crack height for all of the beams and increases steadily for subsequent load increments. However, above a certain crack height, the gradient reduces sharply, possibly due to the yielding of reinforcement, discussed above. This hypothesis is supported by the relatively small change in softening gradient with subsequent increases in crack height. Although these trends are repeated for each of the specimens tested, there is a broad spread of absolute values suggesting that further work is needed to establish the influence of other factors such as crack location, crack angle etc.

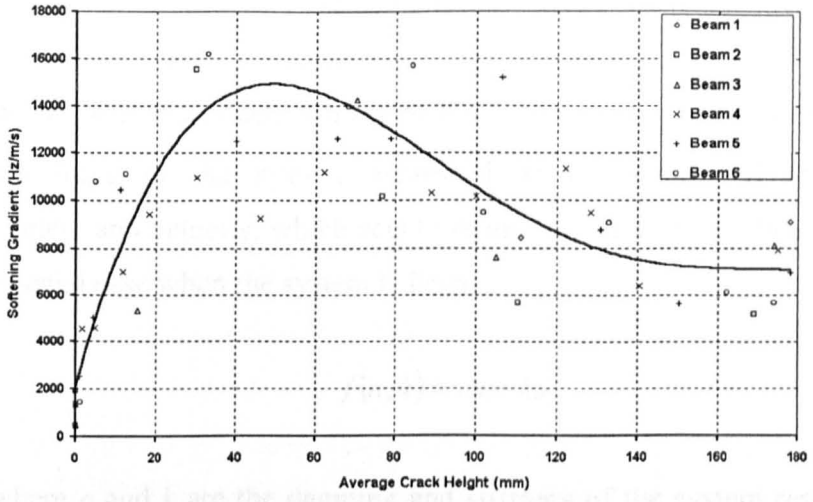

Figure 4.11: Variation of softening gradient with average crack heights

4.5 NON-LINEARITY STUDIES

The results presented so far confirm previous work in showing that there is a significant non-linearity in the vibration behaviour of a cracked reinforced concrete beam. However, although the softening gradient curves discussed above are useful in demonstrating the presence and relative magnitude of this non-linearity, the results cannot readily be applied in the derivation of a suitable model for the processes involved. To achieve the non-linear system identification of a cracked reinforced concrete beam, the author has used the Restoring Force Surface method, for reasons discussed in section 3.7. The following is a brief discussion of the theory and application of this technique of nonlinear system identification method.

4.5.1 RESTORING FORCE SURFACE METHOD

This method, also known as the force-state mapping method (Crawley and Aubert, 1986), was first introduced by Masri and Caughey (1979) and further improved by Worden (1989). As discussed in section 2.4.1.5, the starting point is the equation of motion as specified by Newton's second law:

$$m\ddot{u}(t)+f(u,\dot{u})=p(t) \tag{4.3}$$

where m is the effective mass of the system and $f(u,\dot{u})$ is the internal restoring force of the system expressed as a function of the system displacement and velocity, which acts to return to equilibrium when disturbed. In the special case when the system is linear:

$$f(u,\dot{u})=c\dot{u}+ku \tag{4.4}$$

where c and k are the damping and stiffness of the system respectively. As f is assumed to be dependent only on displacement, u, and velocity, $\dot{u}$, it can be represented by a displacement – velocity plane, i.e. the phase plane. It is possible to rearrange equation 4.1 into the form:

$$f(u,\dot{u})=p(t)-m\ddot{u}(t) \tag{4.5}$$

Provided the effective mass, m, is known, and with excitation force, $p(t)$, and acceleration, $\ddot{u}(t)$, measured or calculated from the test, f can easily be obtained from equation 4.5. For the case of the experiment, velocity and excitation force data are sampled simultaneously at regular intervals. At each sampling instant the value of the displacement and acceleration can respectively be obtained by integrating and differentiating the velocity data. With these, all quantities on the right-hand side of equation 4.5 are known and f at each sampling instant can be calculated from the following equation:

$$f_i = p_i - m\ddot{u}_i \tag{4.6}$$

where p_i is the i^{th} sampled value of the input force etc. It is then possible to obtain a sequence of triplets $(u_i,\dot{u}_i,f_i)$, in which the first two values of the triplets indicate a point in the phase plane and the third value represents the height of the restoring force surface above that point. A representation of the force surface can then be constructed. For SDOF systems, the intersection of this surface with the planes through $\dot{u}=0$ and $u=0$ have physical meanings.

When the plane $\dot{u} = 0$ is used, a relationship between restoring force and displacement for the system is obtained. For a linear system, this would be a straight line and the gradient of the line gives the stiffness of the system. For a nonlinear system, the gradient of the restoring force displacement relationship would provide the instantaneous stiffness values across the vibration of the system. A relationship between restoring force and velocity can be acquired from the intersection of the restoring force surface with the plane through $u = 0$. For an undamped SDOF system, this would be a horizontal line at $f = 0$, as the gradient of the relationship gives the damping value of the system. In the case of this experiment, the effect of damping has not been studied.

4.5.2 DATA PROCESSING

As described earlier each mode of each beam is excited using a single frequency harmonic excitation with a range of different amplitudes. For each test, the time histories of both the input force and the output velocity at a reference position on the top face of the beam are obtained. The following integration and differentiation procedures (Worden and Tomlinson, 2001) are applied to calculate the displacement and acceleration time history data:

Integration:

$$u_i = u_{i-1} + \frac{\Delta t}{2}(\dot{u}_i + \dot{u}_{i-1}) \tag{4.7}$$

Differentiation:

$$\ddot{u}_i = \frac{1}{60\Delta t}(2\dot{u}_{i+3} - 13\dot{u}_{i+2} + 50\dot{u}_{i+1} - 50\dot{u}_{i-1} + 13\dot{u}_{i-1} - 2\dot{u}_{i-3}) \tag{4.8}$$

To eliminate the integration errors, the mean value and best-fit linear trend were removed from the velocity data prior to integration. A moving average procedure was also used to smooth the velocity data and care taken to

ensure all displacement, velocity and acceleration data were at the same point in time.

4.5.3 VALIDATION AND VERIFICATION OF COMPUTER CODE

The routines to perform the restoring force surface calculations are programmed using Matlab and to confirm the algorithm had been correctly programmed a series of standard test cases, using artificially generated data, were processed. These are linear, bi-linear and Duffing's (cubic) oscillators defined by the following equations:

$$\ddot{u} + 0.4\dot{u} + 5u = p\cos(0.8t) \tag{4.9}$$

$$\ddot{u} + 0.4\dot{u} + k_i u = p\cos(0.8t), \quad k_i = \begin{matrix} 3; u \le 0 \\ 1; u > 0 \end{matrix} \tag{4.10}$$

$$\ddot{u} + 0.4\dot{u} + u + 5u^3 = p\cos(0.8t) \tag{4.11}$$

The restoring force displacement curves obtained from these test cases are shown in figures 4.12, 4.13 and 4.14. Appropriate curves are fitted to each set of the restoring force displacement data and the parameters are extracted and compared with the actual data, as shown in table 4.1, 4.2 and 4.3. As can be seen, the code has predicted, with high accuracy, the stiffness relationship for each of the test cases considered. The results of test cases allow the author to suggest two remarks. Firstly, the restoring force surface is able to predict the stiffness of a SDOF non-hysteresis system, in vibration simply from excitation force and velocity data. Secondly, the computer code written for restoring force surface technique gives correct results and therefore can be utilised to process the experimental data.

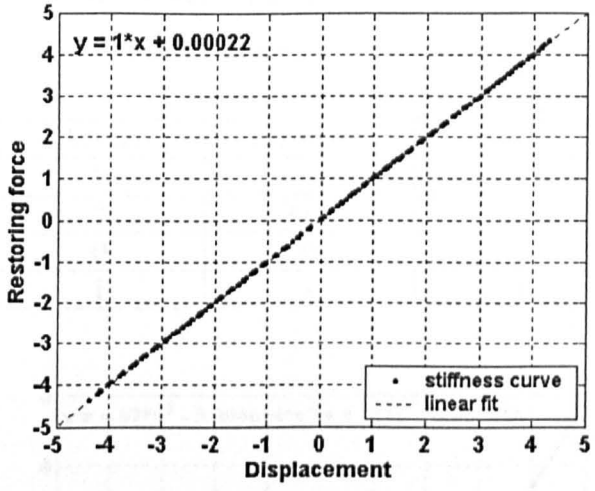

Figure 4.12: Restoring force displacement curve for a linear oscillator (equation 4.9)

Table 4.1: Comparisons between actual and predicted parameters for a linear oscillator (equation 4.9)

Parameters	Actual	Predicted	Difference	Error in %
x^0	0	0.00	-0.00	0
x^1	1	1	1	0

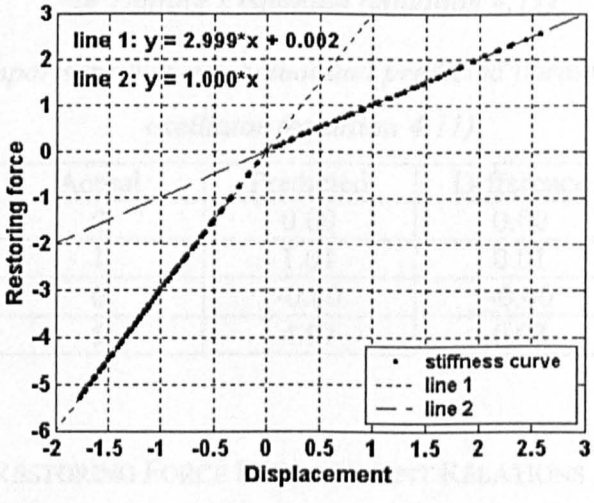

Figure 4.13: Restoring force surface and restoring force displacement curve for a bi-linear oscillator (equation 4.10)

Table 4.2: Comparisons between actual and predicted parameters for a linear oscillator (equation 4.10)

Parameters	Actual	Predicted	Difference	Error in %
Line 1: x^0	0	0.00	0.00	0
Line 1: x^1	3	3.00	-0.00	0
Line 2: x^0	0	0	0	0
Line 3: x^1	1	1	1	0

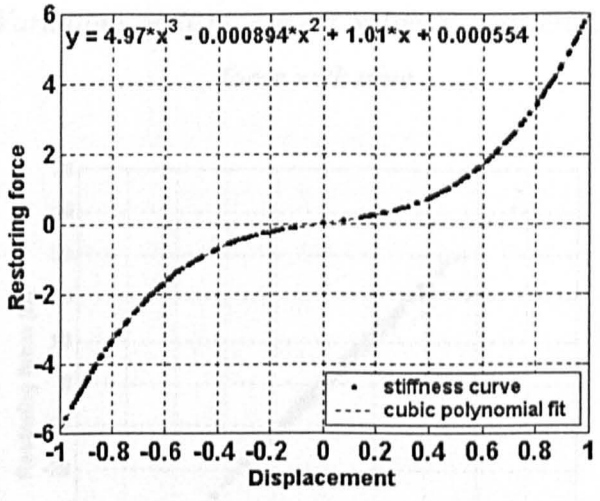

Figure 4.14: Restoring force surface and restoring force displacement curve for Duffing's equation (equation 4.11)

Table 4.3: Comparisons between actual and predicted parameters for a linear oscillator (equation 4.11)

Parameters	Actual	Predicted	Difference	Error in %
x^0	0	0.00	0.00	0
x^1	1	1.01	0.01	1
x^2	0	-0.00	-0.00	0
x^3	5	4.97	0.03	0.6

4.5.4 RESTORING FORCE DISPLACEMENT RELATIONS

As discussed in the above section, to plot a restoring force surface of the test specimen at a specific damage level, a sequence of triplets $(u_i, \dot{u}_i, f_i)$ is needed. To achieve this, velocity data are integrated and differentiated to obtain displacement, u, and acceleration (to calculate f using equation 4.6) respectively. Figure 4.15 shows a typical set of velocity, excitation force, displacement and acceleration data.

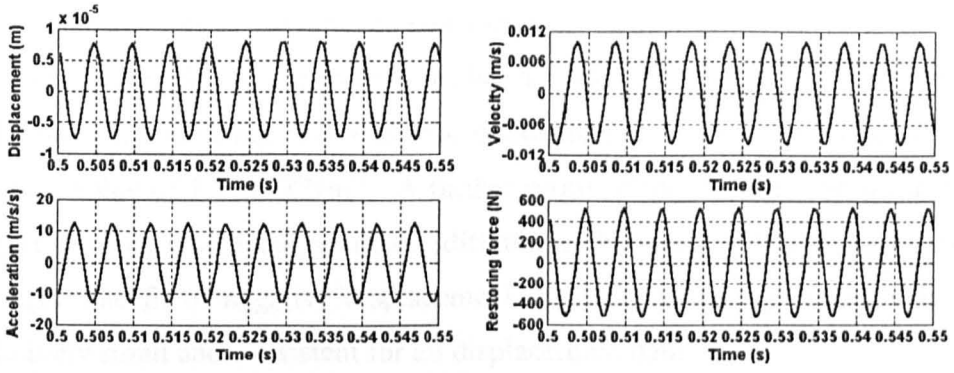

Figure 4.15: Variations of displacement, velocity, acceleration and restoring force with time

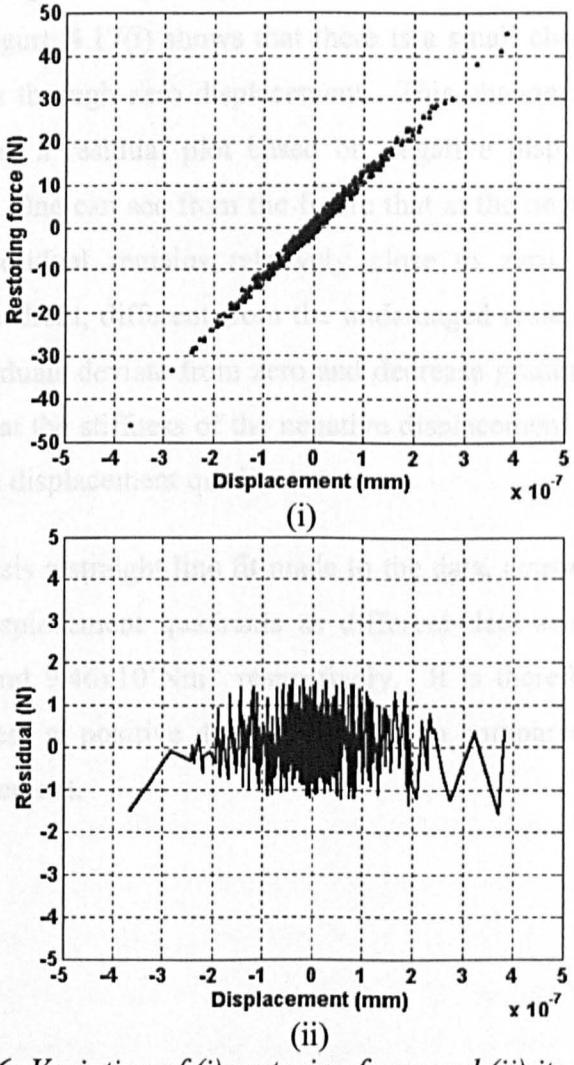

Figure 4.16: Variation of (i) restoring force and (ii) its residual with displacement for undamaged beam 4.

Restoring force surfaces were plotted for each of the beams tested at each of the damage levels considered. Figure 4.16(i) shows the restoring force

displacement curves for undamaged beam 4. One can clearly see that the undamaged reinforced concrete beam has a linear restoring force displacement relationship, indicating that stiffness is constant. A simple straight line fit gives a value of $1.17 \times 10^{8} Nm^{-1}$. A further proof of the linearity can be seen in figure 4.16(ii) where the residuals (differences between restoring force and a straight line fit of negative displacement data) is plotted. The residuals are relatively small and consistent for all displacement data.

Figure 4.17(i) shows a restoring force surface plot for beam 4 at damage level 20kN, i.e. a moderately damaged beam. It can be seen that although the restoring force displacement curve appears linear, a more careful examination of the data in figure 4.17(i) shows that there is a small change of stiffness as the beam passes through zero displacement. This change of stiffness can be better seen using a residual plot based on negative displacement data (see figure 4.17(ii)). One can see from the figure that at the negative displacement quadrant, the residual remains relatively close to zero. At the positive displacement quadrant, different from the undamaged residual plot (see figure 4.16(ii), the residuals deviate from zero and decrease gradually. This residual plot confirms that the stiffness of the negative displacement quadrant is higher than the positive displacement quadrant.

On this basis a straight line fit made to the data, considering the positive and negative displacement quadrants as different data sets, gives values of $8.87 \times 10^{7} Nm^{-1}$ and $9.46 \times 10^{7} Nm^{-1}$ respectively. It is therefore a reduction of 6.27% of stiffness at positive displacement when compared with stiffness at negative displacement.

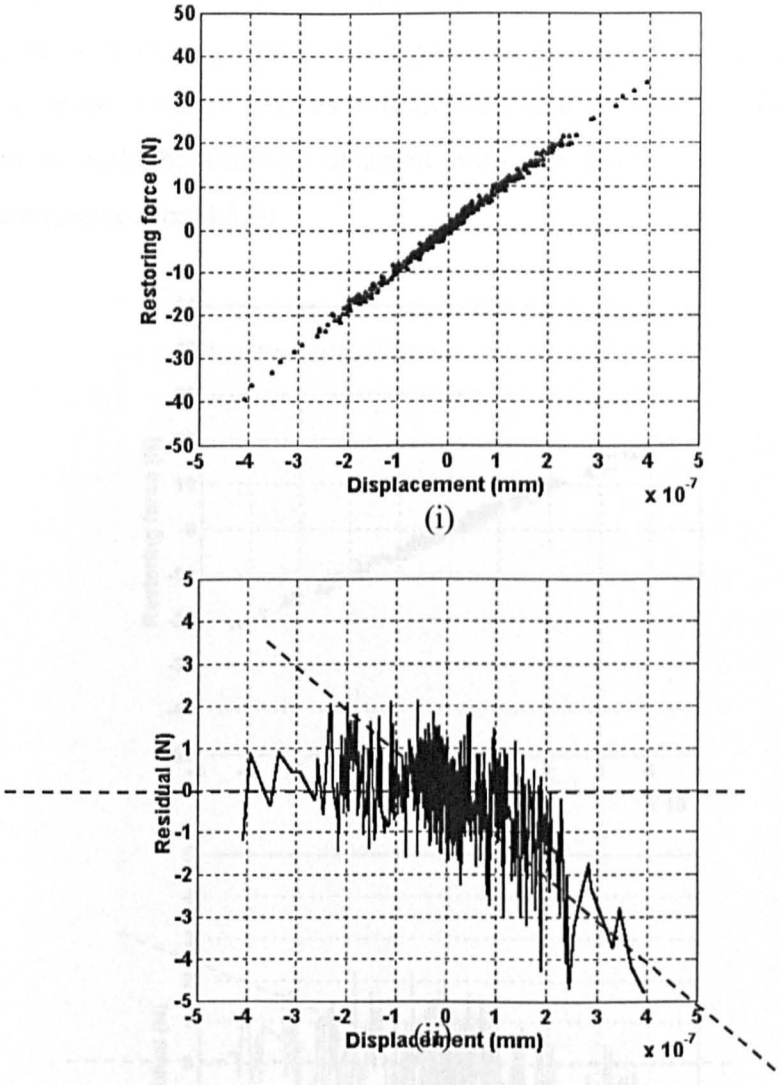

Figure 4.17: Variation of (i) restoring force and (ii) its residual with displacement for a moderately damaged beam.

Figure 4.18(i) shows a restoring force surface plot for beam 4 at damage level 42kN. At 42kN, the reinforced concrete beam is in a badly damaged state and the steel reinforcement has yielded (see static test result shown in figure 4.5). Similarly, a residual plot (see figure 4.18(ii)) shows clearly that that is a change of stiffness between positive and negative displacement. By comparing the magnitude of the figure with figure 4.17(ii), one could also see that the change of stiffness in the badly damaged case is less than a moderately damaged beam. It is also possible to split the restoring force surface into two sections and apply a simple straight line fit to them separately. A gradient of $4.78 \times 10^7 Nm^{-1}$ and $5.01 \times 10^7 Nm^{-1}$ is obtained for positive and negative displacement respectively. There is a stiffness reduction of 4.59% at positive

displacement. If the stiffness reduction ratio is considered as a measure of nonlinearity, there is a drop of nonlinearity in the vibration characteristic at the badly damaged state relative to a moderately damage state. This finding is in agreement with the findings obtained from the analysis using the softening gradient (see section 4.3.4).

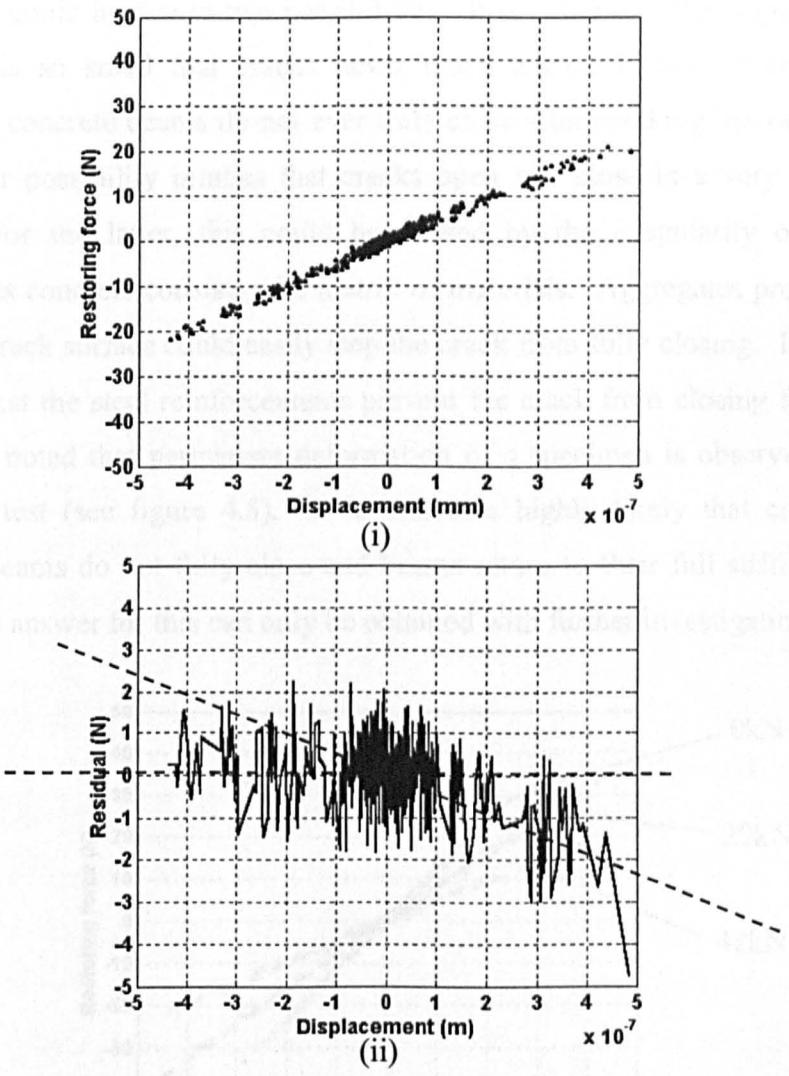

Figure 4.18: Variation of (i) restoring force and (ii) its residual with displacement for a badly damaged beam.

It is also possible to note from the restoring force surfaces that there is a general drop of overall stiffness values (see figure 4.19). In fact, by assuming a linear relationship for all cases, there is a drop as big as 41.8% of stiffness value from the undamaged state to the failed state (at 42kN). Another observation from figure 4.19 is that none of the restoring force displacement curves overlap each other at any part of the curve apart from at the origin. This

has an important implication. If, as suggested by researchers, the beam can be modelled using a bilinear crack model (see section 2.4.2.2) all stiffness values when a crack closes (at negative displacement) should be equal. As shown in figure 4.19, this is obviously not the case and therefore suggests that the bilinear model is insufficient to model cracked reinforced concrete beams.

This could be due to two possibilities. It is either that the amplitude of vibration is so small that cracks never reach a closed state or cracks in reinforced concrete beams do not ever truly close after cracking has occurred. The earlier possibility implies that cracks open and close in a very gradual manner. For the latter, this could be caused by the irregularity of crack surfaces, as concrete consists of a matrix of materials. Aggregates protruding from the crack surface could easily stop the crack from fully closing. It is also possible that the steel reinforcements prevent the crack from closing fully. It should be noted that permanent deformation of a specimen is observed from the static test (see figure 4.5). It is therefore highly likely that cracks in concrete beams do not fully close and beams return to their full stiffness. A conclusive answer for this can only be obtained with further investigations.

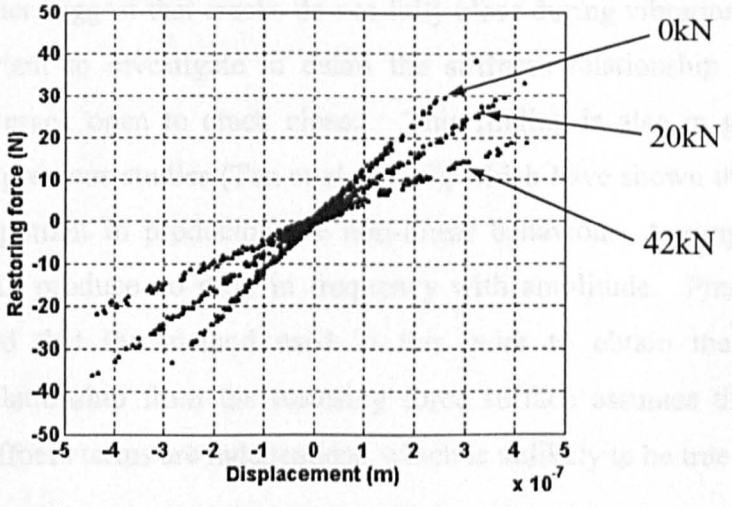

Figure 4.19: Variations of restoring force with displacement for different damage levels

4.6 CONCLUSIONS

The experimental work presented here has confirmed the non-linear behaviour observed during previous experimental studies (Eccles 1999 and Tan et al., 2001) and has shown that the non-linear behaviour has the characteristics of a softening spring. The study of the softening gradient has shown that the level of non-linearity increases with damage up to a certain level at moderate damage state. Above this the softening gradient reduces to a lower level, remaining constant with further damage. In a qualitative sense, this characteristic is in agreement with the findings obtained from the restoring force surface analysis.

Using the restoring force surface method it has been possible to obtain experimental force deflection curves to model the non-linear vibration behaviour of the damaged reinforced concrete beams. Although each restoring force displacement curve from each damage level appears to behave in a bilinear fashion, the overall drop of stiffness with increasing damage level (see figure 4.19) confirms that a bilinear crack model would not be sufficient to replicate the observed vibrating cracked reinforced concrete beams' behaviour. The results further suggest that cracks do not fully close during vibration. It is therefore important to investigate in detail the stiffness relationship of the transition from crack open to crack closed. This finding is also in general agreement with previous studies (Tan et al., 2000), which have shown that this transition is important in producing the non-linear behaviour. A simple bi-linear model will produce no drop in frequency with amplitude. Finally, it should be noted that the method used in this work to obtain the force displacement relationship from the restoring force surface assumes that the damping and stiffness terms are independent, which is unlikely to be true.

An empirical model that recreates the observed experimental behaviour is presented in the next chapter.

CHAPTER 5

NUMERICAL STUDIES

5.1 INTRODUCTION

The work presented so far has demonstrated that there is a consistent pattern of nonlinear behaviour in the vibration of cracked reinforced concrete beams. In this chapter, an empirical model that recreates the observed nonlinear dynamic properties of cracked reinforced concrete beams is presented. The model, in the form of a spring, focuses on the modelling of the cracks themselves. Any stiffness reduction due to the crack is represented by adjusting the spring stiffness at the spring position. The creation of the empirical stiffness model should provide a better understanding of the nonlinear behaviour exhibited in the laboratory tests.

This chapter comprises two main sections. Following this introductory section, a selection of phenomenological models (i.e. models that seek to replicate the observed phenomena rather than the physics of the system), suggested by a number of researchers are discussed and analysed. Results are compared between them and also with the observed experimental behaviour. The most satisfactory model is then selected as the basis of an empirical model. The next section involves deriving an empirical model for the vibration characteristics of the reinforced concrete beams described in chapter three. Applications and limitations of the empirical model are then discussed.

5.2 PHENOMENOLOGICAL STIFFNESS MODELS

As noted in the literature review in chapter 2, most papers discussing the vibration of cracked beams consider the case of a single crack in a uniform, homogenous material. However, these crack models are not applicable to the case of a reinforced concrete beam with multiple distributed cracks such as those used in the experiment. This is not only because there is more than one crack, but also because the exact location and severity of the cracks is extremely difficult to determine due to microcracking, which occurs between the coarse aggregate and cement paste. In addition, the crack behaviour is complicated by the presence of the reinforcement and aggregate interlock. The reinforcement bridges the crack and carries tensile and, by dowel action, shear loads. Aggregate interlock generates friction as the crack surfaces separate in bending and, although tensile forces cannot be resisted without steel, this provides a mechanism to transfer shear across the crack. The accurate modelling of cracks in concrete structures is therefore not a straightforward process and a simplified modal approach has been used here to model the experimental behaviour phenomenologically.

5.2.1 ASSUMPTIONS

The equivalent modal stiffness used in the numerical modelling can be found, assuming the Euler Bernoulli beam theory, from:

$$k = \int_0^L EI(\phi''(x))^2 dx \tag{5.1}$$

There are two more assumptions implicit in using this expression, firstly that there is a uniform reduction in the second moment of area along the length of the beam and secondly that the mode shape does not change with damage. Previous experiments (Das et al, 1996) have shown that, for the reinforced concrete beams discussed here, there is very little change in mode shape with damage and so the second assumption is valid. This also suggests that,

although the first assumption clearly does not hold, the loss of accuracy is acceptable.

5.2.2 METHODOLOGY

With the dynamic response of a cracked reinforced concrete beam modelled using a modal approach, each mode can be described as a SDOF system with non-linear stiffness:

$$m\ddot{u} + c\dot{u} + k(u)u = p(t) \tag{5.2}$$

where m and c are the mass and damping for the system, $p(t)$ is the excitation force and $k(u)$ is a stiffness model which varies across the vibration cycle. The SDOF equations of motion can be simplified by assuming a unit mass (equivalent to mass normalised mode shapes) and expressing the modal damping in terms of the damping ratio, ξ:

$$\ddot{u} + 2\omega_n \xi \dot{u} + \frac{k(u)}{m}u = \frac{p}{m}\cos(t) \tag{5.3}$$

where ω_n is the instantaneous natural frequency of the system at $u=0$. As the system is nonlinear, it does not possess a specific single valued natural frequency. Instead, the natural frequency varies with amplitude and is normally described as an instantaneous natural frequency. In order to simplify the model, the influence of changes in damping on instantaneous natural frequency was ignored.

The equations of motion were then solved numerically using Matlab (*ode45* for non-stiff differential equation, medium-order method). *ode45* is a built-in Matlab routine that uses 4^{th}-order Runge Kutta method to solve nonlinear differential equations numerically. The Runge Kutta method is based on the truncation of Taylor's series technique and an explanation of it

can be found in appendix B. Initial conditions of zero displacement and unit velocity were assumed and the simulations were run until a steady state response was reached. From these, time histories and phase portraits for different states of damage were obtained.

The variation of response with frequency of excitation for each model was obtained by increasing the excitation frequency in steps of $0.005\omega_n$ and calculating the response at each increment. This process was then repeated with varied excitation force to determine the influence of response magnitude on the natural frequency.

The following is a summary of the simulations' routine:

1) Calculate instantaneous frequency, ω_n, at $u=0$ using equation 2.3.

2) Define excitation amplitude, P.

3) Define excitation frequency, $\omega = 0.6\omega_n$.

4) Run *ode45* with time span = $\frac{10}{\pi\omega_n}$ at intervals of $\frac{1}{800\pi\omega_n}$.

5) Split simulated time history into six equal parts, and calculate the difference between maximum and minimum amplitude of time history for each of the last four parts. (Time histories for the first two parts are ignored to ensure the system has reached steady state.)

6) Find and save the mean value of the amplitude differences calculated.

7) Increase ω by $0.005\omega_n$ and go back to step 3 unless ω is greater or equal to $1.1\omega_n$.

8) Increase P and go back to step 2 until desired maximum P is reached (varies with models).

5.2.3 BI-LINEAR CRACK MODEL

A simple bilinear stiffness model is first considered. As stated in the literature review in section 2.4.2, this is by far the most popular approach to model cracking. In this model the stiffness was defined for two states of the crack, open and closed. This model assumes that the crack instantaneously opens when the displacement of the beam creates tensile forces in the crack region, leading to a reduced stiffness value for negative displacements:

$$k = k_i\left(1+\frac{(\mu-1)}{2}\left(\frac{u}{|u|}+1\right)\right) \tag{5.4}$$

where k_i is the stiffness of the uncracked beam and μk_i is the stiffness of the system with an open crack.

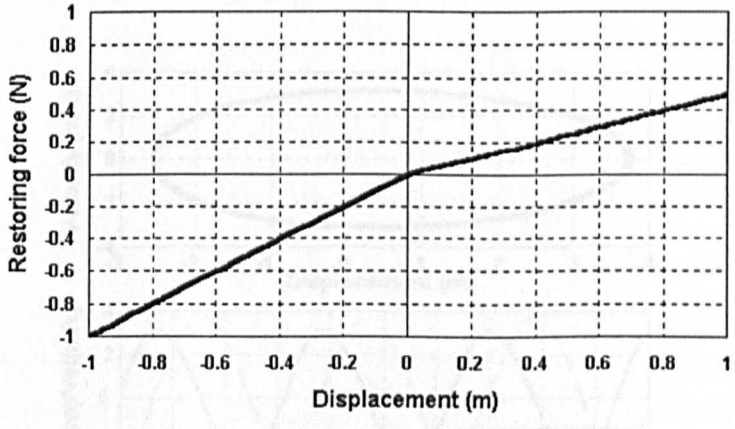

Figure 5.1: Variation of restoring force with displacement for bilinear model

Figure 5.1 is a plot of the variation of the restoring force against displacement for the bilinear model. μ is assumed to be *0.5* in this case, showing a severe damage level. In this figure, the gradient of the line is the stiffness of the model and the bilinear nature of the model's stiffness can clearly be seen as the displacement of the model passes from positive to negative. A curve showing the variation of stiffness with displacement, for the

specific damage level, is shown in figure 5.2. Again, a clear bilinear nature is shown as the stiffness ratio, μ, changes instantaneously from the open cracked state to undamaged state at zero displacement.

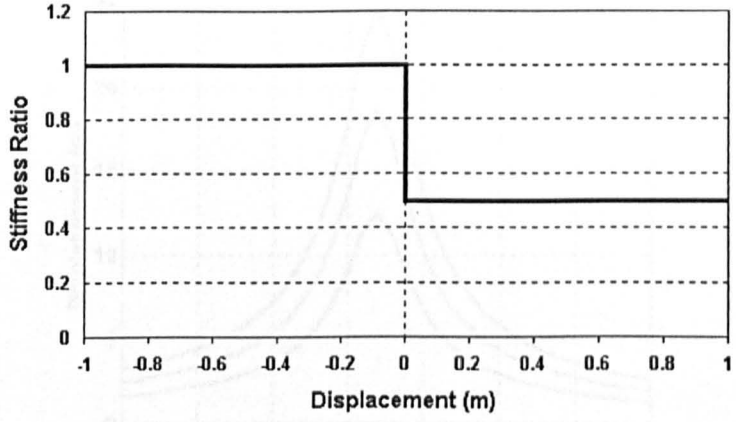

Figure 5.2: Variation of stiffness ratio with displacement for bilinear model

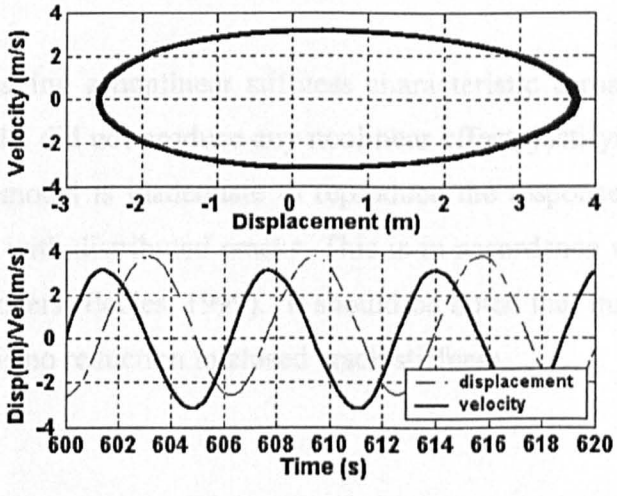

Figure 5.3: Simulated phase plane and time history for bilinear model

Several runs of the model were performed and the typical time history and phase portrait can be seen in figure 5.3. The phase portrait shows a significant asymmetry, which is as expected for a system with a difference in stiffness between each half of the vibration cycle. A plot of amplitude against excitation

frequencies can be found in figure 5.4. The figure shows that the natural frequency of the bi-linear model is independent of excitation level, similar to a linear model.

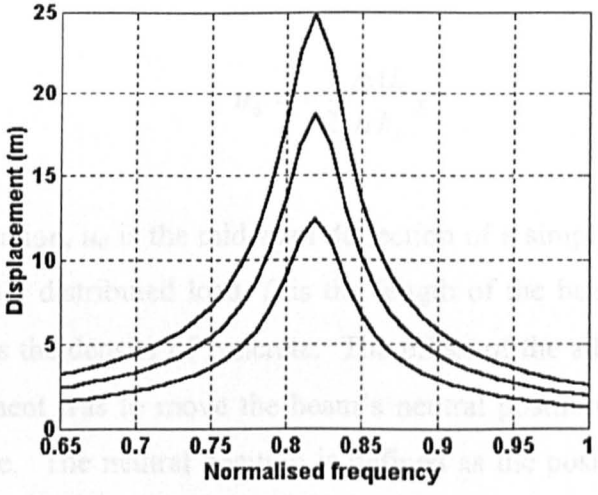

Figure 5.4: Variation of response with normalised frequency for bilinear model

Despite having a nonlinear stiffness characteristic across the oscillation cycle, this model did not produce any nonlinear effect, justifying that a simple bilinear crack model is inadequate to reproduce the response of a reinforced concrete beam with distributed cracks. This is in accordance with the findings of other researchers (Eccles, 1999). It should be noted that this bilinear model assumes there is no reduction in closed crack stiffness.

5.2.4 BI-LINEAR CRACK MODEL WITH ADDITION OF SELF-WEIGHT

The simple bi-linear crack model is often criticised as it neglects the self weight of the beam. Hence, the second model includes the effect of the beam self weight, ρAL:

$$k = k_i\left(1+\frac{(\mu-1)}{2}\left(\frac{(u+u_0)}{|u+u_0|}+1\right)\right) \tag{5.5}$$

where:

$$u_0 = -\frac{1}{2}\frac{\rho AL}{\mu k_i}g \tag{5.6}$$

In the equation, u_0 is the mid-span deflection of a simply supported beam with a uniformly distributed load, L is the length of the beam, A is the cross section and ρ is the density of concrete. The effect of the addition of the self-weight component was to move the beam's neutral position into the cracked stiffness regime. The neutral position is defined as the position to which the beam tends as the oscillation decays, i.e. the equilibrium position.

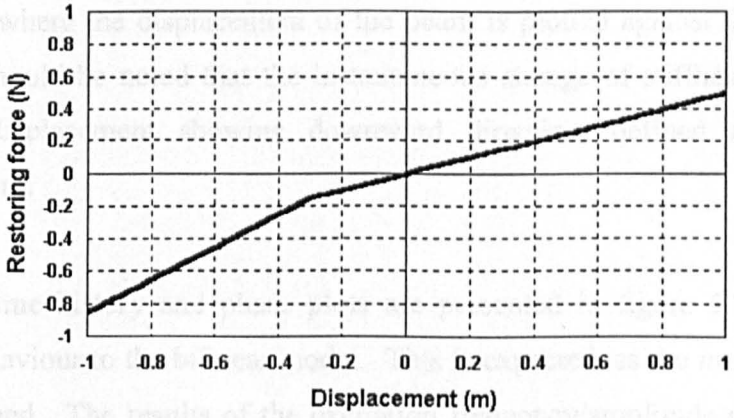

Figure 5.5: Variation of restoring force with displacement for bilinear with self-weight model

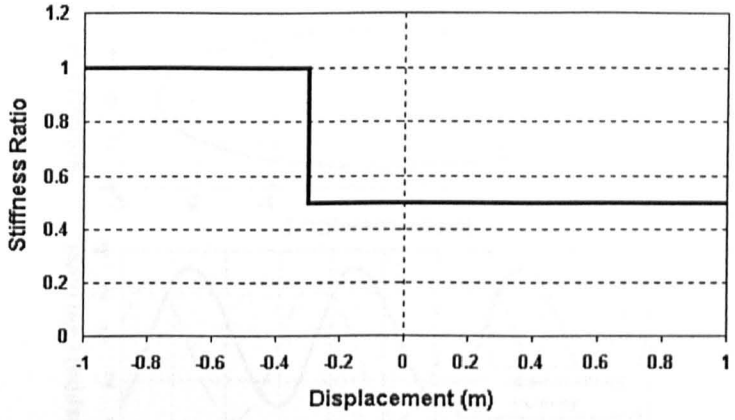

Figure 5.6: Variation of μ with displacement for bilinear with self-weight model

Figure 5.5 presents the restoring force/displacement relationship for this model for $\mu = 0.5$. The inclusion of self-weight has shifted the instantaneous change of stiffness to a location other than the origin. This can be seen in figure 5.6 where the displacement of the beam is plotted against the stiffness ratio. It should be noted that the instantaneous change of stiffness occurs at negative displacement showing downward direction, defined as positive displacement.

The time history and phase plots are presented in figure 5.7, showing similar behaviour to the bilinear model. This is expected, as the model has not been changed. The results of the excitation frequency/amplitude relationship show that when a self-weight is included in the model there is an initial hardening behaviour. This is typified by an increase in natural frequency with amplitude, although for a larger amplitude response the natural frequency remains almost constant (figure 5.8). This is different from the observed experimental behaviour.

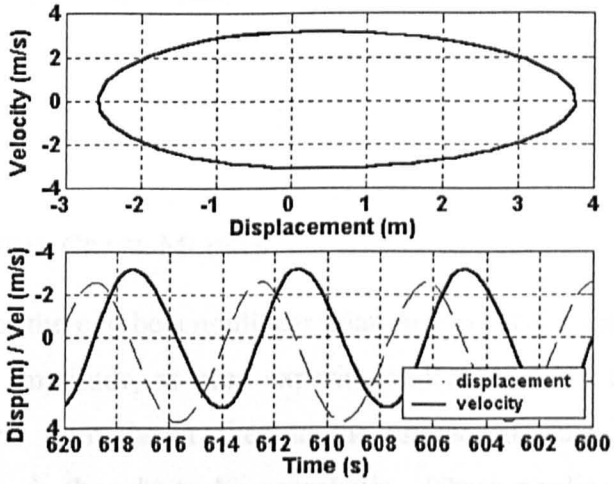

Figure 5.7: Simulated phase plane and time history for bilinear with self-weight model

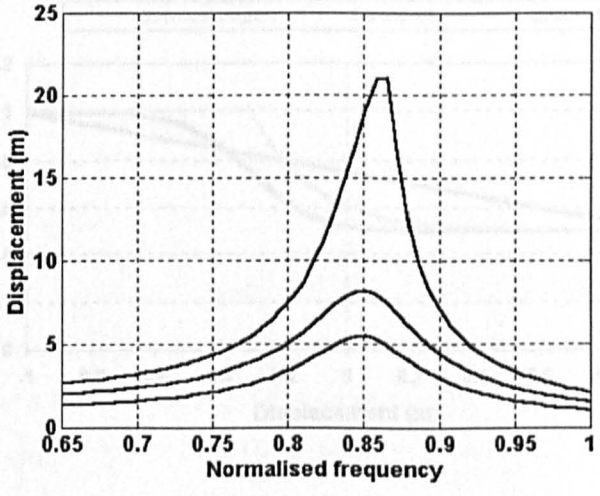

Figure 5.8: Variation of response with normalised frequency for bilinear with self-weight model

In conclusion, the nonlinear behaviour seen experimentally and in the reviewed literature cannot be recreated using the standard bilinear models. This therefore challenges the assumption that the crack opens instantaneously as it moves from positive to negative displacement regions. The suggestion of the possible existence of a transition zone between the open and closed crack

states, by Brandon and Mathias (1995) as discussed in section 2.4.2, is reinforced here.

5.2.5 NONLINEAR CRACK MODELS

In order for there to be a nonlinear relationship between the frequency and the oscillation amplitude, as seen experimentally and from the literature, an abrupt transition from the cracked to the uncracked state, assumed in the bilinear models, is thought to be unrealistic. Three nonlinear crack models suggested by different researchers (Eccles et. al. 1999, Eccles, 1999 and Cheng et. al., 1999) were studied numerically and the results were compared with the experimental behaviour.

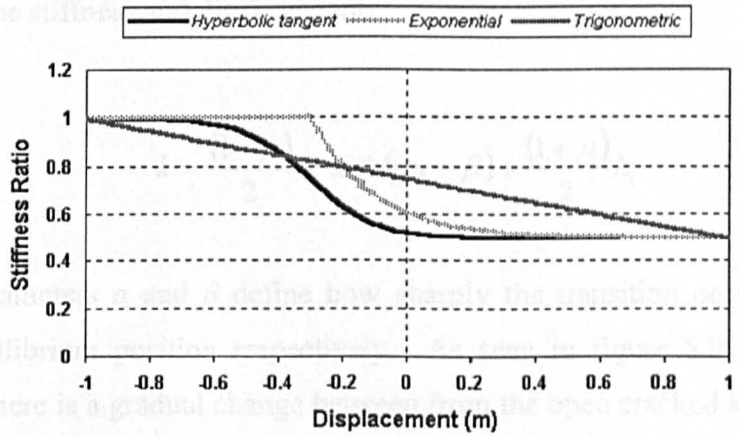

Figure 5.9: Variation of μ with displacement for nonlinear models

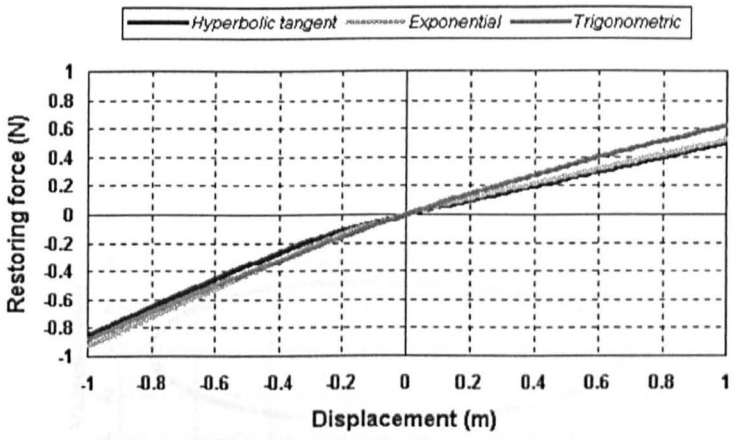

Figure 5.10: Variation of restoring force with displacement for nonlinear models

The first nonlinear crack model assumes a hyperbolic tangent relationship between the stiffness and displacement:

$$k = \frac{(1-\mu)}{2} k_i \tanh(\alpha u + \beta) + \frac{(1+\mu)}{2} k_i \tag{5.7}$$

where parameters α and β define how sharply the transition occurs and the static equilibrium position respectively. As seen in figure 5.9, this model suggests there is a gradual change between from the open cracked state and the closed crack state. Figure 5.10 shows the restoring force/displacement relationship of this model. From this figure, it can be seen that in a cracked beam vibration cycle, the stiffness of the beam changes smoothly from the open cracked state to the closed cracked state and then again returns smoothly to the open cracked state.

The time history and phase plane of the model are shown in figure 5.11. From the figure, it can be seen that the asymmetry is less marked compared to the phase plot, shown in figure 5.3 and 5.7 for bilinear models. The response amplitude/excitation frequency relationship is shown in fig 5.12. From this, a marked softening spring behaviour can be clearly seen, which is in keeping

with previous experimental results discussed in the literature review. This shows that, as compared with the bilinear models, the nonlinear models clearly have an improved qualitative agreement.

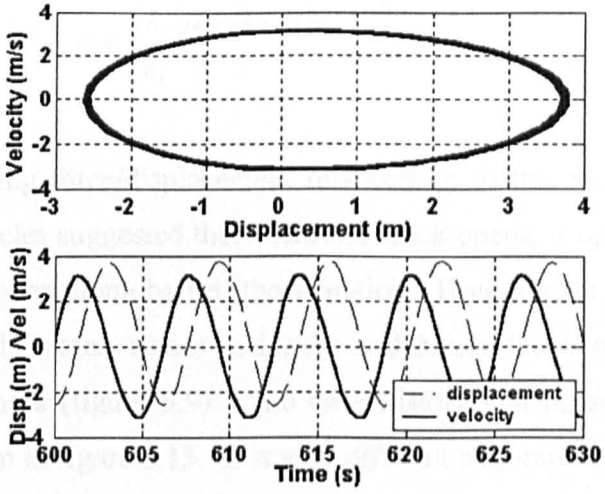

Figure 5.11: Simulated phase plane and time history for hyperbolic tangent model, α = -5, β =1.5

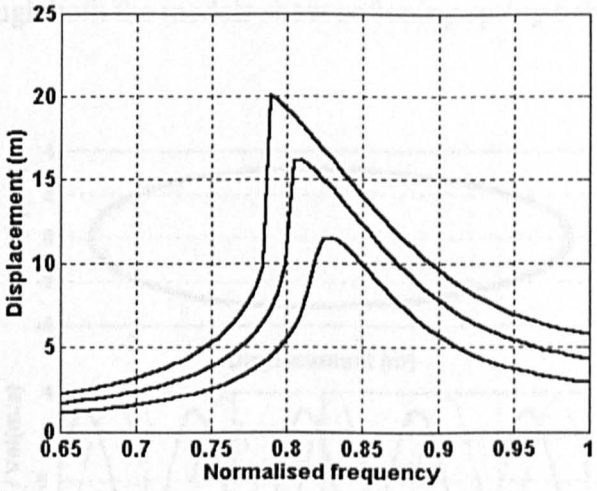

Figure 5.12: Variation of response with normalised frequency for hyperbolic tangent model, α = -5, β =1.5

An alternative model, proposed by Eccles (1999), uses an exponential relationship to describe the change of stiffness, which gives a sudden closure of the crack but a gradual opening:

$$k = \begin{cases} k_i\left(\mu + (1-\mu)e^{\alpha(u+\beta(1-\mu))}\right) & u \geq \beta \\ k_i & u < \beta \end{cases} \tag{5.8}$$

The restoring force/displacement relationship of this model is shown in figure 5.10. Eccles suggested that when the crack opens, it opens gradually as the crack tears open along half of the vibration. However, in the other half of the vibration, the crack closes suddenly and hence the beam maintains its uncracked stiffness (figure 5.9). The time history and phase portrait of the model are shown in figure 5.13. It is very difficult to compare the crack model with the hyperbolic tangent model simply by looking at the time history and phase portrait, as both the models have similar type of nonlinearity. However, if the two models are compared by looking at the response amplitude/excitation frequency relationship, the author found that the hyperbolic tangent model (figure 5.12) is relatively more sensitive than the exponential model (figure 5.14), even though both the models show softening spring behaviour.

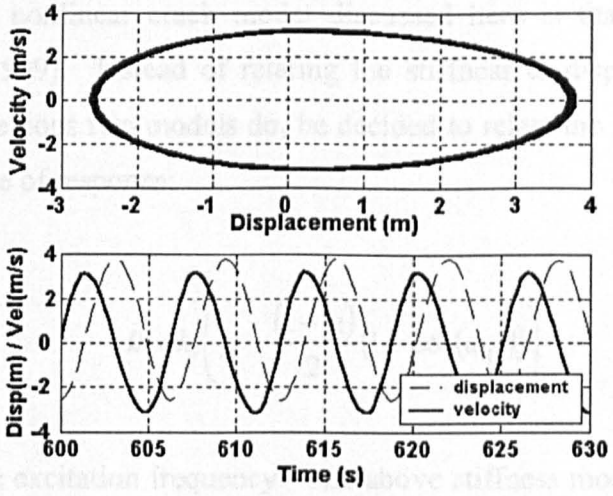

Figure 5.13: Simulated phase plane and time history for exponential model, α = -10, β =0.3

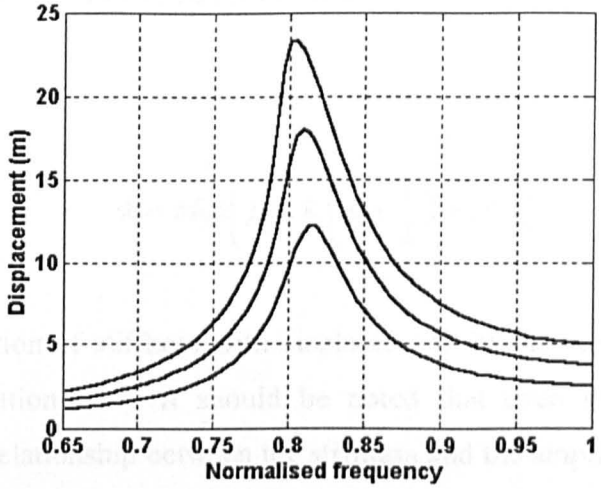

Figure 5.14: Variation of response with normalised frequency for exponential model, $\alpha = -10$, $\beta = 0.3$

It should be noted that both of the nonlinear models have considered the effect of self-weight, as indicated by the changes of stiffness occurring when the displacement is negative, i.e. $\beta>0$. This is a very important point as the nonlinear behaviour of both the models is influenced by the location of the transition. For both models, softening spring behaviour was seen when $\beta>0$, but when $\beta<0$, hardening spring behaviour was seen.

The third nonlinear crack model discussed here is that introduced by Cheng et al (1999). Instead of relating the stiffness to displacement of the beam as the previous two models do, he decided to relate the stiffness directly to the amplitude of response:

$$k = k_i\left(\mu + \frac{(1-\mu)}{2}(1+\cos(\omega_1 t))\right) \tag{5.9}$$

where ω_1 is the excitation frequency. The above stiffness model assumes that the crack is completely closed when $\omega_1 = 2l\pi$ ($l = 1,2,3...$), and completely open when $\omega_1 t = (2l-1)\pi$ ($l = 1,2,3...$). Otherwise the crack is in a state of partial closure. In order to be comparable with the other models discussed in

this chapter, Cheng's model has been recast in terms of u, the displacement of the beam:

$$k = Max\left(\mu k_i, k_i\left(\mu + \frac{1}{2}\left(1-\mu^2\right)\right)\right) \tag{5.10}$$

The variation of stiffness with displacement for the model considered is shown in equation 5.9. It should be noted that even though there is a trigonometric relationship between the stiffness and the amplitude of response, the stiffness changes linearly with displacement. The time history and phase plane (figure 5.15) suggests that due to this gradual change of stiffness, the asymmetry is less marked compared to the other two models. The response amplitude/excitation frequency relationship (figure 5.16) shows that there is a very slight softening behaviour.

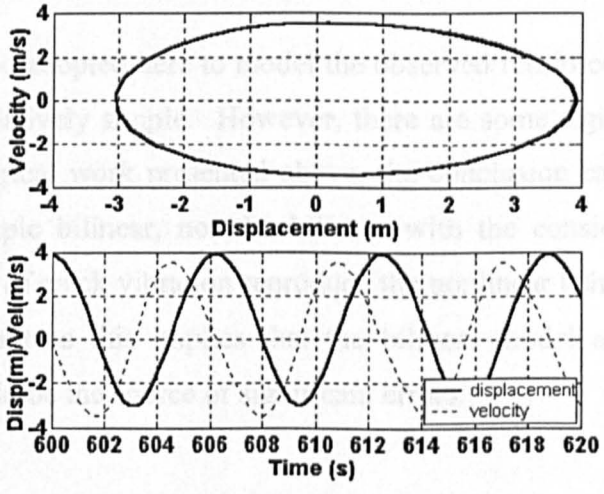

Figure 5.15: Simulated phase plane and time history for trigonometric model

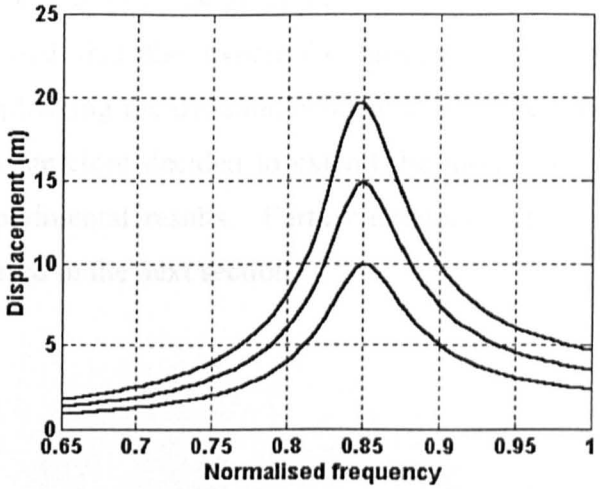

Figure 5.16: Variation of response with normalised frequency for trigonometric model

5.2.6 DISCUSSIONS

The method adopted here to model the observed reinforced cracked beam behaviour is relatively simple. However, there are some significant findings. From the numerical work presented above, the conclusion can be drawn that neither the simple bilinear, nor the bilinear with the consideration of self-weight, models of crack vibration reproduce the nonlinear behaviour correctly. This is important as this implies that the bilinear model adopted by most researchers could be the source of significant errors.

It has also been seen that, in order to model the observed behaviour accurately, it is necessary to consider the transition of the crack from open to closed in more detail. The models considered here do reproduce this behaviour if appropriate parameters are used. It could be questioned that in order to produce this softening spring behaviour, a Duffing's equation with appropriate parameters ($\alpha > 0, \beta < 0$) could be used. However, if a softening Duffing's equation were adopted as a model of cracked vibration, it would show an unrealistic stiffness/displacement relationship in quadratic form.

From the preliminary results of the phenomenological modelling, it has been demonstrated that the hyperbolic tangent model shows the greatest potential for replicating the dynamic behaviour of cracked reinforced concrete beams. It was therefore decided to extend the model empirically, i.e. based directly on experimental results. Further details of the empirical modelling work are discussed in the next section.

5.3 HYPERBOLIC TANGENT EMPIRICAL MODEL

5.3.1 FORCE-DISPLACEMENT RELATIONSHIP

As presented previously, it has been shown that the hyperbolic tangent model does indeed yield a system with softening behaviour, which closely resembles that observed in practice provided appropriate values are selected for these key parameters. However, in order to verify this model it is not enough to simply modify the parameters until the predicted behaviour matches the observed behaviour. More accurately, having proposed a form for the model, it is necessary to obtain the required parameters from the experimental data using some form of curve fitting procedure. The first step in doing this is to integrate equation 5.7 to obtain a force displacement relationship:

$$p = \frac{(1-\mu)}{2}\frac{k_i}{\alpha}\ln(\cosh(\alpha u + \beta)) + \frac{(1+\mu)}{2}k_i u \qquad (5.11)$$

It is worth noting that the force-displacement relationship of the hyperbolic tangent model is actually defined by a natural logarithmic function. Having derived equation 5.11, it is now possible to reproduce the observed restoring force displacement relationship from the experimental studies, and hence, by utilising a curve-fitting routine, extract all values of the parameters.

5.3.2 EFFECTS OF VARIOUS PARAMETERS

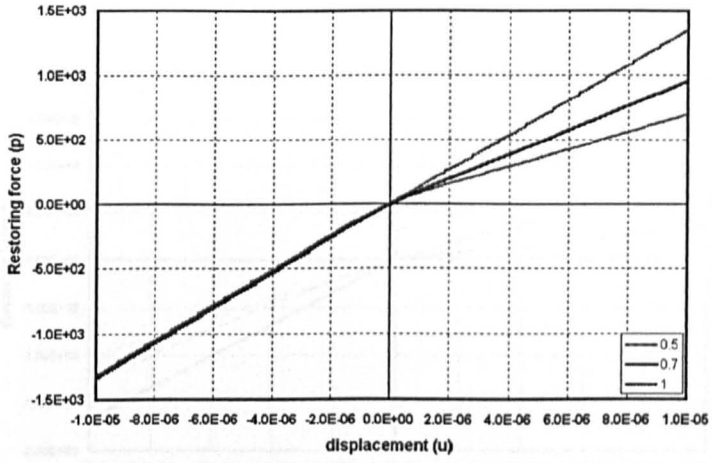

Figure 5.17: Influence of parameter μ on force displacement relationship, $\alpha=8.64\text{x}10^5$

Before proceeding with curve-fitting, it is worth investigating the influence of three parameters, namely μ, α and β. As discussed before, μ is the stiffness ratio of the system and defined as the ratio of open-crack stiffness and closed-crack stiffness. μ is therefore always smaller than unity. Increasing μ reduces the stiffness of the system during the "crack open" phase but does not change the stiffness during the "crack closed" phase (figure 5.17). In other words, μ is a measure used in the empirical model to define the damage level of the system. Varying μ alone therefore, would not be sufficient to replicate the non-linearity observed in the tests.

The parameter α represents the sharpness of the transition and for small values of α, the transition is so gradual that cracks effectively remain half open and the result is an almost linear system with reduced stiffness (figure 5.18). For large values of α, cracks open and close sharply producing a bi-linear system, which again does not replicate the observed non-linearity. However, for intermediate values of α, cracks partly open and close producing a non-linear system with constantly varying stiffness. This shows that stiffness is

reduced in both cracked and uncracked limbs, a system that will replicate both the non-linearity and the stiffness reduction observed in the tests.

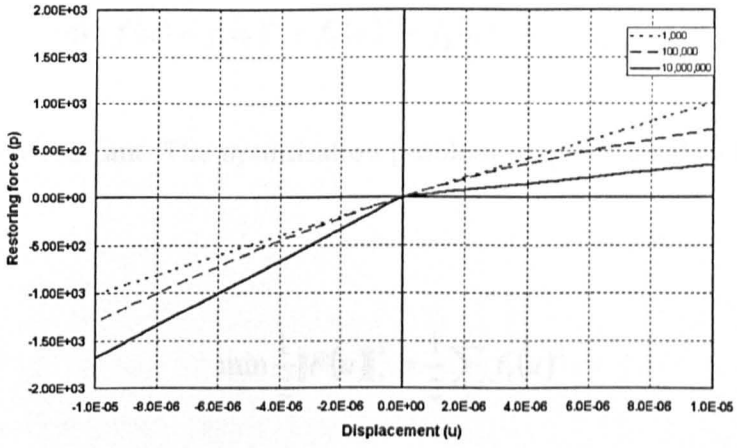

Figure 5.18: Influence of parameter α on force displacement relationship, μ = 0.5

The parameter β defines the static equilibrium position of the vibration. The parameter is predominantly used for the consideration of self-weight and therefore it would only be appropriate to define β as a value greater than zero. It has been discussed in the preliminary study (section 5.2.5) that, provided parameter β is always greater than zero, parameter β does not have a significant effect on simulated nonlinear behaviour. To simplify curve fitting, a value of β was assumed that corresponded to the self-weight deflection of the beam.

5.3.3 NONLINEAR CURVE-FITTING

In order to use equation 5.11 to simulate the behaviour of the cracked reinforced concrete beams the model parameters based on experimental results are needed. These can be obtained by performing a non-linear curve fit to the force displacement data obtained from the experimental restoring force surfaces (figure 4.18). The nonlinear curve-fitting routine adopted here is based on Matlab optimisation toolbox's routine *lsqnonlin*. The routine uses the

least square method to solve a nonlinear curve-fitting problem iteratively in a form:

$$\min_u f(u) = f_1(u)^2 + f_2(u)^2 + f_3(u)^2 + \ldots + f_m(u)^2 + L \qquad (5.12)$$

where L is a constant. The optimisation problem may be stated as least square sense:

$$\min_u \frac{1}{2}\|F(u)\|_2^2 = \frac{1}{2}\sum_i f_i(u)^2 \qquad (5.13)$$

To simplify the curve fitting a value of β was assumed that corresponded to the self-weight deflection of the beam and the value of k_i was fixed as the measured undamaged stiffness of the beam. There were, therefore, only two parameters left to fit, i.e. α and μ, for each damage level. A typical set of curve fitting results can be seen in figure 5.19. It should be noted that there is a reduction in k on both sides of the equilibrium point.

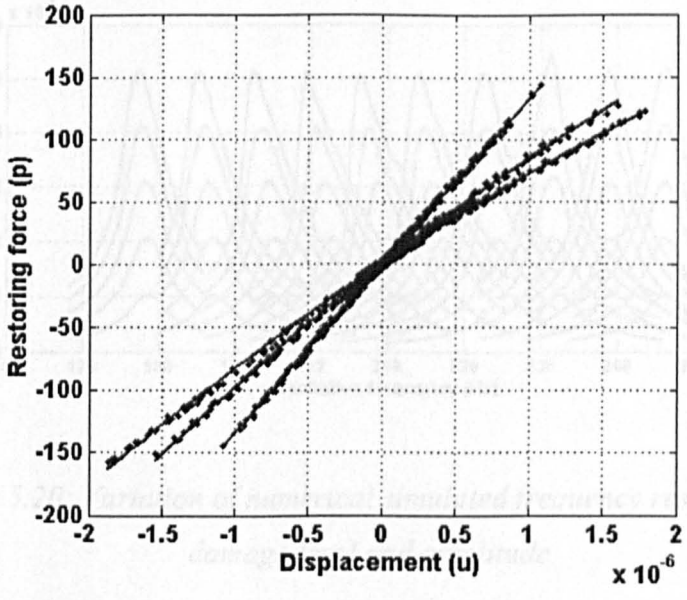

Figure 5.19: Typical curve fit to obtain parameters α and μ

5.3.4 NUMERICAL SIMULATIONS

Having obtained parameters α and μ from the curve fit for each damage level of beam 4, Matlab was then used to simulate the response of the system using the *ode45* routine to solve the SDOF equation of motion, as shown in equation 5.2 and 5.7. Detailed procedures of the methodology can be found in section 5.2.2. The results were then used to recreate the frequency response curves for the system for different amplitudes of excitation and different damage conditions, as shown in figure 5.20.

Simulated results from figure 5.20 clearly show that the hyperbolic tangent model, with empirical coefficients, replicates the observed experimental behaviour. The model not only replicated the drop in natural frequency but also the observed softening behaviour from the laboratory tests. With the simulated frequency response for each damage level obtained, it is then possible to plot a simulated variation of nonlinearity with damage level. The degree of nonlinearity, as shown in the test results, is defined by softening gradient whereas damage level is defined by stiffness ratio. This is shown in figure 5.21.

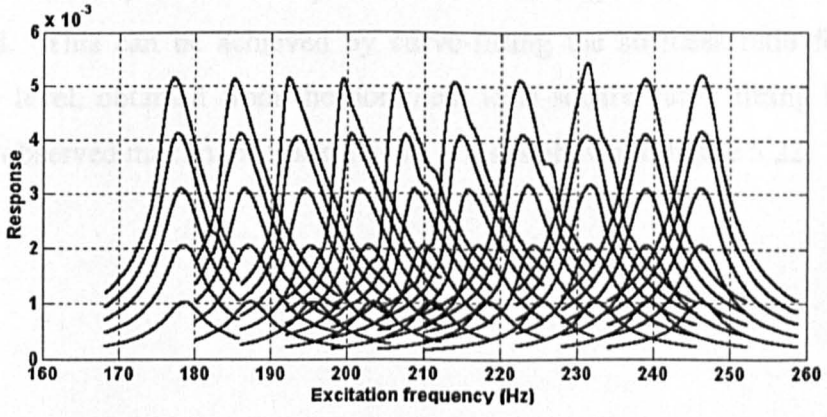

Figure 5.20: Variation of numerical simulated frequency response with damage level and amplitude

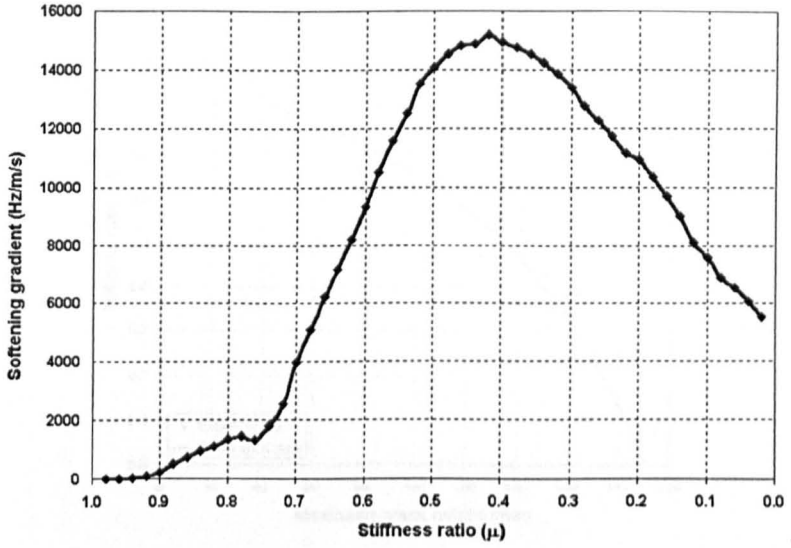

Figure 5.21: Simulated variation of non-linearity with stiffness ratio, μ.

From figure 5.21, it can be seen that the change of nonlinearity of the simulated results has a very similar trend to those observed in the tests (see figure 4.11), i.e. a gradual increase followed by a decrease. However, as damage levels were defined differently in experiments and simulations, it is not possible to compare the two directly. In order to compare the experimental and simulated results, a relationship between crack height and stiffness ratio is required. This can be achieved by curve-fitting the stiffness ratio for each damage level, obtained from the nonlinear least-square curve fitting routine, and the observed maximum crack height. This is shown in figure 5.22.

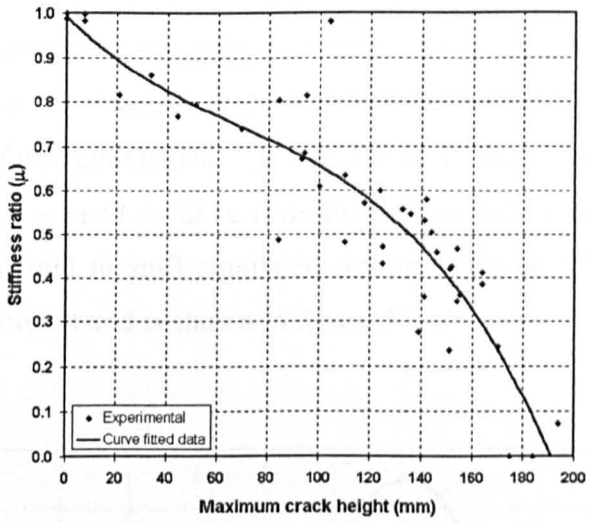

Figure 5.22: Variation of stiffness ratio, μ, with observed maximum crack height.

Each stiffness ratio value, μ, can then be directly related to a physical damage level. A relationship between softening gradient and maximum crack height can then be obtained and compared directly with experimental results, as shown in figure 5.23.

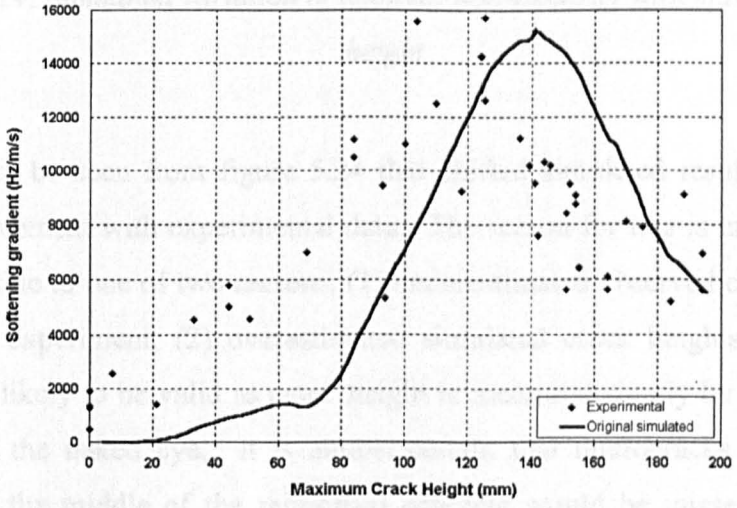

Figure 5.23: Simulated variation of non-linearity with maximum crack height.

From figure 5.23, it can be seen that although the simulated softening gradient with damage relationship showed a similar trend to the experimental behaviour, it did not match entirely with the test results. The reason for this has not been fully understood. It can be seen from figure 5.23 that the empirical model seemed to have consistently overestimated maximum crack heights. An attempt to shift simulated results in figure 5.23 by an arbitrary constant is performed and is shown in figure 5.24.

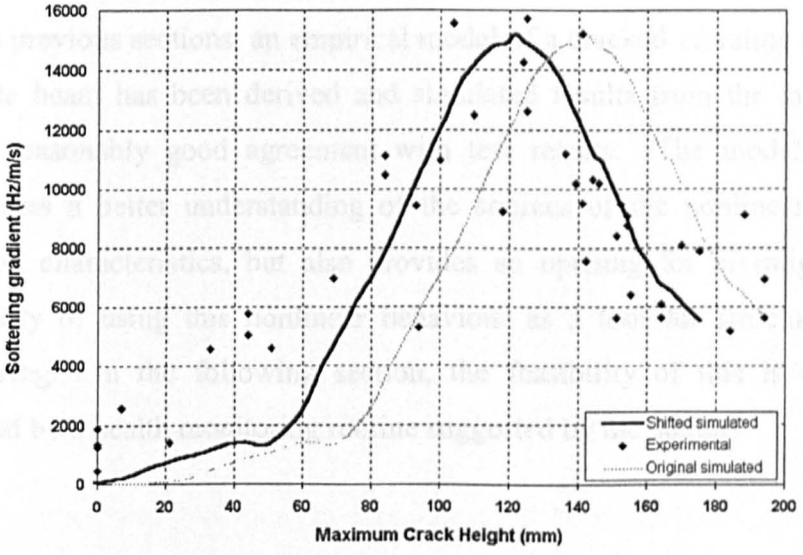

Figure 5.24: Simulated variation of (shifted) non-linearity with maximum crack height

It can be seen from figure 5.24 that shifted simulated results display a better agreement with experimental data. The reason for this is unknown, but could be due to one of two reasons, (1) underestimated observed crack heights from the experiment; (2) overestimated simulated crack heights. The first reason is likely to be valid as crack height is measured simply by the use of a ruler and the naked eye. It is almost certain that microcracks and unseen cracks in the middle of the reinforced concrete would be missed using this method. However, the extent of underestimation would not be as large as that seen in figure 5.24. The second reason might also be valid as the simulated crack height was obtained using a curve fitting routine with μ, which itself is

obtained using a nonlinear curve fitting routine. It is therefore likely that the accuracy of the simulated crack heights has been compromised in some part in the numerical process. It is, however, more likely that both reasons have contributed some part to the error.

5.4 POSSIBLE HEALTH MONITORING TOOL

In previous sections, an empirical model of a cracked vibrating reinforced concrete beam has been derived and simulated results from the model have shown reasonably good agreement with test results. The model not only contributes a better understanding of the sources of the nonlinearity in the vibration characteristics, but also provides an opening for investigating the possibility of using this nonlinear behaviour as a tool for structural health monitoring. In the following section, the feasibility of this is discussed, followed by a health monitoring routine suggested by the author.

5.4.1 DAMAGE INDICATOR

From the study of the nonlinearity in the vibration characteristics in the previous sections, it has been found that measures of nonlinearity, based on softening gradient, change with a specific trend with increasing damage levels (figure 4.11, figure 5.24). It is, therefore, theoretically possible by monitoring the changes of the softening gradient, that the state of the structure, in this case a reinforced concrete beam, can be retrieved. In other words, the softening gradient could possibly be used as a damage indicator. One important feature of a damage indicator is that the indicator has a direct one-to-one, i.e. monotonic, relationship with damage state. However, as seen in figure 5.24, this is clearly not the case for softening gradient. For this reason, using measures of non-linearity based on softening gradient, as a possible damage indicator has been considered unsuitable. More importantly, as nonlinearity

does not have a monotonic relationship with damage, the author expressed doubts over the direct use of the nonlinear characteristic as a damage indicator.

5.4.2 INDIRECT USE OF NONLINEARITY

There is an alternative way of using the nonlinearity found in vibration characteristics as a tool for structural health monitoring. Results in figure 5.22 show a variation of μ with observed maximum crack height. It is monotonic and μ is a physically meaningful parameter. In other words, as long as μ of a reinforced concrete beam (or indeed any other structure) can be determined, the damage condition of the beam is known. By using the restoring force surface method and the nonlinear curve-fitting routine, discussed previously, it is possible to determine μ for given sets of data. This routine is of course based on the suggested empirical crack model, which is itself based on a nonlinear stiffness relationship.

There are nevertheless a few problems to be investigated. Firstly, the data is relatively spread and there is insufficient statistical data to confirm the suggested μ – crack height relationship with confidence. Secondly, the model did not accurately recreate the variation of nonlinearity with damage. This therefore further dampened the confidence and reliability of the model. Thirdly, calculation of μ requires a restoring force surface, which in turn requires the value of the excitation force.

Figure 5.25 compares the variation of the two empirical parameters α and μ. It shows that these are exponentially related. From this, two inferences can be drawn. Firstly, since α and μ are related in some form of exponential relationship, it is possible to reduce the two parameters to one. However, as there was limited time available, the effect of parameter reduction has yet to be investigated. Secondly, it is possible to utilise this relationship as a measure of confidence of μ. With sufficient test data and an accurate exponential relationship obtained, the distance of the point of an unknown damage state

from the exponential curve on the α–μ graph can be a measure of confidence of the data.

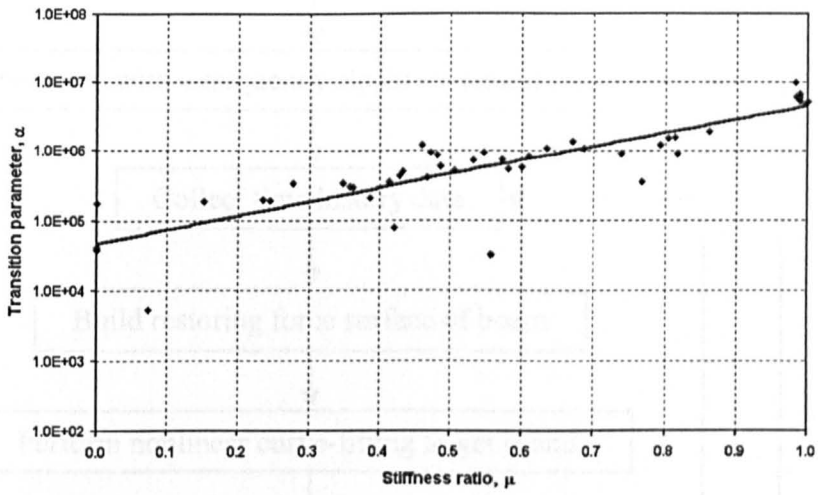

Figure 5.25: Variation of the empirical parameters α with μ,

5.4.3 POSSIBLE HEALTH MONITORING ROUTINE

With issues discussed above, it is clear that the parameters of the empirical crack model have potential to be utilised as health monitoring tools. Based on these, it is now possible to suggest a possible health monitoring routine for a reinforced concrete beam, as shown in figure 5.26.

It should be noted that this routine is based on the assumption that sufficient data has been obtained to build accurate μ-crack height and α-μ figures. This routine could also easily be extended to more complicated structures such as bridges and dams.

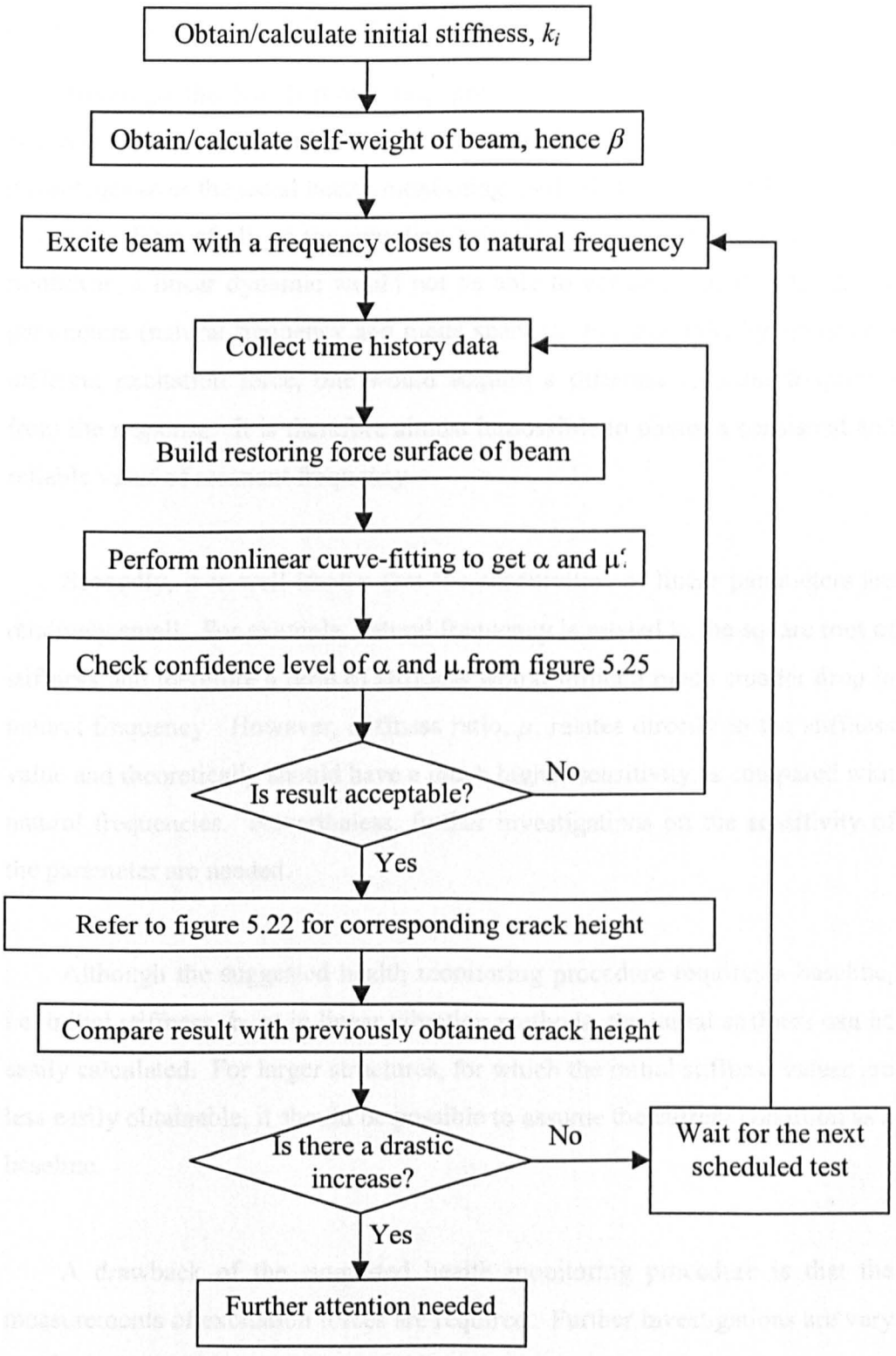

Figure 5.26: Possible routine for health monitoring for reinforced concrete beam

5.4.4 DISCUSSIONS ON HEALTH MONITORING ROUTINE

Although the health monitoring procedure suggested in figure 5.26 is relatively crude and further research is needed, there are some distinct advantages over the usual health monitoring methods that are based on a linear dynamic. First of all, as the vibration behaviour of the test structure itself is nonlinear, a linear dynamic would not be able to correctly identify the linear parameters (natural frequency and mode shapes). For example, by applying a different excitation force, one would acquire a different resonant frequency from the response. It is therefore almost impossible to obtain a consistent and reliable value of resonant frequency.

Secondly, it is well known that the sensitivities of linear parameters are relatively small. For example, natural frequency is related to the square root of stiffness and therefore a drop of stiffness would inflict a much smaller drop in natural frequency. However, stiffness ratio, μ, relates directly to the stiffness value and theoretically should have a much higher sensitivity as compared with natural frequencies. Nevertheless, further investigations on the sensitivity of the parameter are needed.

Although the suggested health monitoring procedure requires a baseline, i.e. initial stiffness, k_i, as in linear vibration methods, the initial stiffness can be easily calculated. For larger structures, for which the initial stiffness values are less easily obtainable, it should be possible to assume the current condition as a baseline.

A drawback of the suggested health monitoring procedure is that the measurements of excitation forces are required. Further investigations are very much needed to overcome these problems.

5.5 CONCLUSIONS

Phenomenological models suggested by different researchers have been investigated and the findings confirm that bilinear models are not capable of replicating dynamic behaviour of reinforced concrete beams as observed in the experiments. Results also show that transitions between open and closed crack need to be considered. An empirical model based on the hyperbolic tangent model has been derived and presented. Simulated results from the empirical model show agreement with observed experimental behaviour although there is a significant offset where further investigation is required.

A possible damage indicator used for structural health monitoring has been studied and stiffness ratio, μ, has the potential to be a damage indicator. Using the crack model proposed in this chapter, the author suggested a means of estimating it, provided that a restoring force surface can be drawn. With this, the author further suggests a possible routine for structural health monitoring for reinforced concrete beam and stresses that it could easily be extended for more complicated structures, like bridges. However, the suggested structural health monitoring procedure requires the measuring of excitation force. This proves to be a problem for implementing this technique to real structures. Further investigations on removing the need for measurement of excitation force would greatly increase the usability of the technique.

CHAPTER 6
THEORETICAL MODELLING – BACKGROUND

6.1 INTRODUCTION

With experimental results and phenomenological/empirical models of reinforced concrete beams presented in previous chapters, it is now appropriate to create an analytical model of the vibrations of a cracked reinforced concrete beam. However, it is important that some issues are discussed before initiating the modelling process.

Firstly, an investigation of the sources of nonlinearity present in reinforced concrete beams is needed. A sensible start for study this would be the concrete material itself and its cracking process, as it is well known that plain concrete is non-homogenous and does not behave in a linear elastic fashion like metals. It is also likely that there are other sources of nonlinear mechanisms, for example, crack closure and dowel action. A discussion of these is presented in the chapter.

Secondly, to produce an accurate model of a reinforced concrete beam requires an accurate plain concrete model. There are many different techniques for creating a constitutive model of plain concrete, ranging from complicated

classical plasticity model based on multi-axial compressive and shear tests to highly simplified design models used in British Standards. It is therefore important to choose a suitable means of modelling concrete for the purpose of this study. As most of these modelling techniques require some form of input from a microscopic model of concrete, a selection of them is also presented in this chapter.

In short, following this introductory section, a brief description of concrete material, paying particular attention to the nonlinear behaviour and cracking process is presented. Other different sources of nonlinear mechanisms are discussed in the next section. This is then followed by the discussions of different techniques for creating a constitutive model of concrete. In the final section, some example of micro-constitutive models of plain concrete are discussed and compared.

6.2 PLAIN CONCRETE

6.2.1 COMPOSITION AND BEHAVIOUR

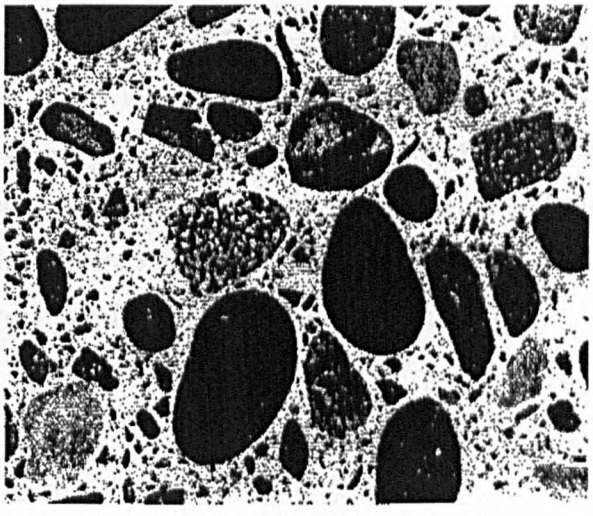

Figure 6.1: The composition of concrete (from Mehta and Monteiro, 1993)

Plain concrete is a non-homogeneous mixture of coarse aggregate, sand and hydrated cement paste (see figure 6.1). For normal-weight, normal-scale concrete mixes, coarse aggregate is usually gravel or crushed rock that is larger than 4.75mm in diameter while sand is aggregate particles with diameter between 0.75mm and 4.75mm. The hydration product of Portland cement and water is also referred as hydrated cement paste (*hcp*) and the *hcp* located in the immediate vicinity of the coarse aggregate particles is normally referred as the transition zone. As the transition zone typically has a slightly higher water to cement ratio than is observed in the entire *hcp* and because of the physical boundary between the different materials, the transition zone is usually slightly weaker than the remainder of the *hcp.* This irregularity in the strength distribution means that plain concrete is considered as a highly inhomogeneous material and nonlinear in nature (Lowes, 1999).

6.2.2 Initiation and Propagation of Cracks

The initiation and propagation of cracks is the dominant mechanism of concrete material response. Under moderate general loading, the response of the concrete mixture is controlled by microcracking in the transition zone between the aggregate and the *hcp.* Under increased loading, microcracks in the transition zone grow and merge and microcracks initiate in the *hcp.* Eventually, a continuous crack system forms, traverses the transition zone and the *hcp*, resulting in the loss of load capacity. When under tensile loading, increased load acts directly to increase the stress at the crack tip and drive crack propagation. As a result, for tensile loading, the sequence of cracking leading up to the development of a continuous crack system and loss of strength occurs very rapidly (Ringot E. and Bascoul, 2001).

6.2.3 ASSUMED BEHAVIOUR OF CONCRETE IN BRITISH STANDARD

For design in bending, the British Standard 8110 (BSI, 1997) assumes that the stress of concrete in compression is initially a parabolic function of strain followed by a region of constant stress with increasing strain before failure. This is shown in figure 6.2 where f_{cu} is the cube strength (in N/mm^2) and γ_m is the partial safety factor. When a beam has been damaged by overloading in bending, the concrete in compression is assumed to behave nonlinearly following the curve in figure 6.2.

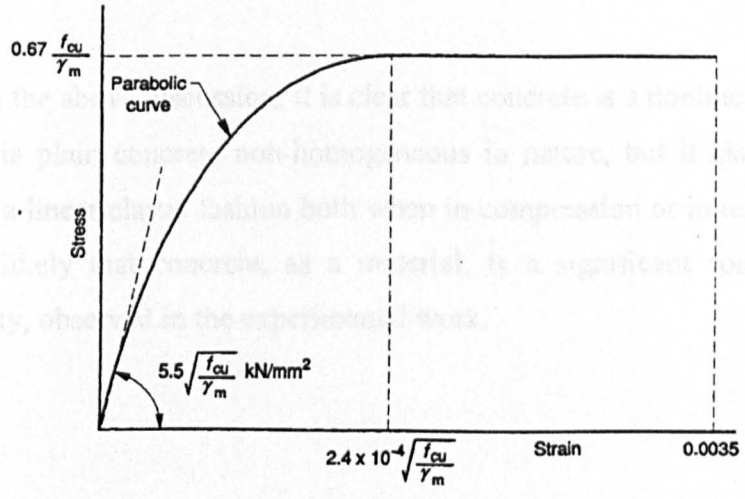

Figure 6.2: Concrete stress-strain relation in compression by British Standard 8110 (BSI, 1997)

British Standard 8110 states that tensile strength of plain concrete is about one tenth of compression and is assumed to be linear elastic. It is also assumed that once cracked, the concrete carries no stress, as shown in figure 6.3(a). This is, however, not exactly true as discussed by a lot of other researchers (Reinhardt et. al., 1986, and Yankelevsky et. al., 1989). In fact, concrete strength often appears to decrease gradually as shown in figure 6.3(b), though this does depend on the loading regime.

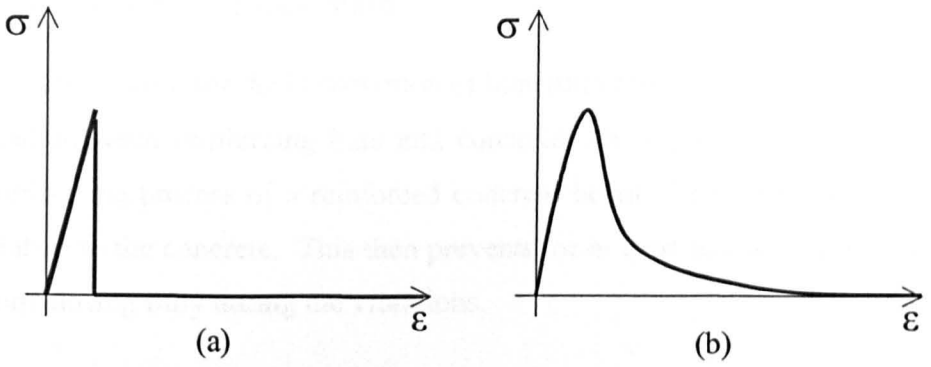

Figure 6.3: Schematic drawing of stress-strain relation of concrete material in tension: (a) British Standard model, (b) observed experimental behaviour

From the above discussion, it is clear that concrete is a nonlinear material. Not only is plain concrete non-homogeneous in nature, but it also does not behave in a linear elastic fashion both when in compression or in tension. It is therefore likely that concrete, as a material, is a significant source of the nonlinearity, observed in the experimental work.

6.3 POSSIBLE NONLINEAR MECHANISMS

One of the possible important sources of nonlinearity other than plain concrete characteristics is the closure of cracks during vibrations. Using phenomenological models, it has been demonstrated in chapter 5 that a crack that opens and closes in a single step, i.e. bilinear behaviour, does not produce nonlinearity. It has also been suggested that transitions between cracks open and cracks closed exist and have marked effect on nonlinear vibration behaviour. However, the reasons for these transitions to exist have yet been mentioned. The following are discussions of some of the possible mechanisms, which may cause transitions in cracks closure, and hence non-linear vibration behaviour.

6.3.1 CONCRETE –STEEL BOND

One reason for the introduction of transition crack closure behaviour is the bond between reinforcing bars and concrete. It is possible that, during the overloading process of a reinforced concrete beam, the reinforcing steel slips relative to the concrete. This then prevents, or at least has an effect on, cracks from closing fully during the vibrations.

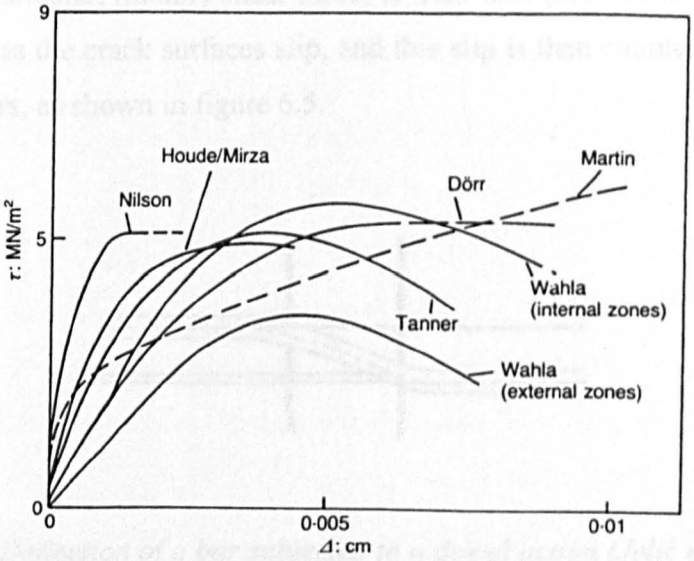

Figure 6.4: Variation of bond stress against slip displacement by various authors. (Data from Kotsovos and Pavlović, 1995)

An investigation of this possibility needs a thorough understanding of the concrete-steel bond behaviour. This is, however, not possible as reliable experimental information of wide applicability of bond slip characteristics is not available (Kotsovos and Pavlović, 1995). In fact, experiments attempting to determine bond stress against slip displacement curves exhibit, typically, a large scatter of data. Figure 6.4 is the comparison of characteristics proposed by various authors. Even if reliable experimental information is available, the use of the information is likely to be limited as the loading pattern experienced by a concrete beam is very different from these bond slip tests.

6.3.2 INTERFACE BEHAVIOUR (DOWEL ACTION, AGGREGATE INTERLOCK)

Reinforced concrete elements are characterised by several interface phenomena which concern either the two constituent materials, concrete and steel, or plain concrete itself. Two of the main interface phenomena, namely dowel action and aggregate interlock, are discussed.

Dowel action can be defined as the capacity of reinforcing bars to transfer forces perpendicular, (mainly shear force) to their axis (Jelić et. al.,1999). This effect arises as the crack surfaces slip, and this slip is then counteracted by the crosswise bars, as shown in figure 6.5.

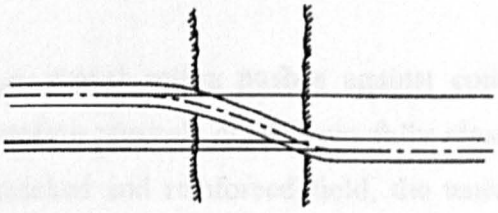

Figure 6.5: Deflection of a bar subjected to a dowel action (Jelić et. al.,1999)

For the deformation of the reinforcing bar over a free length, Pauley et. al. (1974) made a distinction between three different mechanisms (figure 6.6):

(a) bending: the capacity of this mechanism is limited by the formation of plastic hinges in the bar

(b) shear: load transfer by pure shear

(c) kinking: if there is a considerable shift in between the main bar axis, the axial force in the locally deviated part results in a component perpendicular to the bar axis

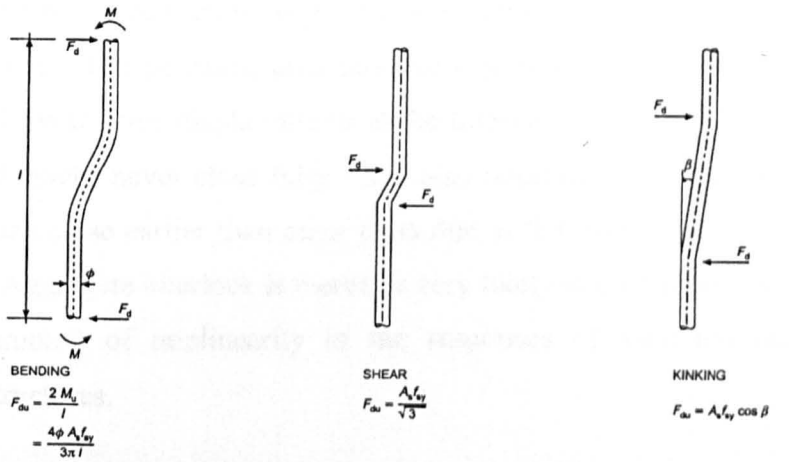

Figure 6.6: Mechanisms of shear transfer over the free length (Paulay et. al., 1974)

During vibration, dowel action pushes against concrete core when in compression and therefore prevents crack from fully closed. It is also likely that in a regularly cracked and reinforced field, the tensile and shear forces induced in the bars by the loads may still be considered as forces applied to the cracked concrete and reinforcement (Gambarova and Di Prisco, 1996).

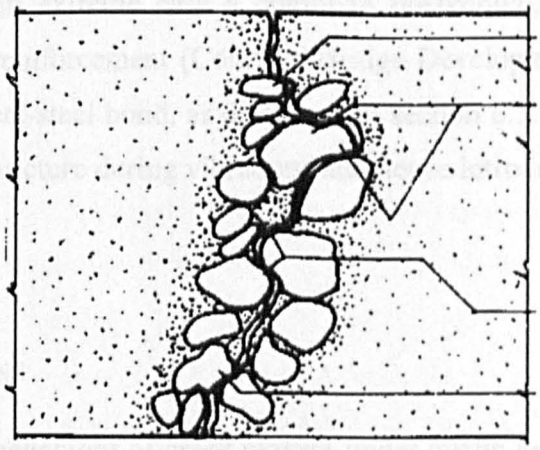

Figure 6.7: Schematic drawing of aggregate interlock in concrete. (Gambarova and Di Prisco, 1996)

Aggregate interlock, as shown in figure 6.7, is arguably a material problem; since the behaviour of a single crack is related to the properties of

concrete, such as maximum aggregate size, aggregate shape and concrete tensile strength. It is generally associated with cracks, which are locally rough. Because of the relative displacements at the interface, it is possible that under cyclic load cracks never close fully. It is also possible that some parts of the crack surface close earlier than other parts due to the irregularity of the crack interface. Aggregate interlock is therefore very likely to contribute some, if not a large, amount of nonlinearity in the responses of vibrating reinforced concrete structures.

6.3.3 CORROSION OF REINFORCEMENT

Another factor that could cause a reinforced concrete structure to behave nonlinearly is corrosion of the reinforcement. It is well known that corrosion of reinforcement would certainly cause changes to the structural capacity. This is because corrosion causes loss of steel area and this is likely to affect the modal parameters of the reinforced concrete beam, particularly the natural frequencies and damping ratios (Purkiss et. al., 1994a, 1994b). Research by the UK Transport Research Laboratory showed corrosion of reinforcement also causes loss, and in extreme case a complete breakdown, of bond between concrete and the reinforcement (Concrete Bridge Development Group, 2002). The loss of concrete-steel bond, as discussed in section 6.3.1, would affect the crack closure of structure during vibrations and hence introduce nonlinearity.

6.3.4 DISCUSSIONS

In short, the behaviour of crack closure under cyclic loading has not been adequately investigated and needs further research (Brandon and Mathias, 1995). The effect of mechanisms such as concrete-steel bond, dowel action and aggregate interlock on crack closure has yet to be investigated (Gambarova and Di Prisco, 1996). Although these microscopic studies of reinforced concrete are beyond the scope of this study, the concept and the effect of these

would be the basis of the modelling work presented in chapter 7. These effects would be represented in some form of stress-strain or stress-deformation relationship of concrete with a gradual softening portion. This therefore involves the constitutive modelling of concrete and will be discussed in the following sections.

6.4 CONSTITUTIVE MODELLING OF CONCRETE

A constitutive model is a phenomenological model often based on material properties, which are usually easily obtainable from material tests or microscopic models. The constitutive model can then be used for structural analysis and, together with structural tests, provides important information about the structural behaviour. There are many methods of creating constitutive models of plain concrete and the following is a brief summary of them.

6.4.1 CLASSICAL PLASTICITY MODELS

These models are the most popular and are based on the theory of plasticity, which consists of three basic components: yield surface, flow rule and hardening law. The yield condition, often using the classical Mohr-Coulomb or Drucker-Prager yield surface for plain concrete, defines the elastic limit. Flow rules prescribe the evolution and amount of plastic strain, and therewith the ratio of axial and lateral deformations. The hardening law controls the shape and size of yield surface after first yield and determines the amount of plastic deformation at a certain stress state. The models' predictions are normally found to be in very good agreement with experimental results for concrete in uni-axial, bi-axial and tri-axial compression and shear and also in tension. The yield surface corresponds at a certain stage of hardening to the strength envelope of concrete, and thus has, a strong physical meaning (Grassi, 2002). The modelling process is normally lengthy and complicated, hence a

very high computational cost. Since the purpose of this study is to the model the crack behaviour of concrete rather than concrete material in general, it is therefore considered that this modelling procedure is unsuitable.

6.4.2 MICROPLANE MODELS

Microplane models, based on a generalization of the slip theory of plasticity, are considered to be more promising and conceptually transparent than the classical approach (Bažant et al., 2000). The constitutive law is formulated in terms of vectors rather than tensors as a relation between the stress and strain components on a plane of any orientation in the material microstructure, called the microplane (Bažant 1984). The microplane model can be seen as a consequence of the hypothesis that the free energy density of the material is a sum of the free energy densities expressed as functions of the strain vector on planes of various orientations (Carol et al. 1999). Recent models have also been extended extensively to cyclic loading.

The penalty to pay for these advantages is an increase in computational work and storage requirements, which is about 10-times greater for the microplane models compared to the classical plasticity models (Caner and Bažant., 2000). Again, it is the crack behaviour rather than plain concrete material that is of interest in this study. Therefore, it is very much unsuitable for the purpose of this study.

6.4.3 DAMAGE MECHANICS MODELS

Another group of constitutive models are the damage mechanics models. The models created based on fracture and damage mechanics are particularly useful to describe the mechanical behaviour of concrete in tension (Mazars and Pijaudier-Cabot, 1996, Carol et. al.,2001a, 2001b, Peerlings, 1999). As this

modelling technique is later adopted in this study, it will be discussed in considerable detail.

Fracture mechanics (damage mechanics is a branch of fracture mechanics) is based on the theory that the weakening of material by a crack can be treated as an equilibrium problem in which the reduction in strain energy of a body containing a propagating crack can be equated to the increase in surface energy due to the increase in surface area (Ceriolo and Di Tommaso, 1998). The early field of fracture mechanics bases predominantly on Irwin's linear elastic fracture mechanical (LEFM) theory, which states that a crack will only begin to extend when the stress intensity factor has been increased to the fracture toughness of the material and commonly denoted K_{Ic} for mode I plane strain deformation (Broek, 1988). As LEFM assumes cracks as straight lines, it is unsuitable for the study of cracks and fractures in non-homogenous material. It is therefore not surprising that when several researchers (Kaplan, 1961 and Blakey and Baresford, 1962) attempted to apply LEFM analysis on notched concrete beams subjected to three- and four- point bending they were unsuccessful. It was later realised that LEFM is subject to a size effect and is only applicable to large-scale initially cracked structures and ultra-brittle concrete (Planas and Elices, 1989), and that it is necessary to apply nonlinear fracture mechanics to describe fracture in ordinary concrete structures.

There are two main damage mechanics models, the fictitious crack model (FCM), developed by Hillerborg et. al. (1976), and blunt crack model (BCM), developed by Bažant and Oh (1983).

6.4.3.1 Fictitious Crack Model (FCM)

In the FCM, cracks are described using a stress, σ, versus crack opening displacement, w, relationship. Two mechanisms contribute to the stress transfer over the crack. The crack width is the collected deformation of a band of microcracks. Within this crack band material bridges transfer the load.

After the formation of a real single crack, the stress transfer is possible due to aggregate interlock. A crack runs along the interface between the aggregate grains and the cement matrix. The grains are pulled out of the matrix and due to this, friction forces between grains and matrix occur. The grains act like friction blocks and transfer friction forces over the crack (König and Duda, 1996). In the FCM, material points on the crack extension path are assumed to be in one or three possible states: (1) A linear elastic state; (2) a fracture state where material softened, caused by cohesive forces in the fracture process zone; and (3) a state of no stress transmission. In the fracture state, the cracking process is described by a softening relation that relates stress normal to the crack surface σ to the crack opening displacement, w (distance between the cracked surfaces)

$$\sigma = f(w) \tag{6.1}$$

where $f(\,)$ is a material function determined by uniaxial tensile tests. The area under the curve is termed the specific fracture energy, G_f, which is assumed to be a material constant (Elfgren, 1989). Figure 6.8 shows an example of a FCM model of concrete.

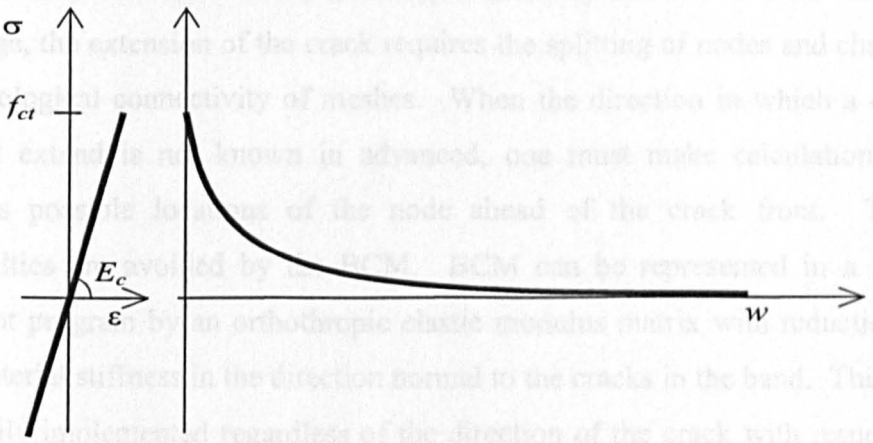

Figure 6.8: An example of FCM

6.4.3.2 *Blunt Crack Model*

In BCM, similar to FCM, the central hypothesis is that fracture in a heterogeneous material can be modelled as a band of densely distributed microcracks, but with a blunt front. Instead of representing the softening portion of concrete with a stress-displacement relationship, an effective stress-strain relationship is adopted using a "nonlocal continuum" concept.

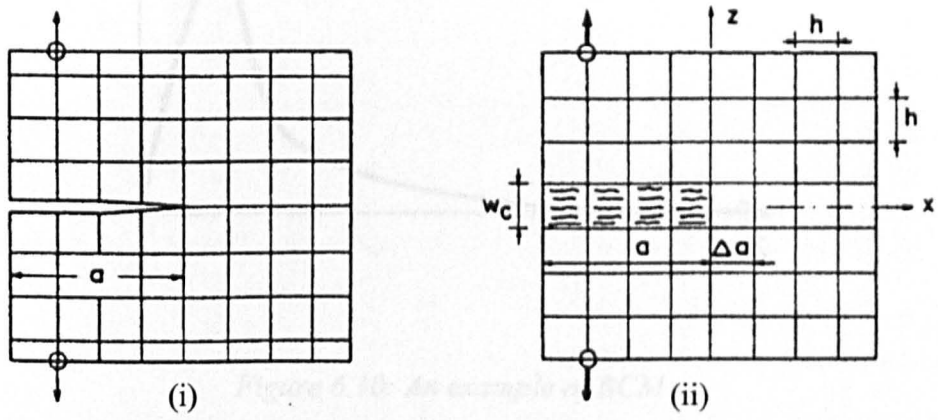

Figure 6.9: Representations of (i) FCM and (ii) BCM in FE package.

The key advantage of BCM is that it is highly computational effective for finite element models. For a crack represented by FCM in a finite element package, the extension of the crack requires the splitting of nodes and changes of topological connectivity of meshes. When the direction in which a crack should extend is not known in advanced, one must make calculations for various possible locations of the node ahead of the crack front. These difficulties are avoided by the BCM. BCM can be represented in a finite element program by an orthothropic elastic modulus matrix with reduction of the material stiffness in the direction normal to the cracks in the band. This can be easily implemented regardless of the direction of the crack with respect to mesh lines (see figure 6.9).

As there is no finite element model used in this study, BCM is effectively identical to FCM. The only difference is that FCM assumes that the stress

displacement behaviour observed in tensile specimens is a material property whereas BCM assumes stress strain behaviour is. Figure 6.10 shows an example of a BCM of concrete.

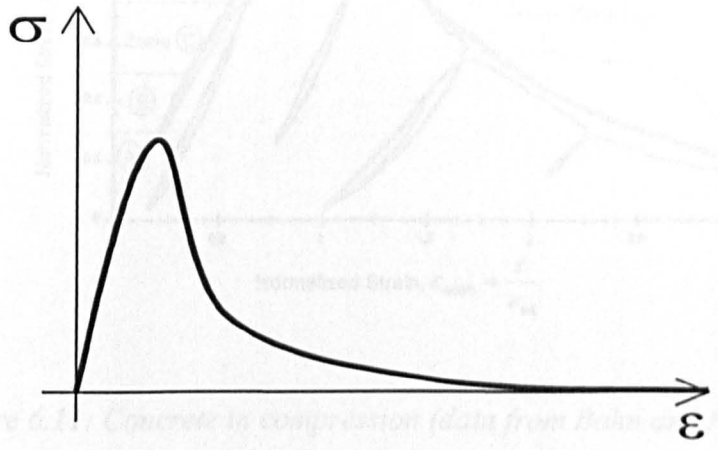

Figure 6.10: An example of BCM

6.5 MICROSCOPIC CONSTITUTIVE MODELS

As all constitutive model predictions are based on the input of material properties, it is very important that a sufficiently accurate microscopic constitutive model is use. For the purpose of this study, only two of the concrete properties are of interest, concrete subject to compression and tension.

6.5.1 CONCRETE IN COMPRESSION

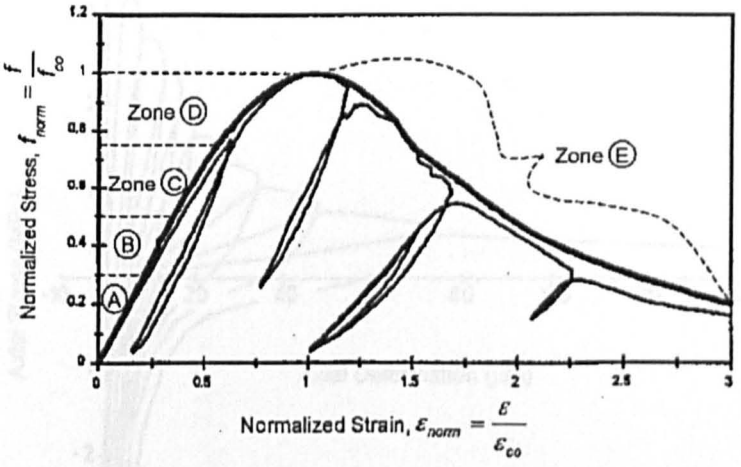

Figure 6.11: Concrete in compression (data from Bahn and Hsu, 1998)

Figure 6.11 shows a plot of stress-strain response of a typical concrete mix subjected to uni-axial monotonically increasing and cyclic compressive strain. The response of the plain concrete is essentially linear-elastic until the load reaches approximately 30 percent of the peak compressive strength (Zone A). There is a very slight reduction in material stiffness when compressive stress increase to between 30 and 50 percent (Zone B) but would still be sufficient to model as a linear-elastic model (Mehta and Monteiro, 1993). Cyclic test results showed there is negligible residual strain when unloading from compressive stresses below 50 percent.

Concrete behaviour under high compressive stress would not be relevant to this study as the specimens in the experiments were specifically designed to fail in tension, and therefore would not sustain high levels of compressive stress. It is therefore sufficient to model concrete in compression as a linear-elastic material.

6.5.2 CONCRETE IN TENSION

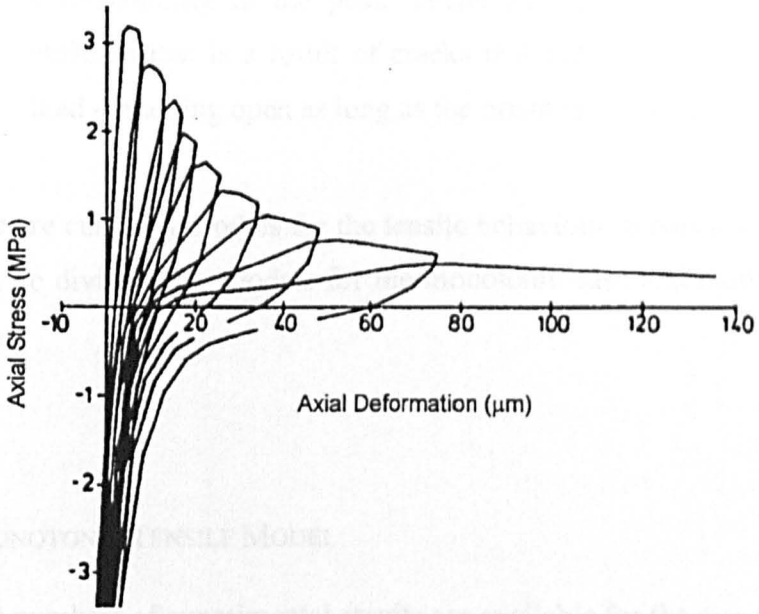

Figure 6.12: Concrete under cyclic tensile loading (Data from Reinhardt et. al., 1987)

Figure 6.12, shows a typical stress-deformation response of plain concrete prisms subjected to uniaxial tensile deformation under reversed cyclic loading. The response of plain concrete in tension is characterised by initiation, opening and propagation of cracks, thus it is inappropriate to consider tensile strain, since strain measurement depends entirely on the gauge length associated with the investigation. Important characteristics of these material responses, as described by Lowes (1999), include:

1. Concrete responds in an essentially linear-elastic manner until the tensile strength is achieved. This response corresponds to the initiation of a small number of stable microcracks.

2. Loading of the concrete to tensile strains in excess of that corresponding to the peak tensile strength results in loss of load capacity. This response corresponds to the development of a crack.

3. Unload-reload cycles that initiate at strains in excess of that corresponding to the peak tensile strength occur at a material stiffness that is a result of cracks that formed under peak tensile load remaining open as long as the prism is carrying tensile stress.

There are currently models for the tensile behaviour in concrete available, which can be divided into models for the monotonic case and models for the cyclic case.

6.5.3 MONOTONIC TENSILE MODEL

Large numbers of experimental results are available for the σ-*w* relation of concrete in tension in the case of monotonic loading. Figure 6.13 shows two examples of the more popular models (Petersson, 1981, Cornelissen et. al., 1986). These models all show good agreement with the experimental results, as shown in Figure 6.12.

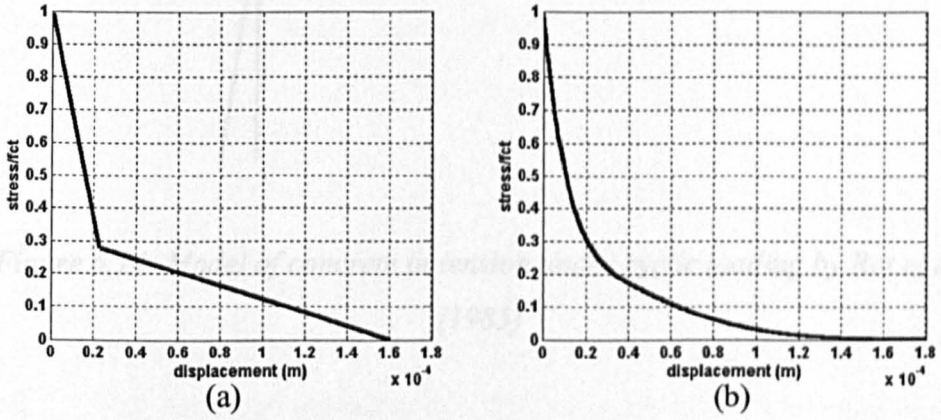

Figure 6.13: Models for concrete in tension under monotonic loading suggested by: (a) Petersson, 1981, (b) Cornelissen et. al., 1986.

6.5.4 CYCLIC TENSILE MODEL

In contrast to monotonic models, only very few models are available for the case of cyclic loading. The simplest of them all is a model by Rots et. al. (1985) (see figure 6.14). The model proposed by Rots et. al. is based solely on stress and strain, and therefore is easily adoptable for BCM in damage mechanics. More importantly, Rots et. al. suggested the unloading curves of concrete material always pass through the origin. This effectively assumed there is no residual strain in cracked plain concrete after unloading. This model would only be suitable if cyclic effects have negligible relevance in the overall behaviour.

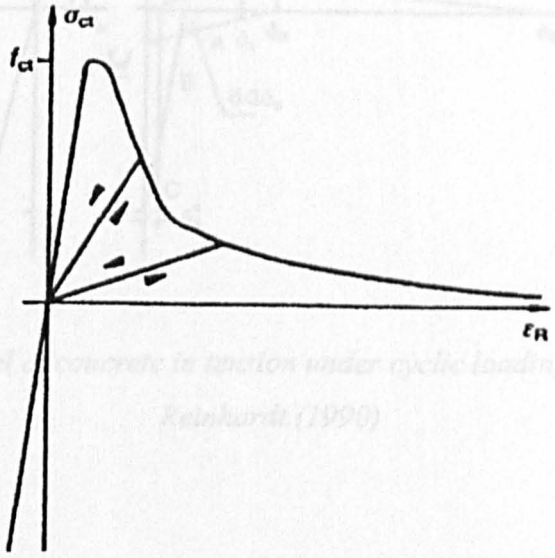

Figure 6.14: Model of concrete in tension under cyclic loading by Rot et al. (1985)

The next concrete model to be considered is the model suggested by Hordijk and Reinhardt (1990) (see figure 6.15). Hordijk and Reinhardt's model is subdivided into two parts, a general stress-strain relation and a stress-displacement relation for the additional localised deformations. It is therefore easily adoptable for FCM in damage mechanics. The general section of stress-strain relation consists of a linear relationship in all of the compressive region and in the tensile region up to f_{ct}, the maximum tensile stress of concrete.

Hordijk and Reinhardt's model has a fairly accurate prediction of concrete under cyclic tension, paying particular attention to the hysteresis behaviour. It should be noted that the model also includes residual deformations of concrete when the maximum tensile stress is reached. As compare to model by Rots et. al., it is a far more detailed and accurate representation of concrete under cyclic tensile loading.

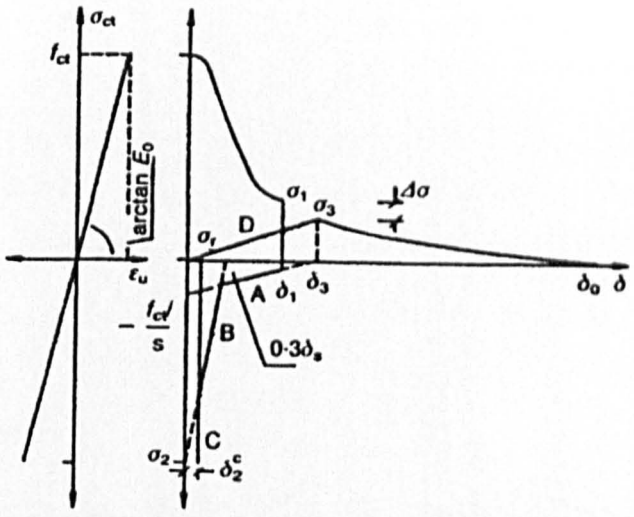

Figure 6.15: Model of concrete in tension under cyclic loading by Hordijk amd Reinhardt.(1990)

6.6 SUMMARY

In this chapter, several background issues of theoretical modelling were studied. The nonlinear behaviour of concrete material has been highlighted. Different possible nonlinear mechanisms including crack closure, interface behaviour, concrete-steel bond, corrosion of reinforcement and tension stiffening were also discussed. Several concrete modelling techniques were then presented, with attention paid particularly to the suitability of each technique in achieving the aim set for this study. Among these, damage mechanics modelling techniques were discussed in relative detail, as it was the author's opinion that it would be well suited for the work. A variety of uni-

axial microscopic concrete models were also examined. With these background issues investigated, we are now in a position to derive an analytical model of a cracked reinforced concrete beam, presented in the next chapter.

CHAPTER 7

DAMAGE MECHANICS MODEL OF VIBRATING CRACKED REINFORCED CONCRETE BEAMS

7.1 INTRODUCTION

As discussed in the previous chapter, the field of damage mechanics provides a convenient framework for this study to develop an analytical model. In this chapter, a model of vibrating cracked reinforced concrete beam using damage mechanics technique is presented. The difficulty in modelling a vibrating cracked beam lies in the modelling of the crack itself. It was therefore sensible to first derive a simple analytical model of a reinforced concrete crack. With this, it can then be incorporated into a beam model to predict the behaviour of a cracked beam.

The aim of the cracked beam modelling presented here is to recreate the nonlinear vibration behaviour observed in the experimental work and consequently improve understanding of the source of nonlinearity. To achieve this, a sensible starting point was modelling the material response of plain concrete itself. The plain concrete model was then validated by comparing it

with models developed by other researchers. The validated model of plain concrete was later extended to incorporate steel reinforcements. The behaviour of the model under the unloading condition was then investigated. A reinforced concrete crack model can be derived from the changes of stiffness during the loading and unloading conditions. By assuming the crack model as a rotational SDOF spring, vibration analysis was carried out to study its dynamic behaviour. Finally, the rotational SDOF spring was included in a beam model to represent a cracked reinforced concrete beam. Again, vibration analysis was carried out for the cracked beam model.

This chapter is divided into several sections. Following this introductory section, the assumptions made for deriving the analytical crack model are presented and justified. The next section comprises methodology and procedure used in the modelling process. Numerical results for the plain concrete and reinforced concrete models are proposed in the following section. Validations of these models are then discussed. Finally, the model was extended to incorporate the unloading, and subsequently cyclic, behaviour of cracked reinforced concrete beams.

7.2 ASSUMPTIONS AND JUSTIFICATIONS

Several assumptions were made in the derivation of the analytical crack model. They are:

- Strain softening behaviour of concrete in tension plays a key role in nonlinear vibration behaviour of a reinforced concrete beam. This implies that other possible sources of nonlinearity discussed in chapter 6, such as concrete-steel bond and interface behaviour, have not been included in the model. There are two reasons for this: (1) concrete-steel bond and interface behaviour have been suggested by Nield (2001) to have minimal effect on nonlinearity; (2) to allow the author to investigate the effect of strain softening behaviour of concrete on nonlinearity alone.

- The vibration of concrete material does not contain hysteresis behaviour. This assumption is incorrect as depicted by Reinhardt et. al. (1986) and Hordijk and Reinhardt (1990) (see figure 6.12). However, experimental results presented in chapter 4 showed very little, if any, hysteresis effect. The result suggested that hysterisis behaviour of concrete material in the reinforced concrete beams tested in chapter 4 has minimal effect. As the purpose of the modelling is to recreate this behaviour, the assumption that no hysteresis effect is experienced is therefore acceptable.

- Only uni-axial behaviour of plain concrete is considered. This assumption is not strictly correct, as confinement would possibly have some effect on the vibration behaviour. However, the effect is thought to be minimal and is outweighed by the benefits of ease of modelling using uni-axial behaviour.

- Torsion and shear effect has not been considered. As all beams in the experiment have failed in bending, it is reasonably safe to assume that torsion and shear have very limited effect on the observed behaviour.

- The effect of compressive steel reinforcement has also been ignored. As no crack was observed in the compressive zone, it is safe to assume that no contribution of nonlinear effect from the compressive zone and therefore the effect of compressive steel reinforcement can be ignored.

- Plane sections remain plane.

The assumed concrete behaviour and fracture process are discussed in the following sections.

7.2.1 STRESS-STRAIN/DISPLACEMENT RELATION

It was decided to model the crack in the concrete using a FCM approach (see section 6.4.3.2. Concrete in compression is modelled as a linear-elastic material due to the fact that tested specimens were designed to fail in tension and experienced relatively little compression. Concrete in tension was modelled using a modified Reinhardt's model, as shown in figure 7.1.

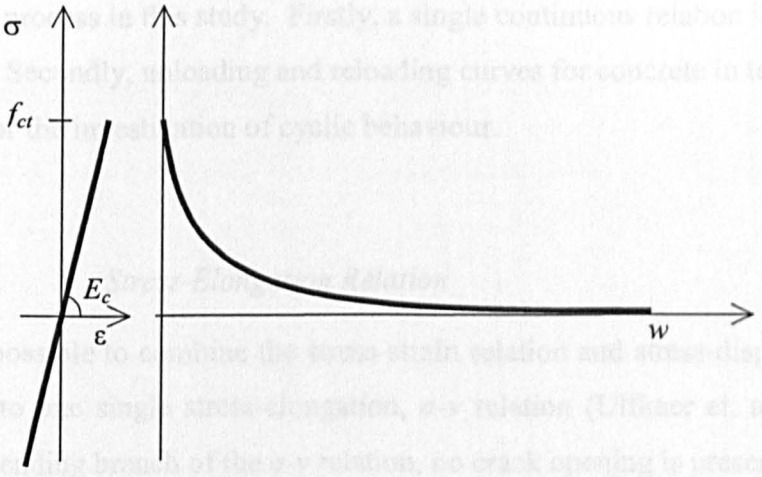

Figure 7.1: Assumed stress-strain/displacement envelope.

As every FCM, Reinhardt's model is subdivided into two parts, a general stress-strain relation and a stress-displacement relation for the additional localised deformations. The general section of stress-strain relation consists of a linear relationship in all of the compressive region and in the tensile region up to f_{ct}, the maximum tensile stress of concrete. The maximum tensile stress is assumed to be one tenth of the maximum compressive stress. The stress-displacement section of the model follows the stress-displacement envelope suggested by Cornelissen et. at. (1985):

$$\sigma_c(i) = f_{ct}\left\{\left[1+\left(C_1\frac{\varepsilon_c(i)-f_{ct}}{w_c}\right)^3\right]e^{-C_2\frac{\varepsilon_c(i)-f_{ct}}{w_c}} - \frac{\varepsilon_c(i)-f_{ct}}{w_c}\left(1+C_1^3\right)e^{-C_2}\right\} \quad (7.1)$$

where f_{ct} is the concrete tensile strength, E_c is the Young's modulus of concrete, w_c is the critical crack opening displacement at the complete release

of stress and is equal to $160\mu m$ for concrete (assuming fracture energy = $100N/m$). C_1 and C_2 are empirical parameters that are taken as equal to *3* and *6.93* respectively.

7.2.2 MODIFICATION OF REINHARDT'S MODEL

Two modifications of Reinhardt's model are required for the crack modelling process in this study. Firstly, a single continuous relation is required for stress. Secondly, unloading and reloading curves for concrete in tension are required for the investigation of cyclic behaviour.

7.2.2.1 Stress-Elongation Relation

It is possible to combine the stress-strain relation and stress-displacement relation into one single stress-elongation, σ-v relation (Ulfkaer et. al., 1990). On the ascending branch of the σ-v relation, no crack opening is present and the elongation is linear elastic,

$$v = \frac{\sigma h_c}{E_c} \tag{7.2}$$

where h_c is the thickness of the equivalent elastic layer, which will be discussed below. On the descending branch, the total elongation v consists of two contributions, elongation from the linear elastic behaviour and displacement from crack opening,

$$v = \frac{\sigma h_c}{E_c} + w \tag{7.3}$$

where w is the crack width opening.

The equivalent elastic layer, h_c, represents the local stiffness of the tested beams. Ulfkaer et. al. (1995) found that h_c can be assumed to be proportional to the depth of the beam, $h_c = k_c h$, independent of crack length, provided k_c is smaller than 1 (see figure 7.2). This is in agreement with Krenk et. al. (1994)

who performed computations on cohesive joints and showed that the local flexibility associated with a crack penetrating half the beam depth is equivalent to an elastic layer with a k_c of value of around 0.5-0.7. k_c = 0.7 is used throughout the modelling process. Combining equations 7.2 and 7.3 gives a stress-elongation relation as shown in figure 7.3.

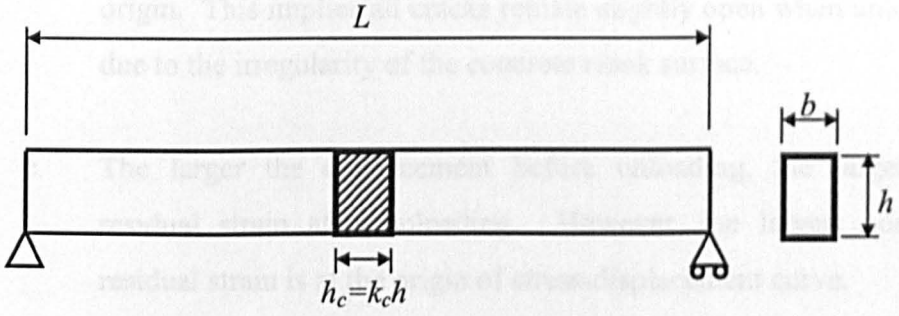

Figure 7.2: Equivalent elastic layer suggested by Ulfkaer et. al. (1995)

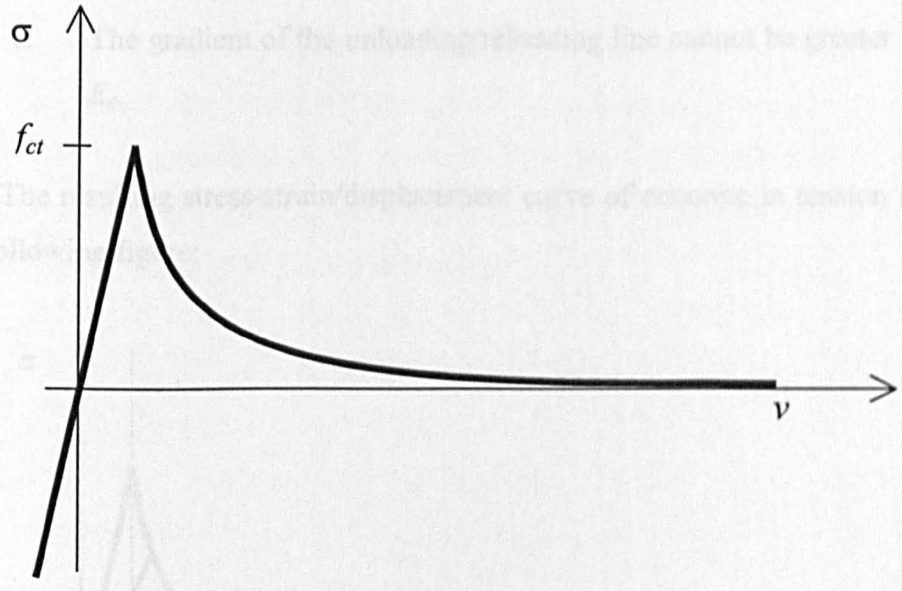

Figure 7.3: Assumed stress – elongation curve

7.2.2.2 *Unloading / Reloading Curve*

Unloading and reloading are assumed to run on the same line, i.e. there is no hysteresis loop. To incorporate the effect of residual strain, the author suggested the unloading/reloading line follows the following rules

a. When the displacement, w, is zero, i.e. uncracked state, all unloading/reloading curves pass through the origin of the stress strain curve.

b. If the concrete has started to crack, i.e. the load history has passed the peak; all unloading/reloading curves must not pass through the origin. This implies all cracks remain slightly open when unloaded due to the irregularity of the concrete crack surface.

c. The larger the displacement before unloading, the larger the residual strain after unloading. However, the largest possible residual strain is at the origin of stress-displacement curve.

d. All unloading curves join the uncracked stress-strain curve at the intercept of two curves.

e. The gradient of the unloading/reloading line cannot be greater than E_c.

The resulting stress-strain/displacement curve of concrete in tension is as the following figure:

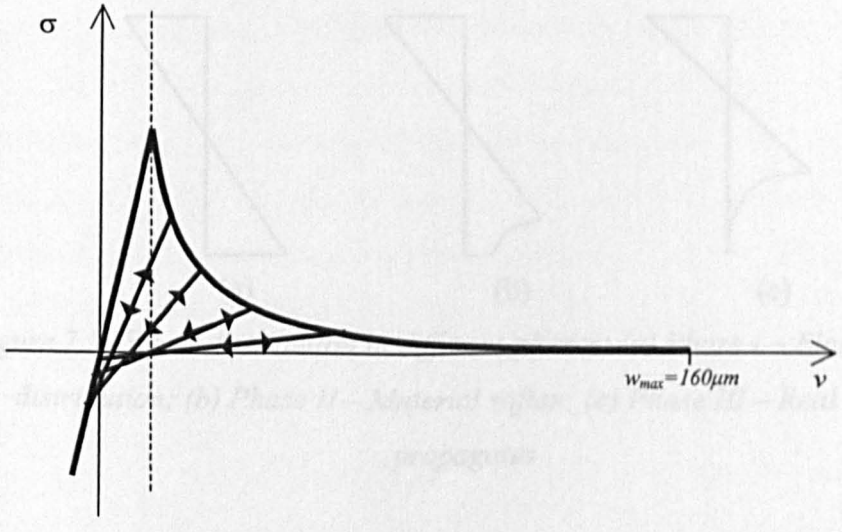

Figure 7.4: Unloading/reloading curve of assumed stress-strain/displacement relation

7.3 CRACK MODELLING PROCESS

7.3.1 CONCEPT

Before presenting the modelling process, it is best to discuss the concept adopted in the modelling process. As suggested by Iyengar and Raviraj (2001), the fracture process can be divided into three phases:

1. Phase I – before the tensile strength is reached in the tensile side of the beam

2. Phase II – development of crack in the region where the material softens

3. Phase III – real crack propagation

In phase I, the stress-strain relation is linearly elastic in all layers of the beam. In phase II, the tensile softening behaviour of concrete comes into effect and a crack starts to develop. In phase III, the concrete has softened so much that it has very little effect on the overall behaviour. The stress distribution in each of these phases is illustrated in Figure 7.5.

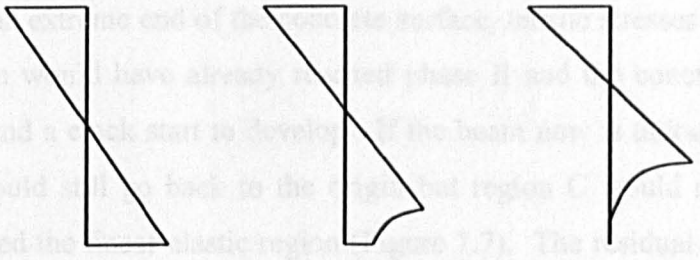

Figure 7.5: Stress distribution in different phases: (a) Phase I – Elastic stress distribution; (b) Phase II – Material soften; (c) Phase III – Real crack propagates

The concept of the modelling process is best described in the following cases:

Case 1: Consider a section of uncracked concrete beam under slight bending, regions below the neutral axis all experiencing different degrees of tensile stresses. Provided the tensile stresses experienced are sufficiently low in all cases and none of them has reached the peak of the stress-elongation curve, unloading the beam will bring it back to the original position and there would not be any residual strain in the concrete. (Figure 7.6)

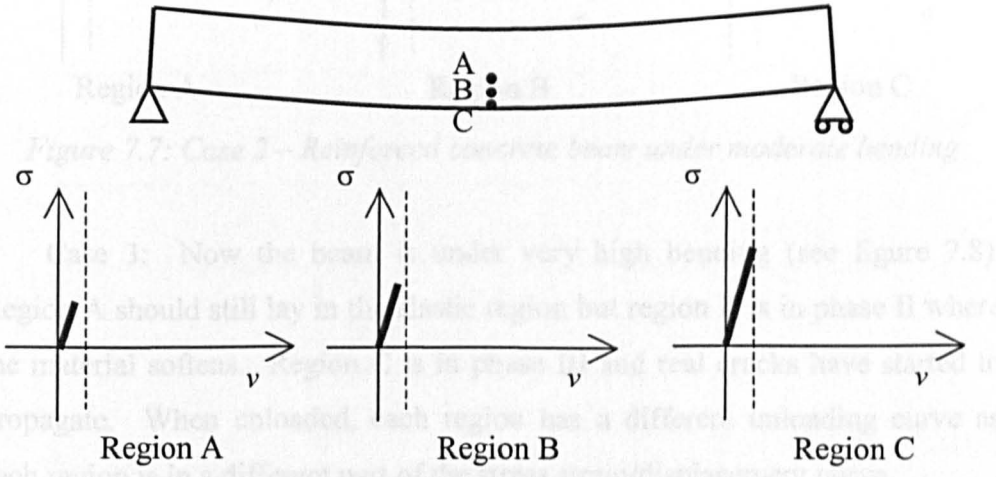

Figure 7.6: Case 1—Reinforced concrete beam under slight bending

Case 2: Consider the beam now under higher bending stress, region A immediately under the neutral axis would still experience reasonably low stresses and remains in the elastic region. Region B would just have reached the peak and further increase in stress would see a crack start to develop. Region C, the extreme end of the concrete surface, tensile stresses experienced in the region would have already reached phase II and the concrete material will soften and a crack start to develop. If the beam now is unloaded, Region A and B would still go back to the origin but region C would not as it has already passed the linear elastic region (Figure 7.7). The residual deformation shows that region C is cracked.

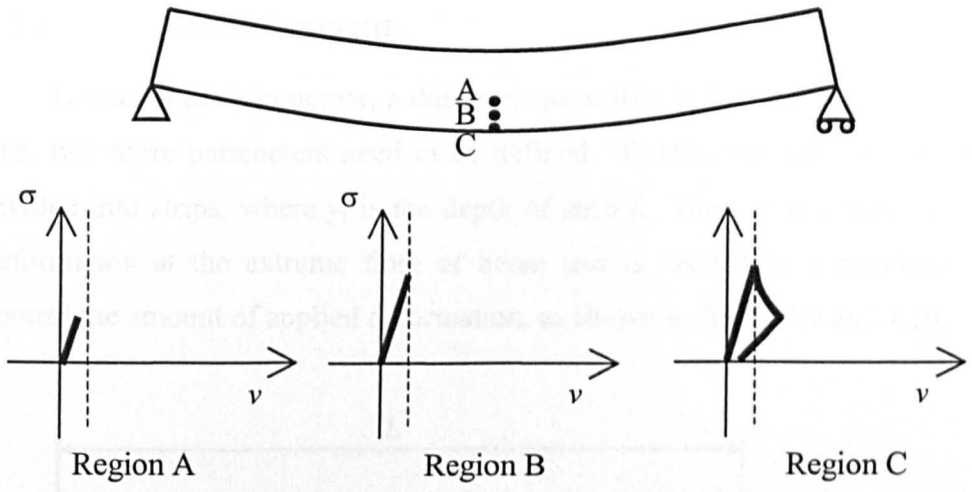

Figure 7.7: Case 2 – Reinforced concrete beam under moderate bending

Case 3: Now the beam is under very high bending (see figure 7.8). Region A should still lay in the elastic region but region B is in phase II where the material softens. Region C is in phase III and real cracks have started to propagate. When unloaded, each region has a different unloading curve as each region is in a different part of the stress strain/displacement curve.

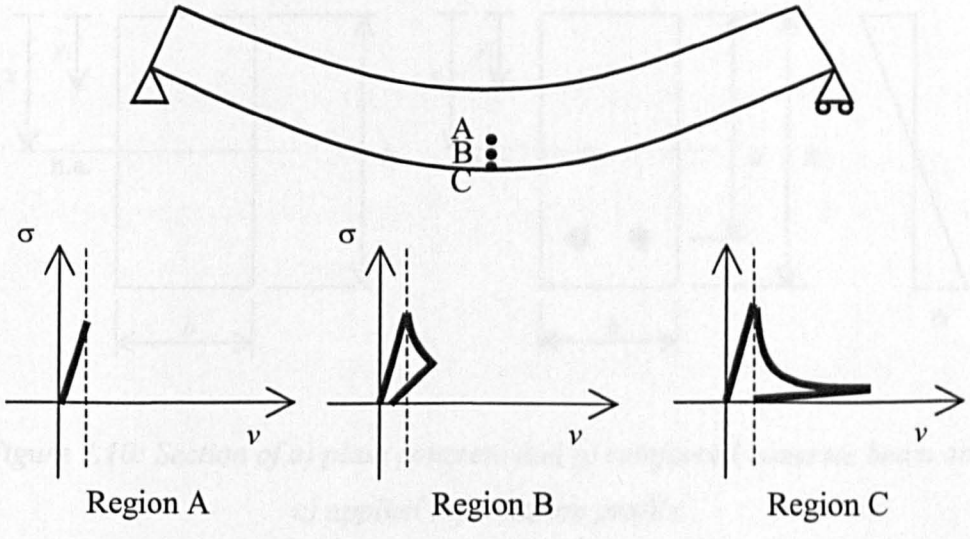

Figure 7.8: Case 3 – Reinforced concrete beam under heavy bending

Although the unloading curve of each layer of concrete is bilinear in fashion, the combined effect of all layers would create a nonlinear unloading curve and hence, a nonlinear behaviour in vibration characteristic. It is therefore important to model each layer of concrete

7.3.2 PLAIN CONCRETE

To model plain concrete, a deformation profile is first calculated. To do this, two more parameters need to be defined. Firstly, the depth of beam is divided into strips, where y_i is the depth of strip i. Then, v_x is defined as the deformation at the extreme fibre of beam and is needed as a parameter to control the amount of applied deformation, as shown in figure 7.9 and 7.10.

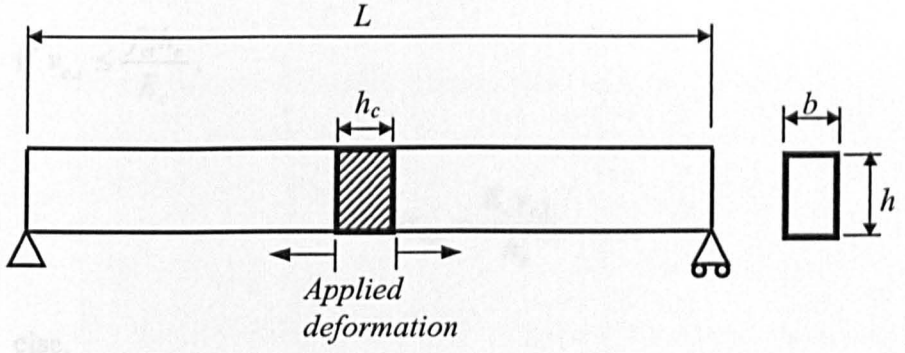

Figure 7.9: Applied deformation at extreme fibre of beam

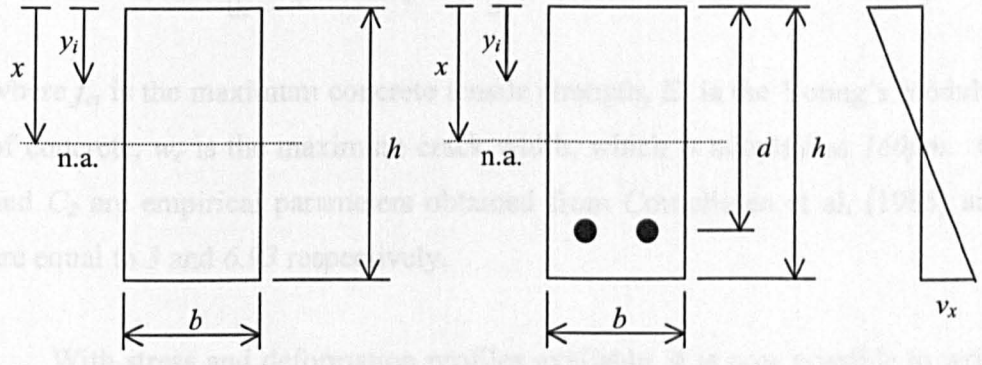

Figure 7.10: Section of a) plain concrete and b) reinforced concrete beam and c) applied deformation profile

Since plane sections are assumed to remain plane at either face of the beam, the deformation at each strip can be calculated using rules of similar triangles and the deformation profile across beam can be easily obtained:

$$v_{c,i} = \frac{y_i - x}{h - x} v_x \tag{7.4}$$

where $v_{c,i}$ is deformation of concrete at strip i and most other parameters can be found in figure 7.10.

With the deformation profile calculated, it is possible to calculate the stress profile across the beam. The stress in the concrete at each strip, σ_i, is calculated using the stress-deformation curve discussed in previous sections and can be written in equation form as:

if $v_{c,i} \leq \frac{f_{ct} h_c}{E_c}$,

$$\sigma_{c,i} = \frac{E_c v_{c,i}}{h_c} \tag{7.5}$$

else,

$$\sigma_{c,i} = f_{ct}\left\{\left[1+\left(C_1 \frac{v_{,c,i} - f_{ct}}{w_c}\right)^3\right] e^{-C_2 \frac{v_{c,i}-f_{ct}}{w_c}} - \frac{v_{c,i} - f_{ct}}{w_c}\left(1+C_1^3\right)e^{-C_2}\right\} \tag{7.6}$$

where f_{ct} is the maximum concrete tensile strength, E_c is the Young's modulus of concrete, w_c is the maximum crack width, which is adopted as $160\mu m$. C_1 and C_2 are empirical parameters obtained from Cornelissen et al. (1985) and are equal to *3* and *6.93* respectively.

With stress and deformation profiles available, it is now possible to write force equations for the crack region:

$$F_{com} = b\int_0^x \sigma dy \tag{7.7}$$

$$F_{ten} = b\int_x^{(h-x)} \sigma dy \tag{7.8}$$

where F_{com} and F_{ten} are total compressive and tensile force respectively. For equilibrium, there must be no net force between the compressive and tensile forces:

$$F_{com} + F_{ten} = 0 \tag{7.9}$$

It is therefore safe to assume that if there is a net force, there is an error in the estimated neutral axis depth, x, and x needs to be adjusted. To achieve this, error, ε_r, is defined as:

$$\varepsilon_r = \frac{F_{com} + F_{ten}}{\sqrt{F_{com}^{\ 2} + F_{ten}^{\ 2}}} \tag{7.10}$$

and x can then be adjusted by adding the product of x and 1% of ε_r:

$$x_{n+1} = x_n\left(1 + \frac{\varepsilon_r}{100}\right) \tag{7.11}$$

The deformation, stress profile and forces are then recalculated using the new neutral axis depth, x, and the process is repeated until a satisfactory level of accuracy is achieved. Then, the contribution of each strip to the bending moment in the beam can be calculated and a moment profile is obtained:

$$\mu_i = \sigma_{c,i}(y_i - x) \tag{7.12}$$

where μ_i is the moment contribution from strip i. The total bending moment, M, can be attained by integrating the moment profile across the whole section:

$$M = \int_0^h \mu dy \tag{7.13}$$

As plane sections remain plane, the rotation, θ, of the beam can easily be obtained:

$$\theta = \tan^{-1}\left(\frac{v_x}{h-x}\right) \approx \frac{v_x}{h-x} \tag{7.14}$$

A repeat of the above procedures using different v_x would allow a full moment rotation curve to be plotted.

7.3.3 REINFORCED CONCRETE

This analytical model can easily be extended to incorporate reinforcement in concrete. In calculating the deformation profile (equation 7.4) and stress profile (equation 7.5, 7.6), the deformation in the reinforcement, v_s, needs be incorporated and can be obtained using the following equation:

$$v_s = \frac{d-x}{h-x} v_x \tag{7.15}$$

where d is the depth of reinforcement from top surface of beam. Stress in the reinforcement, σ_s, can then calculated:

$$\sigma_s = \frac{E_s v_s}{h_c} \tag{7.16}$$

where E_s is Young's modulus of steel. The calculation of total tensile force (equation 7.8) now needs to incorporate a tensile force component from reinforcement and the total tensile force becomes:

$$F_{ten} = F_{ten.c} + F_{ten.s} = b\int_{x}^{(h-x)} \sigma dy + \sigma_s A_s \tag{7.17}$$

where A_s is the area of steel reinforcement. Similarly, the component from reinforcement needs to be added in the calculation of bending moment and equation 7.13 becomes:

$$M = M_c + M_s = \int_{0}^{(h-x)} \mu dy + \frac{E_s v_s A_s}{h_c}(d-x) \tag{7.18}$$

7.3.4 SUMMARY OF MODELLING PROCEDURES

The following is a summary of the modelling routine, implemented in Matlab:

1. Divide beam section into 500 strips

2. Give an initial value of neutral axis depth, x
3. Apply deformation in extreme fibre, v_x
4. Adjust deformation accordingly in all strips to obtain a deformation profile using equation 7.4 or 7.15 for plain concrete and reinforced concrete respectively
5. Calculate stress in each strip using the stress deformation curve described before to obtain a stress profile
6. Integrate stress profile using trapezoidal rule and calculate tension and compression forces from the integrated stress profile
7. Calculate error using equation 7.10
8. Update estimate of neutral axis depth using equation 7.11
9. Go to step 4 unless error calculated in line 6 is smaller than ±1%.
10. Calculate final deformation profile using the correct neutral axis depth, x
11. Calculate final stress profile using calculated deformation profile
12. Calculate moment profile using equation 7.12 or 7.18 for plain concrete and reinforced concrete respectively
13. Integrate moment profile to calculate bending moment as in equation 7.13
14. Calculate rotation using equation 7.14
15. Save bending moment and rotation
16. Return to step 3 by increasing applied deformation until required load level is reached

7.4 MODEL VALIDATIONS

To ensure the above crack modelling technique is reasonably accurate, a standard beam as suggested by Ulkjær et. al. (1995) is first considered. The properties of the standard beam are given in table 7.1.

Table 7.1: Geometry and material properties of a standard beam

Property	Value
Beam depth, h	100 mm
Beam width, b	100 mm
Beam length, L	800 mm
Specific fracture energy, G_f	100 Nm^{-1}
Tensile strength, f_{ct}	3 MPa
Modulus of elasticity, E_c	20 GPa

In order for the results to be comparable with the work from Iyengar and Raviraj (2001) and Ulkjær et. al. (1995), bending moment, M and rotation, θ, are expressed in normalised form:

$$M_{norm} = \frac{6M}{f_{ct}h^2b} \tag{7.19}$$

$$\theta_{norm} = \frac{\theta E_c}{h_c f_{ct}} \tag{7.20}$$

Elastic deformation in the beam parts outside the elastic layer is taken into account in the manner described by Iyengar and Raviraj (2001). This gives the total rotation, θ_{total}

$$\theta_{total} = \theta_{norm} + (\gamma - 1)M_{norm} \tag{7.21}$$

where $\gamma = \frac{\beta\lambda}{3k_c}$; $\beta = 1 + \frac{2.85}{\lambda^2} - \frac{0.84}{\lambda^3}$; $\lambda = \frac{L}{h}$ and k_c chosen to be 0.5.

Simulated normalised moment-rotation curve is presented in figure 7.11.

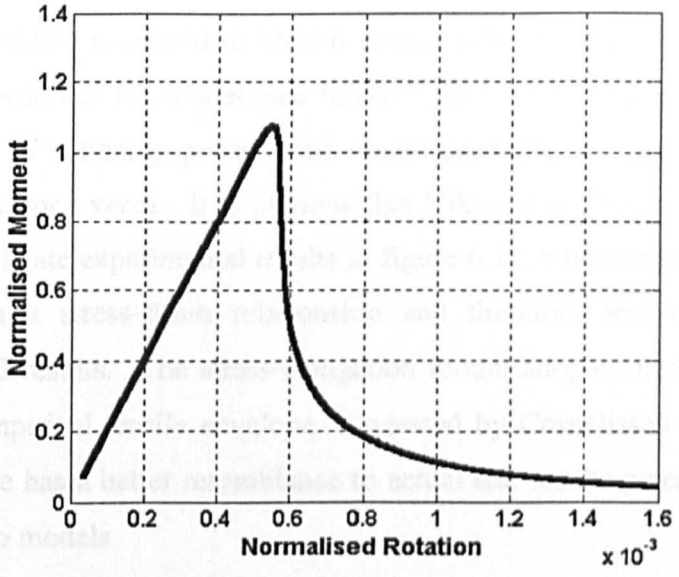

Figure 7.11: Simulated moment-rotation relation using suggested crack modelling technique

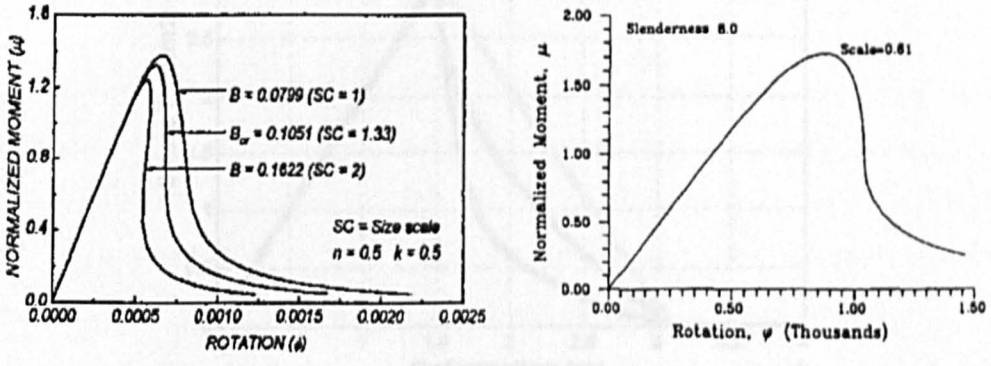

(a) (b)

Figure 7.12: Simulated moment-rotation relation from: (a) Iyengar and Raviraj's model (2001); (b) Ulkjær et. al.'s model (1995)

Figure 7.12 shows the simulated normalised moment-rotation by other researchers. When comparing the results from figure 7.11 with figure 7.12, the simulated results in this study show more similarity with Iyengar and Raviraj's results but less with Ulkjær et. al.'s. This is because Iyengar and Raviraj (2001) used a BCM with a softening portion described by a curvilinear relation, defined by a power law whereas Ulkjær et. al. (1995) simply used a linear softening behaviour in the FCM (see figure 7.13). Simulated results from this study also predicted a relatively lower maximum moment when

compared with both the other simulated results. This is because the maximum moment predicted is related to critical energy release rate, i.e. area under the softening portion of the model (see figure 7.13). As Iyengar's model has the largest area of softening portion, the model predicted the highest maximum moment, and vice versa. It is obvious that Ulkjær's model is unrealistic and does not replicate experimental results in figure 6.12, whereas Iyengar's model is based on a stress-strain relationship and therefore less comparable to experimental results. The stress-elongation model adopted here, however, is based on empirical tensile envelope, suggested by Cornelissen et. at. (1985), and therefore has a better resemblance to actual test results when compared to the other two models.

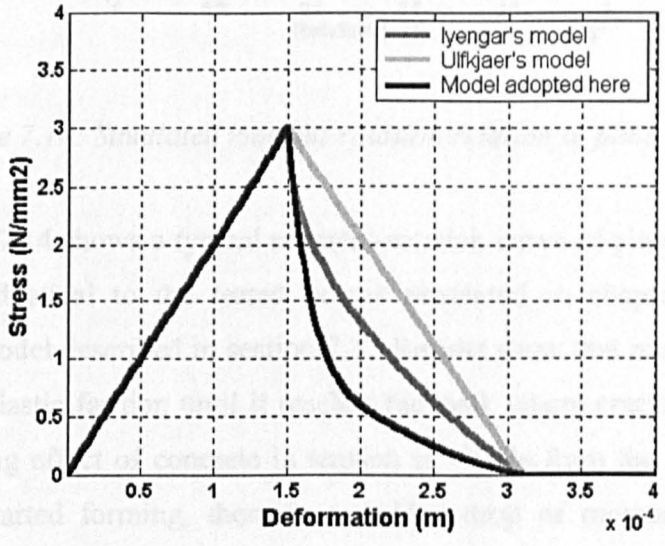

Figure 7.13: Adopted stress-elongation relation for different models

One should note that both groups of researchers have worked extensively on analytical models of cracks in plain concrete beams and focused their work mainly on the size effect. Size effect has not been considered in the model presented in this study. Nevertheless, as the aim of the model is to recreate the nonlinear vibration response, the analytical model suggested in the report can therefore be considered sufficient.

7.5 NUMERICAL RESULTS

7.5.1 PLAIN CONCRETE

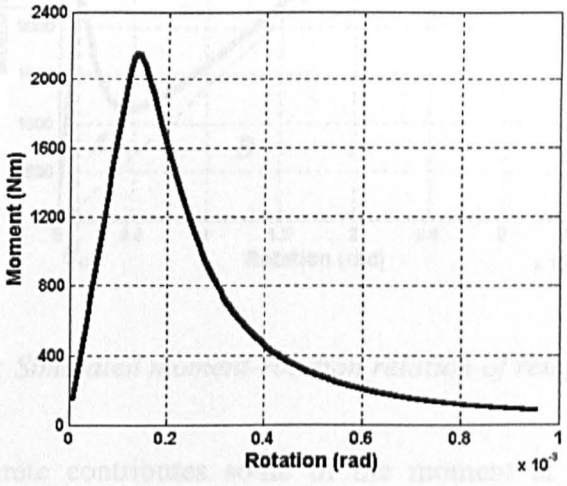

Figure 7.14: Simulated moment-rotation relation of plain concrete

Figure 7.14 shows a typical moment-rotation curve of plain concrete with properties identical to the tested beams presented in chapter 4 using the analytical model described in section 7.3. Results show that moment increases in a linear elastic fashion until it reaches the peak where cracks start to form. The softening effect of concrete in tension is visible from the graph as when the crack started forming, there is a sudden drop of moment, which then gradually decreases further as the deformation increases.

7.5.2 REINFORCED CONCRETE

Figure 7.15 shows a typical moment-rotation curve of reinforced concrete obtained by the analytical crack model. As expected, the incorporation of reinforcement into the model greatly increases the moment capacity of the beam. In fact, it can clearly be seen that the moment rotation relation consists of two parts: 1) plain concrete in area A, whose shape is the same as figure 7.14, and 2) steel reinforcement in area B, which has a linear elastic behaviour, and hence linear moment rotation relation.

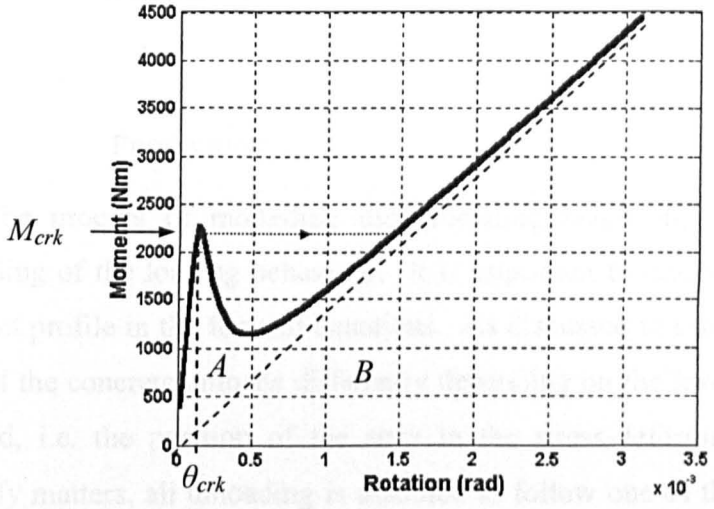

Figure 7.15: Simulated moment-rotation relation of reinforced concrete

Plain concrete contributes some of the moment at lower load levels. When deformation increases, moment increases and once the concrete is cracked, at M_{crk}, its contribution significantly reduces and subsequently becomes negligible as all moment now is contributed by the steel reinforcement. It is also interesting to see that at θ_{crk} where concrete cracks, there is a sudden apparent drop of moment indicating that the crack growth is unstable. However, in reality, the moment would not reduce, instead, there would be a sudden increase of rotation following the dotted arrow shown in figure 7.15, indicating that a crack has formed. This is a snap through effect.

The load at which the first crack can be seen can be easily calculated. Under three-point loading, the cracking load, F_{crk}, is

$$F_{crk} = \frac{4M_{crk}}{l} \tag{7.22}$$

where l is the effective length of beam. Considering the case of beams tested in the experiment where $l=1.62m$, the numerical solution shows that cracks start at 5.7kN. This is in good agreement with experimental results where the first crack is seen at around 6kN.

7.6 UNLOADING

7.6.1 PROCEDURE

The process of modelling the unloading behaviour is similar to the modelling of the loading behaviour. It is important to describe the unloading moment profile in the form of equations. As discussed in section 7.2.2.2, each strip of the concrete unloads differently depending on the level of deformation reached, i.e. the position of the strip in the stress-deformation curve. To simplify matters, all unloading is assumed to follow one of the following five routes:

If $v_{c,i} \leq \frac{f_{ct} h_c}{E_c}$,

$$E_{unloading}(i) = \frac{\sigma_{c,i} h_c}{v_{c,i}} \tag{7.23}$$

Elseif $v_{c,i} \leq \frac{2 f_{ct} h_c}{E_c}$,

$$E_{unloading,i} = \frac{\sigma_{c,i}}{\frac{v_{c,i}}{h_c} - \frac{f_{ct}}{4E_c}} \tag{7.24}$$

Elseif $v_{c,i} \leq \frac{3 f_{ct} h_c}{E_c}$,

$$E_{unloading,i} = \frac{\sigma_{c,i}}{\frac{v_{c,i}}{h_c} - \frac{f_{ct}}{2E_c}} \tag{7.25}$$

Elseif $v_{c,i} \leq \frac{4 f_{ct} h_c}{E_c}$,

$$E_{unloading,i} = \frac{\sigma_{c,i}}{\frac{v_{c,i}}{h_c} - \frac{3 f_{ct}}{4E_c}} \tag{7.26}$$

Else,

$$E_{unloading,i} = \frac{\sigma_{,c,i}}{\frac{v_{c,i}}{h_c} - \frac{f_{ct}}{E_c}} \tag{7.27}$$

By following the above mention rules, is possible that some of the unloading curves having stiffness (gradient) higher than Young's modulus of concrete. It is therefore crucial to also apply the following rule:

If $E_{unloading,i} \geq E_c$,

$$E_{unloading,i} = E_c \tag{7.28}$$

The unloading process is similar to the loading process but is carried out by gradually decreasing the deformation at the extreme end, v_x. While the deformation profile is calculated in exactly the same manner as the loading process, the stress profile, at load case n, is calculated as follow:

If $\sigma_{c,n-1,i} \geq \frac{E_c v_{c,i}}{h_c}$,

$$\sigma_{c,n,i} = \sigma_{c,n-1,i} + E_{unloading} \Delta v_{c,i} \tag{7.29}$$

Else,

$$\sigma_{c,n,i} = \sigma_{c,n-1,i} + E_c \Delta v_{c,i} \tag{7.30}$$

where

$$\Delta v_{c,i} = v_{c,n,i} - v_{c,n-1,i} \tag{7.31}$$

The *if-else* statement is to incorporate the joining of the unloading curve to the original stress deformation curve in compression region. The rest of the

procedure of the unloading process is in the same manner as the loading process.

7.6.2 NUMERICAL RESULTS

Figure 7.16 shows a typical moment-rotation curve of reinforced concrete with increasing deformation, followed by decreasing deformation, obtained by the analytical crack model. As expected, the unloading curve does not pass through the origin, just as the adopted stress-deformation curve. However, unlike the stress-deformation curve, even though each strip of the model unloads in a bilinear fashion, a full combination of strips produces a smooth unloading curve.

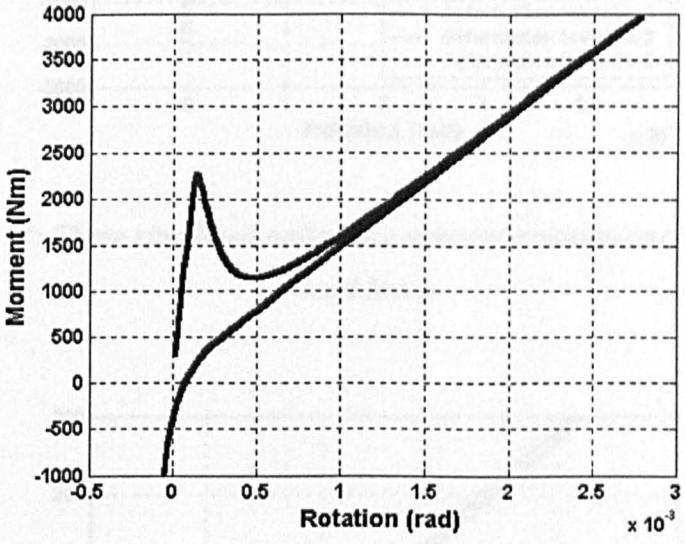

Figure 7.16: Simulated loading/unloading moment-rotation curve of reinforced concrete

Figure 7.17 shows three sets of loading and unloading curves, all loaded to different levels. It can be seen from the figure that all three unloading curves started on the same gradient and end at a similar gradient. However, the numerical results show that the higher the reinforced concrete beam is loaded, the less steep it is when it cuts through M=0 and the higher the residual rotation. During a vibration test, as the magnitude of excitations are normally

very small, it is the region of the unloading curve with very small magnitude which is of interest. In other words, the moment and rotation of the beam in a vibration cycle should follow only a minute section of the unloading curve. By shifting the unloading curve to the left by the amount of residual rotation at $M=0$, all unloading curves pass through the origin as shown in figure 7.18.

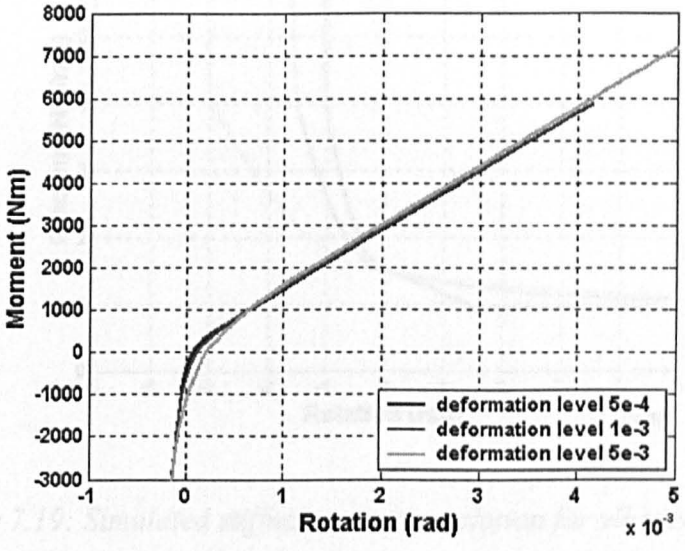

Figure 7.17: Three simulated unloading moment-rotation curves at different load levels

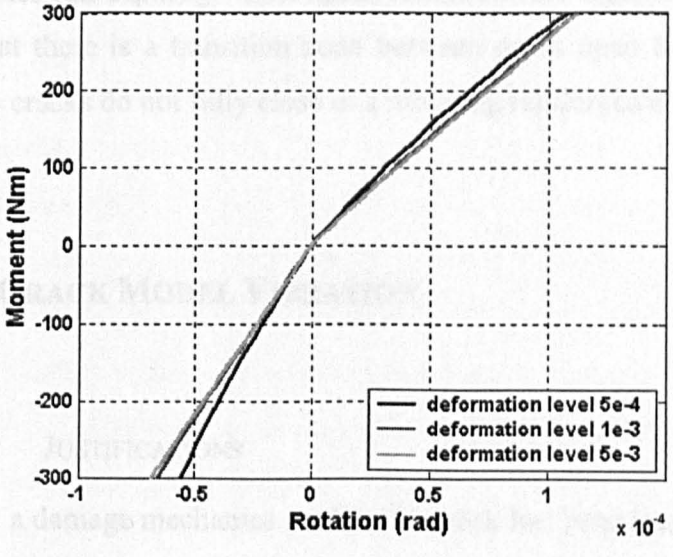

Figure 7.18: Simulated moment-rotation relations for vibration analysis

Since the gradient of the unloading moment rotation curve gives bending stiffness, differentiating the unloading moment rotation curve would obtain a relation of bending stiffness across a vibration cycle (see figure 7.19).

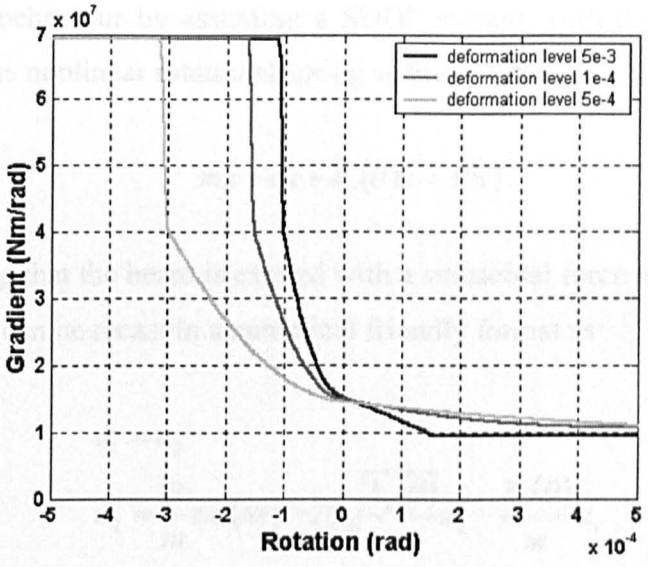

Figure 7.19: Simulated stiffness-rotation relation for vibration analysis

The curve has a similar shape to the mixture of hyperbolic tangent and exponential models discussed in chapter 5. One key thing to note from the figure is that when vibrating, i.e. for small rotations, the bending stiffness hardly reaches full capacity. This again reinforces the arguments from earlier chapters that there is a transition zone between crack open and crack closed and that the cracks do not fully close in a vibrating reinforced concrete beam.

7.7 CRACK MODEL VIBRATION

7.7.1 JUSTIFICATIONS

So far, a damage mechanics model of a crack has been introduced. Based on strain softening behaviour of concrete material under tension, the crack model correctly simulated that there is a transition zone between crack open and crack closed and that cracks do not fully close in a vibrating reinforced

concrete beam. In this section, a further investigation of the vibration characteristic of the crack model is presented. This is carried out by assuming the crack model as a nonlinear rotational spring, with a stiffness that varies with rotation in the fashion shown figure 7.19. It is then possible to study the crack model behaviour by assuming a SDOF system, with the stiffness term replaced by the nonlinear rotational spring stiffness term:

$$m\ddot{u} + c\dot{u} + k_c(\theta)u = P(t) \tag{7.32}$$

Assuming that the beam is excited with a sinusoidal force at frequency, ω, equation 7.26 can be recast in a numerical friendly format as:

$$\begin{aligned} \dot{u}_1 &= u_2 \\ \dot{u}_2 &= \frac{P}{m}\sin(\omega t) - 2\xi\sqrt{\frac{k_c(\theta)}{m}}u_2 - \frac{k_c(\theta)}{m}u_1 \end{aligned} \tag{7.33}$$

where $k_c(\theta)$ is stiffness interpolated linearly from figure 7.18. m is the model mass of the system. The damping ratio, ξ, used is 0.05, which is a typical value of reinforced concrete material.

7.7.2 METHODOLOGY

The methodology used in investigating the dynamic behaviour of the crack model is very similar to the characterisations of phenomenological models discussed in chapter 5. The crack model is excited using a single sinusoidal excitation at a frequency close to the fundamental frequency. A sinusoidal excitation at a slightly higher frequency is then applied. This is continued until a full response of the mode is covered. The whole process is then repeated using a higher excitation magnitude. Amplitude of the response time history of each excitation frequency at each excitation magnitude is recorded. The detailed procedure can be found in section 5.2.2.

7.7.3 NUMERICAL RESULTS

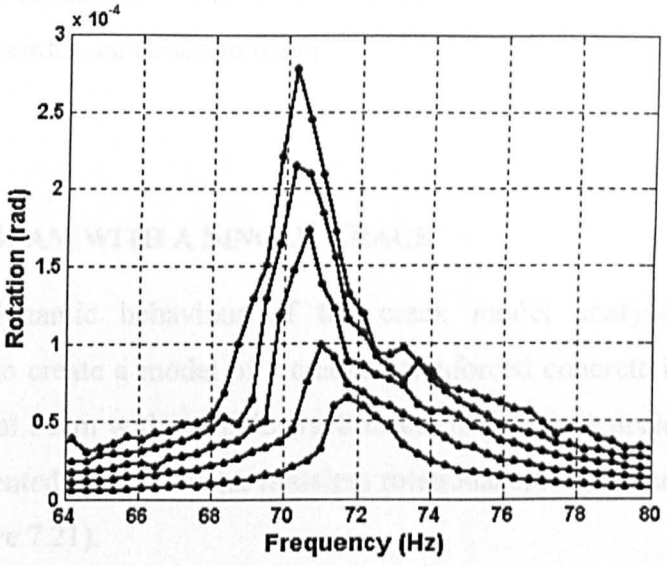

Figure 7.20: Variation of excitation frequency with response

Figure 7.20 shows a simulated response frequency curve for the analytical crack model, in which a marked softening behaviour is observed. One should note that the value of the resonant frequency shown in figure 7.20 should not be compared with the resonant frequency of the experimental results. This is because the resonant frequency here is calculated simply from the stiffness of the crack and modal mass in which the stiffness of the crack is an arbitrary value that does not carry any physical meaning. However, it is possible to compare the relative drop of frequencies with varying amplitude of excitations. There is a drop of 1.8Hz, which is equivalent to 2.56% of fundamental frequency, between the smallest and the largest amplitude of excitation applied. This is relatively higher than those observed in the tested beams presented in chapter 4 (less than 1.9%). This shows that the crack model behaves more nonlinearly in vibration than the test beams.

These results from the vibration analysis of crack model were quite encouraging. It is expected that the crack model would show a higher degree of nonlinearity, typified by softening behaviour. This is because the model is only representing a crack in a reinforced concrete beam. Although the crack model itself is nonlinear, the rest of the beam is very much linear and this

linearity of the beam would mask the nonlinearity of the crack. As a result, a much lower nonlinearity would be observed in the overall vibration response of the cracked reinforced concrete beam.

7.8 BEAM WITH A SINGLE CRACK

With dynamic behaviour of the crack model analysed, it is now appropriate to create a model of a cracked reinforced concrete beam. Here, a 2-dimensional beam with a single crack in the mid span is presented, with the crack represented by a nonlinear massless rotational spring discussed in section 7.7 (see figure 7.21).

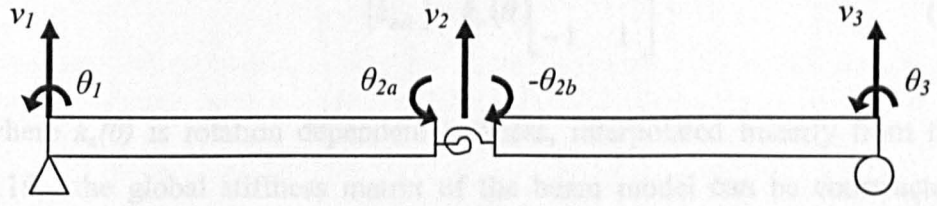

Figure 7.21: Beam with a single crack a mid span model

7.8.1 CONSTRUCTION OF STIFFNESS, MASS AND DAMPING MATRICES

To reduce computational cost, the beam model is assumed to be comprised of only two beam elements, which are represented by corresponding stiffness and mass matrices. From almost any structural analysis textbook, one can find that the stiffness and mass matrices (assuming consistent mass matrix), of a beam element, *[k]* and *[m]*, are as follows:

$$[k]=\begin{bmatrix} k_{11} & k_{12} & k_{13} & k_{14} \\ k_{21} & k_{22} & k_{23} & k_{24} \\ k_{31} & k_{32} & k_{33} & k_{34} \\ k_{41} & k_{42} & k_{43} & k_{44} \end{bmatrix} = \frac{EI}{L^3}\begin{bmatrix} 12 & 6L & -12 & 6L \\ 6L & 4L^2 & -6L & 2L^2 \\ -12 & -6L & 12 & -6L \\ 6L & 2L^2 & -6L & 4L^2 \end{bmatrix} \quad (7.34)$$

$$[m]=\begin{bmatrix} m_{11} & m_{12} & m_{13} & m_{14} \\ m_{21} & m_{22} & m_{23} & m_{24} \\ m_{31} & m_{32} & m_{33} & m_{34} \\ m_{41} & m_{42} & m_{43} & m_{44} \end{bmatrix} = \frac{\overline{m}L}{420}\begin{bmatrix} 156 & 22L & 54 & -13L \\ 22L & 4L^2 & 13L & -3L^2 \\ 54 & 13L & 156 & -22L \\ -13L & -3L^2 & -22L & 4L^2 \end{bmatrix} \tag{7.35}$$

A normal two-dimensional beam model constructed using two beam elements would have a total of six degrees of freedom, i.e. displacement, (v_1, v_2, v_3), and rotation, (θ_1, θ_2, θ_3), at each ends of the beam element. Inclusion of the rotational spring uncouples the rotation connection at the mid-span and therefore degree of freedom θ_2 has been divided into two separate degrees of freedom, θ_{2a} and θ_{2b}. By assuming the stiffness matrix of the rotational spring, k_{crk}, as

$$[k_{crk}]=k_c(\theta)\begin{bmatrix} 1 & -1 \\ -1 & 1 \end{bmatrix} \tag{7.36}$$

where $k_c(\theta)$ is rotation dependent stiffness, interpolated linearly from figure 7.19, the global stiffness matrix of the beam model can be constructed as below:

$$[K]=\begin{bmatrix} k_{11} & k_{12} & k_{13} & k_{14} & 0 & 0 & 0 \\ k_{21} & k_{22} & k_{23} & k_{24} & 0 & 0 & 0 \\ k_{31} & k_{32} & k_{33}+k_{11} & k_{34} & k_{12} & k_{13} & k_{14} \\ k_{41} & k_{42} & k_{43} & k_{44}+k_{crk,11} & k_{crk,12} & 0 & 0 \\ 0 & 0 & k_{21} & k_{crk,21} & k_{22}+k_{crk,22} & k_{23} & k_{24} \\ 0 & 0 & k_{31} & 0 & k_{32} & k_{33} & k_{34} \\ 0 & 0 & k_{41} & 0 & k_{42} & k_{43} & k_{44} \end{bmatrix} \tag{7.37}$$

As the rotational spring is defined as zero mass, the global mass matrix, *[M]*, constructed in a similar fashion, is

$$[M]=\begin{bmatrix} m_{11} & m_{12} & m_{13} & m_{14} & 0 & 0 & 0 \\ m_{21} & m_{22} & m_{23} & m_{24} & 0 & 0 & 0 \\ m_{31} & m_{32} & m_{33}+m_{11} & m_{34} & m_{12} & m_{13} & m_{14} \\ m_{41} & m_{42} & m_{43} & m_{44} & 0 & 0 & 0 \\ 0 & 0 & m_{21} & 0 & m_{22} & m_{23} & m_{24} \\ 0 & 0 & m_{31} & 0 & m_{32} & m_{33} & m_{34} \\ 0 & 0 & m_{41} & 0 & m_{42} & m_{43} & m_{44} \end{bmatrix} \tag{7.38}$$

For the construction of damping matrices, Rayleigh damping has been adopted for the model in which the damping is proportional to a combination of mass and stiffness matrices, as shown as below:

$$[C]=a_0[M]+a_1[K] \tag{7.39}$$

where a_o and a_1 are the proportionality constants. The proportionality constants are calculated using the following formula (Clough and Penzien, 1993):

$$\begin{Bmatrix} a_0 \\ a_1 \end{Bmatrix}=\frac{2\xi}{\varpi_m+\omega_n}\begin{Bmatrix} \omega_m\omega_n \\ 1 \end{Bmatrix} \tag{7.40}$$

where ξ is the damping ratio, assumed to be 0.05, ω_m is generally taken as the fundamental frequency of the system and ω_n is set among the higher frequencies of the modes that contribute significantly to the dynamic response, in which the resonant frequency for mode 2 of the system has been be taken for this case.

7.8.2 DYNAMIC ANALYSIS

With mass, stiffness and damping matrices constructed, it is then possible to perform a dynamic analysis for an undamaged reinforced concrete beam. Similar to a SDOF system, equations of motion can be written as

$$[M]\{\ddot{u}\}+[C]\{\dot{u}\}+[K]\{u\}=\{F(t)\} \tag{7.41}$$

Assuming the beam is excited with a sinusoidal force at frequency, ω, and for the ease of numerical analysis, equation 7.35 can be rewritten as

$$\begin{Bmatrix} \dot{u}_1 \\ \dot{u}_2 \end{Bmatrix} = \begin{bmatrix} 0 & I \\ -[M]^{-1}[K] & -[M]^{-1}[C] \end{bmatrix} \begin{Bmatrix} u_2 \\ u_1 \end{Bmatrix} + \begin{Bmatrix} 0 \\ [M]\{F\sin(\omega t)\} \end{Bmatrix} \quad (7.42)$$

As the case in analytical crack model, the beam is set to be excited with increasing frequencies around first mode and with different amplitudes, where the detailed routine is presented in section 5.2.2.

7.8.3 NUMERICAL RESULTS

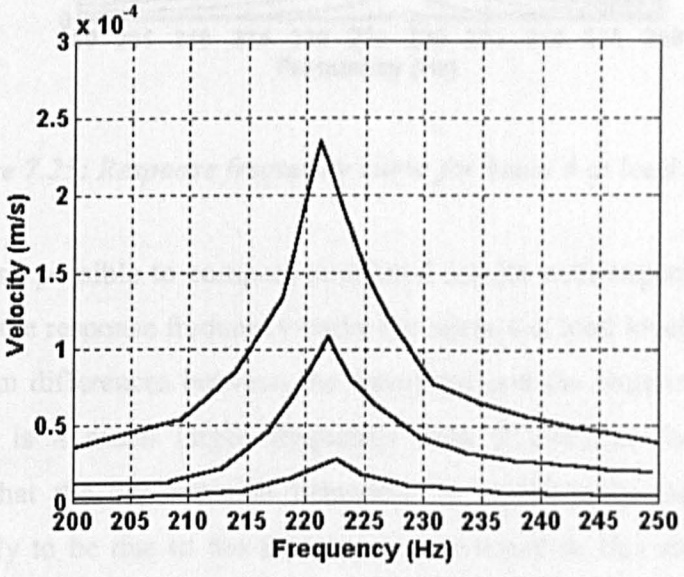

Figure 7.22: Simulated response frequency relation for a beam with a crack

As discussed in section 7.7.3, simulated responses for the beam model are expected to show lesser softening behaviour than the response of the crack model (see figure 7.20). This is because linearity of beam element models has significantly masked the nonlinearity of the crack model and hence showing much lower overall nonlinear features. A typical set of simulated response frequency curves for a beam model with a crack at mid span is shown in figure 7.22. The simulated results appear to behave in a linear fashion. However, a close examination shows that there is a very slight softening effect. In fact, in

the case shown in figure 7.22, there is a frequency drop of 1.4Hz (222.7Hz - 221.3Hz) between the smallest and the largest amplitude of excitation applied.

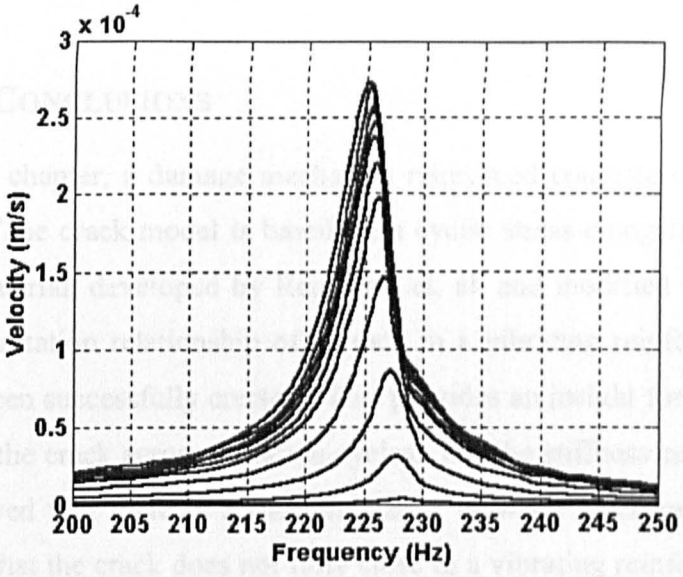

Figure 7.23: Response frequency curve for beam 4 at load level 22

It is also possible to compare simulated results with experiment. Figure 7.23 shows the response frequency curve for beam 4 at load level 22kN. There are two main differences between the simulated and the experimental results. First, there is a much larger frequency drop (3.6Hz) in the experiment, indicating that the experimental behaviour is significantly more nonlinear. This is likely to be due to the fact that beams tested in this study showed a distributed crack pattern, i.e. more than one crack, whereas the beam model here only incorporated a single crack. An increase of number of cracks indicates an increase of nonlinear spring and hence an increase of degree of nonlinearity. Second, experimental results show a slightly narrower peak. This is likely to be due to the choice of damping. It is thought that damping ratio of 1% used for the beam model in this study could have slightly overestimated the damping of the tested beams. It should be noted that as the beam model only consists of two beam elements, the point of excitation of the model was located at the centre of the beam whereas in the experiment, it was located closer to the node of the first mode (see figure 3.6). As a result of this,

although the input forces on both occasions are the same, the magnitude of response should not be compared.

7.9 CONCLUSIONS

In this chapter, a damage mechanics reinforced concrete crack model is presented. The crack model is based on a cyclic stress-elongation relation of concrete material, developed by Reinhardt et. al. and modified by the author. A moment rotation relationship of a crack in a vibrating reinforced concrete beam has been successfully created. This provides an insight for the change of stiffness of the crack across vibration cycles. For the stiffness curve, the crack model showed that there is a transition zone between crack open and crack closed and that the crack does not fully close in a vibrating reinforced concrete beam.

Vibration analysis shows that the response frequency curve of the crack model exhibits a marked softening behaviour. The degree of nonlinearity of the crack model is relatively higher than responses observed in the experiment presented in chapter 4. Incorporating the crack model, represented by a rotational spring, into a beam model with a single crack, limited softening behaviour was observed. It was, however, generally less marked then results observed from the experiment. It is possible to conclude from the study that strain-softening behaviour of concrete under tensile force caused cracked reinforced concrete beams to vibrate in a nonlinear fashion, exhibited as a softening spring behaviour. As the beam model only consists of a single crack whereas tested beams as presented in chapter 4 comprise more than one crack, full comparisons between two were therefore impossible.

CHAPTER 8

CONCLUSIONS AND FURTHER WORK

8.1 CONCLUSIONS

A literature review has revealed that although a great deal of work in investigating the possibility of using linear vibration techniques to detect damage in bridges has been carried out for the past 25 years, there are still some major concerns, such as poor sensitivity of modal parameters to damage, requirement of baseline data, need of measuring excitation force and environmental effects. The existence of nonlinearity in the vibration characteristics when the structure is damaged further complicates the problem and causes doubts on the feasibility of applying these techniques on actual structures. Understanding of the nonlinear behaviour is therefore crucial. An investigation of the nonlinearity found in the vibration characteristics of reinforced concrete beams has been presented here.

The experimental work presented here has confirmed the non-linear behaviour observed during previous experimental studies (Eccles 1999 and Tan et. al., 2001) and has shown that this non-linear behaviour has the characteristics of a softening spring. The study of the softening gradient has shown that the level of non-linearity increases with damage up to a certain

moderate damage state, above which the softening gradient reduces to a lower level then remains constant with further damage. This characteristic is in agreement with the findings from restoring force surface analysis in a qualitative sense.

Using the restoring force surface method it has been possible to obtain experimental force deflection curves to model the non-linear vibration behaviour of the damaged reinforced concrete beams. Although the restoring force displacement curve from each damage level appears to behave in a bilinear fashion, the overall drop of stiffness with increasing damage level (see figure 4.19) confirms that a bilinear crack model would not be sufficient to replicate the observed vibrating cracked reinforced concrete beams' behaviour. The results also showed that the crack does not fully close in a vibrating cracked reinforced concrete beam. It is therefore important to investigate in detail the stiffness relationship of the transition from crack open to crack closed.

The finding that bilinear models are not capable of replicating the dynamic behaviour of reinforced concrete were confirmed by investigating phenomenological crack models suggested by different researchers. Results also indicate that the dynamic behaviour of the hyperbolic tangent model suggested by Owen et. al (1999) shows good resemblance to the observed experimental behaviour phenomenologically. As a result, the hyperbolic tangent model has been used as the basis for an empirical model. Although further investigation is needed, simulated results from the empirical model show good agreement with observed experimental behaviour.

Another reason for creating the empirical model is to investigate the possibility of using the nonlinear behaviour for structural health monitoring. A possible damage indicator has been studied and stiffness ratio, μ, is an obvious damage indicator. Using the empirical crack model proposed, the author suggested a means of estimating the stiffness ratio, provided a restoring force surface could be drawn. The author further suggested a possible routine for

structural health monitoring for reinforced concrete beams and stressed that it could easily be extended for more complicated structures, like bridges. However, the suggested structural health monitoring procedure requires the measuring of excitation force. This proves to be a problem for implementing this technique to real structures. Further investigation on removing the need of measurement of excitation force would greatly increase the usability of the technique.

Possible mechanisms that may cause the observed nonlinearity were then studied and discussed. By incorporating a strain softening behaviour of concrete material developed by Reinhardt et. al. and modified by the author, a damage mechanics reinforced concrete crack model has been created. The crack model replicated a transition zone between crack open and crack close and also the fact that crack does not fully close in a vibrating reinforced concrete beam.

When the crack model, represented by a rotational spring, was incorporated into a beam model, limited nonlinear behaviour was observed, exhibited by a softening response frequency curve. The nonlinearity observed was generally less marked then results from the experiment. It is possible to conclude from the study that strain-softening behaviour of concrete under tensile force caused cracked reinforced concrete beams to vibrate in a nonlinear fashion, exhibited as a softening spring behaviour. As the beam model only consists of a single crack whereas tested beams as presented in chapter 4 comprise more than one cracks, full comparisons between the two were impossible.

To summarise, the major contributions of this study are:

- Confirmed the presence of nonlinearity and showed a characteristic of softening response, i.e. decreasing peak frequencies with increasing excitation magnitudes.

- The nonlinear behaviour is of its greatest when reinforced concrete beam is lightly damaged. Degree of nonlinearity, defined using softening gradient, decreases and stays relatively constant with further increase of overloading damage. This is suggested to be due to the yielding of reinforcement.

- Experimental restoring force deflection relations of the vibrating reinforced concrete beams showed that there is an overall drop of stiffness across the vibration cycles with increasing damage levels. This confirms that a bilinear crack model is insufficient to replicate vibrating cracked reinforced concrete beams' behaviour.

- Showed, from the restoring force deflection curves, that cracks in vibrating reinforced concrete beams do not fully close.

- Investigated the suitability of different phenomenological stiffness models and confirmed that the consideration of transitions between crack open and crack closed are required.

- Proposed an empirical model for vibrating cracked reinforced concrete beams. Based on the empirical model, a structural health monitoring routine is suggested.

- Presented a damage mechanics model for cracked reinforced concrete beam based on strain softening behaviour of concrete. It has been shown that strain softening behaviour of concrete contributes some of the observed nonlinear behaviour.

8.2 FURTHER WORK

As all of the reinforced concrete beams studied here have failed predominantly by bending, all cracks grow almost vertically upward from the bottom surface of the beam. It would be interesting to see if a different configuration of cracks would exhibit a similar type of nonlinearity in the vibration characteristic. Therefore, a study of the effect of different damage mechanisms on the nonlinearity in vibration characteristics should be investigated.

It is also suggested that restoring force surface system identification technique be applied on more realistic structures. As it is crucial to assume that each mode of the structure is a SDOF system, the fact that complex structures have closely-spaced modes will complicate the problem. On another matter, in this study, the restoring force surface technique has been utilised simply for stiffness study. There is no reason why the same technique would not be possible to extend to the study of damping.

The reliability of the suggested possible health monitoring procedure can be enhanced by carrying out more tests on different configurations of reinforced concrete beam structures. For the suggested procedure to be able to implement on real structures, investigations of possible ways of removing the reliance of the input excitation are required.

On the issue of analytical crack modelling, studies of inclusions of hysteresis behaviour of concrete under cyclic loading into the model are required. An analytical crack model based on a multi-axial relationship should also provide a better representation of cracks in reinforced concrete structures. Furthermore, a static load test of measuring moment rotation relationship could be performed. This would provide a comparison of the model with experimental results.

It is also possible to extend the suggested beam model in chapter 7 to incorporate distributed cracks. A reinforced concrete beam model with distributed crack is a more realistic model as most reinforced concrete beams damaged by overloading show a form of distributed cracks. This can be carried out by increasing the number of beam element segments in the beam model and by joining the beam elements with rotational springs as discussed in chapter 7 at the intended crack locations. Figure 8.1 shows an example of reinforced concrete beam model with distributed cracks.

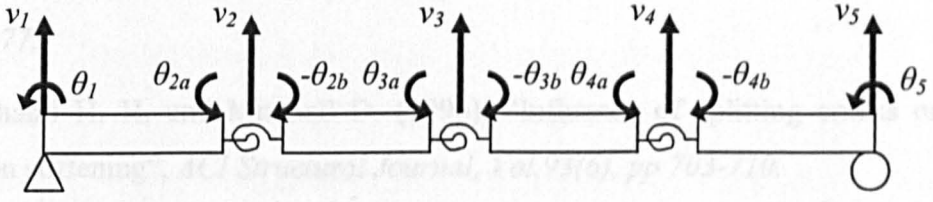

Figure 8.1: Beam model with distributed cracks

Additional work is required to assess the possible nonlinear damage mechanisms discussed in chapter 6. In this study, the strain softening behaviour of concrete under tensile force has been used to represent a host of different possible nonlinear mechanisms for the modelling process. In order to improve understanding, each of these possible nonlinear mechanisms should also be investigated separately.

REFERENCES

Abdel Wahab M. and De Roeck G. (1997), "Effect of temperature on dynamic system parameters of a highway bridge", *Structural Engineer International, Vol. 4, pp 266-270.*

Abraham O. N. L. and Brandon J. A. (1995), "The modelling of the opening and closure of a crack", *ASCE Journal of Vibration and Acoustics, Vol. 117, pp 370-377.*

Abrishami H. H. and Mitchell D. (1996), "Influence of splitting cracks on tension stiffening", *ACI Structural Journal, Vol.93(6), pp 703-710.*

Actis R. L. and Dimarogonas A. D. (1989), "Non-linearеffects due to closing cracks in vibrating beams", *ASME Design Engineering Division Publication, DE-Structural Vibration and Acoustics, Vol. 18(3), pp 99-104.*

Adams D. A. and Allemang R. J. (1998), "Survey of nonlinear detection and identification techniques for experimental vibrations", *Proceedings on the 23rd International Seminar on Modal Analysis, September 1998, Lueven, Belgium.*

Bahn B. Y. and Hsu C. T. T. (1998), "Stress-strain behaviour of concrete under cyclic loading", *ACI Materials Journal, Vol.955, No.2, pp 178-193.*

Bazant Z. P. and Oh B. H. (1983), "Crack band theory for fracture of concrete", *Materials and Structures, Vol. 16, No. 93, pp 155-177.*

Bazant Z. P. and Prat P. C. (1988a), "Microplane model for brittle-plastic material. I: Theory", *ASCE Journal of Engineering Mechanics, Vol. 114, No. 10, pp 1672-1687.*

Bazant Z. P. and Prat P. C. (1988b), "Microplane model for brittle-plastic material. II: Verification", *ASCE Journal of Engineering Mechanics, Vol. 114, No. 10, pp 1689-1702.*

Bazant Z. P., Caner F. C., Adley M. D. and Akers S. A. (2000), "Microplane Model M4 for Concrete: I. Formulation with Work-Conjugate Deviatoric Stress", *ASCE Journal of Engineering Mechanics, Vol. 126(9), pp 994-953.*

BCI (1997), British Standard 8110: Structural Use of Concrete, Part 1. Code pf Practice for Design and Construction.

BD 21/93 (Design manual for roads and structures 3.4.3.), *The Assignment of Highways Bridges and Structures, Highways Agency, UK, January 1993.*

BD 44/95 (Design manual for roads and structures 3.4.14.), *The Assignment of Highways Bridges and Structures, Highways Agency, UK, January 1995.*

BD 63/94 (Design manual for roads and structures 3.1.4.), *Inspection of highways Structures, Highways Agency, UK, October 1994.*

Bendat J. S. (1998), Nonlinear Systems Techniques and Applications, *John Wiley & Sons, New York, USA.*

Bendat J. S. and Piersol A. G. (1986), Random data: analysis and measurement procedure, *second edition, John Wiley & Sons, New York, USA.*

Billing J.R. (1984), "Dynamic loading and testing of bridges in Ontario", *Canadian Journal of Civil Engineering, Vol. 11, pp 833-843.*

Blakey F. A. and Baresford F. D. (1962), "Discussion of crack propagation and the fracture of concrete by M. E. Kaplan", *Journal of American Concrete Institution, Vol. 59, pp 919-923.*

Brandon J. A. and Mathias M. H. (1995), "Complex oscillatory behaviour in a cracked beam under sinusoidal excitation", *Journal of Sound and Vibration, Vol. 186(2), pp 350-354.*

Brandon J. A. and Richards J. (1989), "A conjecture on the interface mechanics fractures based on the interpretation of impulse tests", *Proceeding of the Institute of Mechanical Engineering in Medicine, Vol. 203(4), pp 203-205.*

Brandon J. A. and Sudraud C. (1998), "An experimental investigation into the topological stability of a cracked cantilever beam", *Journal of Sound and Vibration, Vol. 211(4), pp 555-569.*

Brincker R., Anderson P., Kirkegaard P. H. and Ulfkjaer J. P. (1995), "Damage detection in laboratory concrete beams", *Proceedings of the 13th International Modal Analysis Conference, Nashville, Tennessee, USA, pp 661-667.*

British Standards 8110 –1:1997, Structural Use of Concrete – Part 1: Code of practice for design and construction, *British Standards Institutions, United Kingdom.*

Broek D. (1988), The practical use of fracture mechanics, *Kluwer Academic Publishers, The Netherlands.*

Bueckner H. F. (1958), "The propagation of cracks and the energy of elastic deformation", *Trans. ASME, Vol 80, pp 1225-1229.*

Caner F. C. and Bazant Z. P. (2000), "Microplane model M4 for concrete: II. algorithm and calibration", *ASCE Journal of Engineering Mechanics, Vol. 126(9), pp 954-963.*

Carol I., Jirasek M. and Bazant Z. P. (2001), "A thermodynamically consistent approach to microplane theory . Part I: Free energy and consistent microplane stresses", *International Journal of Solods and Structures, Vol. 38, No. 17, pp 2921-2931.*

Carol I., Lopez C. M. and Roa O. (2001), "Micromechanical analysis of quasi-brittle materials using fractruresd-based interface elements", *International Journal for Numerical Methods in Engineering, Vol. 55, No. 1-2, pp 193-215.*

Casas J. R. and Aparicio A. C. (1994), "Structural damage identification from dynamic test data", *ASCE Journal of Structural Engineering, Vol. 120(8), pp 2437-2450.*

Cawley P. and Adams R. D. (1979), "The location of defects in structures from measurement of natural frequencies", *Journal of Strain Analysis, Vol. 6(2), pp 34-37.*

Ceriolo L. and Di Tommaso A. (1998), "Fracture mechanics of brittle materials: a historical point of view", *Proceedings of 2nd International PhD Symposium in Civil Engineering, Budapest, Hungary.*

Chaudhari T. D. and Maiti S. K. (1999), "Modelling of transverse vibration of beam of linearly variable depth with edge crack", *Engineering Fracture Mechanics, Vol. 63, pp 425-445.*

Cheng S. M., Wu X. j. and Wallace W. (1999), "Vibrational response of a beam with a breathing crack", *Journal of Sound and Vibration, Vol. 225(1), pp 201-208.*

Chowdhury S. H., Loo Y. C. and Fragomeni S. (2000), "Damping formulae for reinforced and partially prestressed concrete beams", *Advances in Structural Engineering, Vol. 3(4), pp.327-335.*

Chu Y. C. and Shen M. H. H. (1992), "Analysis of forced bilinear oscillators and the application to cracked beam dynamics", *AIAA journal, Vol. 30(10), pp 2512-2519.*

Clark R., Dover W. D. and Bond L. J. (1984), "The effect of crack closure on the reliability of NDT predictions of crack size", *NDT International, Vol. 20, pp 269-275.*

Concrete Bridge Development Group (2002), *Guide to testing and monitoring the durability of concrete structures – technical guide 2, The Concrete Society, UK.*

Cornelissen H. A. W. (1986), "Experiments and theory for the application of fracture mechanics to normal and lightweight concrete", *Fracture Toughness and Fracture Energy of Concrete, F. H. Wittman (ed.), Elsevier, Amsterdam, pp 565-575.*

Creed S. G. (1987), "Assessment of large engineering structures using data collected during in-service loading', *Structural Assessment, Buttersworths, London, pp 55-62.*

Crespo P., Ruotolo R and Surace C. (1996), "Nonlinear modelling of a cracked beam", *Proceedings of 14th International Modal Analysis Conference, USA, pp 1017-1022.*

Das C. P., Davidson N. C. and Colla C. (1995), "Potential applications of non-destructive testing methods for bridge assessment and monitoring", *presented in IStructE Seminar, Analysis and Testing Bridges,, 26th April.*

Das P. C., Owen J. S., Eccles B. J., Woodings M. A. and Choo B. S. (1997), "The role of dynamic testing in the assessment of bridges", *76th Annual Meeting of the Transport Research Board, Washington D. C., USA.*

Dimarogonas A. D. (1996), "Vibration of cracked structures: A state of the art review", *Engineering Journal of Fracture Mechanics, Vol. 55(5), pp 831-857.*

Doebling S. W. (1995), "Measurement of structural flexibility matrices for experiments with incomplete reciprocity", *PhD Dissertation, Department of Aerospace Engineering Science, University of Colorado, Boulder, Colorado, USA.*

Doebling S. W., Farrar C. R., Prime M. B. and Shevitz D. W. (1996), "Damage identification and health monitoring of structural and mechanical systems from changes in their vibration characteristics: a literature review", *Report to Los Alamos National Laboratory, LA-13070-MS, USA.*

Doebling S.W., Farrar C. R., Aktan E., Beck J., Cornwell P., Helmicki, A, Safak, E. and Yao J. (1999), "The state of the art in structural identification of constructed facilities", *Report(draft) by the ASCE Committee on Structural Identification of Constructed Facilities, Los Alamos National Laboratory, Texas, USA, 28 June.*

Donskoy D. M., Ekimov A. E. and Sutin A. M. (2000), "Detection and characterisation of defects with vibro-acoustic modulation technique", *Emerging Technologies in NDT, pp 153-157.*

Eccles B. J. (1999), "The use of non-linear vibrations in the health monitoring of reinforced concrete structures", *PhD thesis, School of Civil Engineering, University of Nottingham, Nottingham, UK.*

Elfgren L. (1989), "Fracture mechanics of concrete structures – from theory to application", *RILEM, Chapman and Hall Limited, London, U.K.*

Eurocode 8: Design provisions for earthquake resistance of structures, *DD ENV1998 : 1996, British Standards Institutions, United Kingdom.*

Farrar C. R., Baker W. E., Bell T. M., Cone K. M., Darling T. W., Duffrey T. A., Eklund A. and Migliori A. (1994), "Dynamic characterisation and damage

detection in the I-40 Bridge over the Rio Grande", *Report to Los Alamos National Laboratory, LA-12767-MS, USA.*

Farrar C. R., Doebling S. W. and Nix D. A. (2001), "Vibration-based structural damage identification", *Philosophical Transactions – Royal Society of London: Mathematical Physical and Engineering Sciences. Vol. 1778, pp 131-150.*

Felber A. J., Ventura C. E. and Steimer S. F. (1993), Queensborough Bridge Ambient Vibration Study, *EDI Experimental Dynamics Ltd.*

Freund L. B. (1998), Dynamic Fracture Mechanics, *Cambridge University Press, Cambridge, UK.*

Friswell M. I. (1992), "A simple non-linear model of a cracked beam", *Proceedings of the 10th International Modal Analysis Conference, San Diego, California, USA, pp 516-521.*

Friswell M. I. and Mottershead J. E. (1995), "Finite Element Model Updating in Structural Dynamics", *Kluwer Academic Publishers, the Netherlands.*

Friswell M. I., Penny J. E. T. and Wilson D. A. L. (1994), "Using vibration data and statistical measures to locate damage in structures", *Modal Analysis: The International Journal of Analytical and Experimental Modal Analysis, Vol. 9(4), pp 239-254.*

Gambarova P. and Di Prisco M. (1996), "Interface behaviour", *RC Element Under Cyclic Loading, Thomas Telford Publications, London.*

Goldsmith A. (1999), "Damage detection in concrete beams using vibration measurement", *Fourth Year Undergraduate Project Report, Department of Engineering Science, University of Oxford, UK.*

Grassi P. (2002), "Constitutive modelling of concrete in compression", *Thesis for the degree of Licentiate of Engineering, Department of Structural Engineering, Concrete Structures, Chalmers University of Technology, Boulder, Göteborg, Sweden*

Gudmundson P. (1982), "Eigenfrequency changes of structures due to cracks, notches, or other geometrical changes", *Journal of the Mechanis and Physics of Solids, Vol. 30(5), pp 339-353.*

Hearn G. and Testa R. B. (1991), "Modal analysis for damage detection in structures", *ASCE Journal of Engineering Structural Engineering, Vol. 117(10), pp 3042-3063.*

Hemez F. M. (1993), "Theoretical and experimental correlation between finite element models and modal tests in the context of large flexible space structures", *PhD Dissertation, Department of Aerospace Engineering Science, University of Colorado, Boulder, Colorado, USA.*

Heylen W., Lammens S. and Sas P. (1998), Modal Analysis Theory and Testing, *Katholieke Universiteit Leuven, Leuven, Belgium.*

Hillerborg A., Modeer M. and Patersson P. E. (1976), "Analysis of crack formation and crack growth in concrete by means of fracture mechanics and finite elements", *Cement and Concrete Research, Vol. 6, pp 773-782.*

Hordijk D. A. and Reinhardt H. W. (1990), "A constitutive model for crack cyclic behaviour of plain concrete", *Proceedings of ECF 8 Fracture Behaviour and Design of Materials and Structures, Turin, Italy, pp 579-584.*

Irwin G. R. (1957), "Relation of stresses near a crack to the crack extension force", *9th Congress Applied Mechanics, Brussels.*

Ismail F. A., Ibrahim and Martin H. R. (1990), "Identification of fatigue cracks from vibration testing", *Journal of Sound and Vibration, Vol. 140, pp 305-317.*

Iyengar K. T. and Raviraj S. (2001), "Analytical study of fracture in concrete beams using blunt crack model", A*SCE Journal of Engineering Mechanics, Vol. 127(8), pp 828-834.*

Jelić I., Pavlović M. N. and Kotsovos D. (1999), "A study of dowel action in reinforced concrete beams", *Magazine of Concrete Research, Vol. 51(2), pp 131-141.*

Johnson P. A., Sutin A. and Van Den Abelee K. (2000), "Application of nonlinear wave modulation spectroscopy to discern material damage", *Emerging Technologies in NDT, pp 159-166.*

Kaplan M. F. (1961), "Crack propagation and the fracture of concrete", *Journal of American Concrete Institution, Vol. 58(11), pp 591-610.*

Kirmsher P. G. (1944), "The effect of discontinuities on the natural frequency of beams", *Proceedings of American Society of Testing and Materials, Vol. 44, pp 897-904.*

Ko J. M., Wong C. W. and Lam H. F. (1994), "Damage detection in steel framed structures by vibration measurement approach", *12th Proceedings of International Modal Analysis Conference, Honolulu, Hawaii, USA, pp 280-286.*

König G. and Duda H. (1996), "Concrete in tension", *RC Element Under Cyclic Loading, Thomas Telford Publications, London.*

Kotsovos M. D. and Pavlović M. N. (1995), *Structural Concrete – Finite-element analysis for limit state design, Thomas Telford Publications, London.*

Kramer C., De Smet C. A. M. and De Roeck G. (1999), "Z24 bridge damage detection tests", *Proceedings of 17th International Modal Analysis Conference, Kissimmee, Florida, USA, Vol. 17, pp 1023-1029.*

Kulla J. (2001), "A vibration-based structural health monitoring system", *Proceedings of the International Conference on Structural System Identification, Vol. 1, pp 263-272, Kassel, Germany.*

Kwarczuk M. and Ostacowicz W. M. (1992), "Parametric vibrations of a cantilever beam with a crack", *Archive of Applied Mechanics, Vol. 62, pp 463-473.*

Lamonaca B. G. (1997), "Crack identification in nonlinear vibrating beams", *Proceedings of the 15th International Modal Analysis Conference, Orlando, Florida, USA, pp 1904-1911.*

Lowes L. N. (1999), "Finite element modelling of reinforced concrete beam-column bridge connections", *PhD Dissertation, Department of Civil Engineering, University of California, Berkeley, California, USA*

Lungdren K. and Gylltoft K. (2000), "A model for the bond between concrete and reinforcement", *Magazine of Concrete Research, Vol. 52(1), pp 53-63.*

Maeck J., Abdel Wahab M., Peeters B., De Roeck G., De Visscher, De Wilde W. P., Ndambi J. –M. and Vantomme J. (2000), "Damage identification in

reinforced concrete structures by dynamic stiffness determination", *Engineering Structures, Vol. 22, pp 1339-1349.*

Mahmoud M. A., Abu Ziad M. and Al Harashani S. (1999), "Numerical frequency analysis of uniform beam with a transverse crack", *Communications in Numerical Methods in Engineering, Vol. 15, pp 709-715.*

Masri S. F. and Caughey T. K. (1979), "A non-parametric identification technique for non-linear dynamic problems", *Journal of Applied Mechanics, Vol. 46, p.p. 433-447.*

Mazars J. and Pijaudier-Cabot G. (1996), "From damage to fracture mechanics and conversely: a combined approach", *Int. J. Solids Structures, Vol. 33, No. 20-22, pp 3327-3342.*

Mehta P. K. and Monteiro P.J.M., *Concrete: structures, properties and methods.* Eagle-wood Cliffs: Prentice-Hall, New York, 1993.

Messina A., Jones I. A. and Willians E. A. (1996), "Damage detection and localisation using natural frequencies", *Proceedings of International Conference on Identification in Engineering Systems, Swansea, UK, pp 67-76.*

Modena C., Sonda D. and Zonta D. (1999), "Damage localization in reinforced concrete structures by using damping measurements", *Key Engineering Materials, Vols. 167-168, pp 132-141.*

Mörsch E. (1909), Concrete Steel Construction, McGraw-Hill, New York, pp 368.

Mottershead J. E. and Friswell M. I.(1993), "Model updating in structural dynamics: A survey", *Journal of Sound and Vibration, Vol. 167(2), pp 347-375.*

Nandwana B. P. and Maiti S. K. (1997), "Detection of the location and size of a crack in a stepped cantilever beams based on measurement of natural frequencies", *Journal of Sound and Vibration, Vol. 203(3), pp 435-466.*

Narkis Y (1994), "Identification of crack location in vibrating simply supported beam", *Journal of Sound and Vibration, Vol. 172(4), pp 549-558.*

Neville A. M. (1990), "Properties of concrete", *Longman Scientific and Technical, 3rd Edition.*

Nield S. A. (2001), "Using non-linear vibration techniques to detect damage in concrete bridges", *DPhil thesis, Department of Science, University of Oxford, Oxford, UK.*

Nield S. A., Williams M. S. and McFadden P. D. (2001), "A discrete model of a vibrating beam using a time-stepping approach", *Journal of Sound and Vibration, Vol. 239(1), pp 99-121*

Nield S. A., Williams M. S. and McFadden P. D. (2002), "Non-linear behaviour of reinforced concrete beams under low-amplitude cyclic and vibration loads", *Engineering Structures, Vol. 24, pp 707-718*

Okauchi I. (1997), "Field vibration test of a long span cable-stayed bridge using large exciters", *Japanese Society of Civil Engineering, Vol. 14, No.1, p.p. 83-93.*

Owen J. S., Eccles B. J., Choo B. S. and Woodings M. A. (1999), "Non-linear vibrations of cracked reinforced concrete beams", *Proceedings of the 4th European Conference of Structural Dynamics, Prague, Czech Republic, pp 357-364.*

Owen J. S. and Choo B. S. (1998), "The use of dynamic testing methods for bridge assessment and monitoring", *report no. SR98006, University of Nottingham, Nottingham, UK.*

Owen J. S., Pearson S. R., Tan C. M. and Choo B. S. (2001), "The classification of damaged/repaired bridge beams using vibration signatures", *Transportation Research Records, Washington D. C., USA, January 2002.*

Owen J. S., Tan C. M. & Choo B. S. (2002) "Empirical model of the nonlinear vibration of cracked reinforced concrete beams", *Proceedings of The First European Workshop on Structural Health Monitoring – SHM, pp 195-202, Paris, France, July 2002.*

Pandey A. K., Biswas M. and Samman M. M. (1991), "Damage detection from changes on curvature mode shapes", *Journal of Sound and Vibration, Vol. 145(2), pp 321-332.*

Pearson S. R., Owen J. S., and Choo B. S. (2001), "The use of vibration signatures to detect flexural cracking in reinforced concrete bridge decks", *Proceedings of the 4th International Conference on Damage Assessment of Structures (DAMAS 2001), Cardiff, Wales, UK.*

Pearson S.R. (2003), "On using vibration data to detect damage in model-scale reinforced concrete bridges", *PhD thesis, School of Civil Engineering, University of Nottingham, Nottingham, UK.*

Peerlings R. H. J. (1999), "Enhanced damage modelling for fracture and fatigue", *PhD Thesis, Eindhoven University of Technology, Eindhoven, The Netherlands.*

Petersson P. E. (1981), "Crack growth and development of fracture zones in plain concrete and similar materials", *Report TVBM-1006, Division of Building Materials, University of Lund, Sweden.*

Planas J. and Elices M. (1989), "Asymptotic analysis of the development of a cohesive crack zone in mode I loading for arbitrary softening curves", *Proceedings of SEM-RILEM Conference of Fracture of Concrete and Rock, Society of Experimental Mechanics, Houston, Texas, USA, pp 384-393.*

Pugno N., Surace C. and Ruotolo R. (2000), "Evaluation of the nonlinear dynamic response to harmonic excitation of a beam with several breathing cracks", *Journal of Sound and Vibration, Vol. 235(5), pp 749-762.*

Purkiss J. A., Bailey M., Friswell M. I., Penny J. E. T. and Wood M. G. (1994a), "The dynamic response of prestressed concrete bridge decks', *Institution of Structural Engineering Library, London, UK.*

Purkiss J. A., Bailey M., Friswell M. I., Penny J. E. T. and Wood M. G. (1994b), "Analysis of the effect of ambient conditions on the dynamic response of prestressed concrete bridge decks", *Institution of Structural Engineering Library, London, UK.*

Qian G. L., Gu S. N. and Jiang J. S. (1990), "The dynamic behaviour and crack detection of a beam with a crack", *Journal of Sound and Vibration, Vol. 138(2), pp 233-243.*

Raghavendrachar M. and Aktan A. E. (1992), "Flexibility by multi-reference impact testing for bridge diagnostics", *ASCE Journal of Structural Engineering, Vol. 118(8), pp 2186-2203.*

Reinhardt H. W., Cornelissen H. A. W. and Hordijk D. A. (1986), "Tensile tests and failure analysis of concrete", *ASCE Journal of Structural Engineering, Vol. 112(11), pp 2462-2477.*

Ringot E. and Bascoul A., (2001), "About the analysis of microcracking in concrete", *Cement and Concrete Composites, Vol. 23, pp. 261-266.*

Rizos P. F., Aspragathos N. and Dimarogonas A. D. (1990), "Identification of crack location and magnitude in a cantilever beam from vibration modes", *Journal of Sound and Vibration, Vol. 138(3), pp 381-388.*

Roberts G. P. (1995), "Recent experience in dynamic monitoring of a multi-span bridges", *Analysis and Testing of Bridge Seminar, Institution of Structural Engineers, London, UK.*

Rohrmann et. al. (2001), "Damage distribution of a RC footbridge evaluated by neural networks and classical update procedures", *presented in the International Conference on Structural System Identification, Kassel, Germany.*

Rots J. G. (1985), "Smeared crack approach and fracture localisation in concrete", *Heron Journal, Vol. 30, Delft.*

Ruotolo R. (1996), "Harmonic analysis of the vibrations of a cantilevered beam with a closing crack", *Computers and Structures, Vol. 61(6), pp 1057-1074.*

Ruotolo R. and Surace C. (1997), "Damage assessment of multiple cracked beams: numerical results and experimental validation", *Journal of Sound and Vibration, Vol. 206(4), pp 567-588*

Ruotolo R., Surace C. and Mares C. (1996), "Theoretical and experimental study of the dynamic behaviour of a double-cracked beam", *Proceedings of the 14th International Modal Analysis Conference, pp 1560-1564.*

Rytter A.(1993), "Vibration based inspection of civil engineering structures", *PhD thesis, Department of Building Technology and Structural Engineering, Aalborg University, Denmark.*

Salane H. J. and Baldwin J. W. (1990), "Identification of modal properties of bridges", *ASCE Journal of Structural Engineering, Vol. 116(7), pp 2008-2021.*

Salawu O. S. (1997a), "Detection of structural damage through changes in frequency: a review", *Engineering Structures, Vol. 19(9), pp 718-723.*

Salawu O. S. (1997b), "Assessment of bridges: use of dynamic testing", *Canadian Journal of Civil Engineering, Vol. 24, pp 218-228.*

Salawu O. S. and Williams C. (1995a), "Review of full scale dynamic testing of real bridge structures", *Engineering Structures, Vol. 17(2), pp 113-121.*

Salawu O. S. and Williams C. (1995b), "Bridge assessment using forced-vibration testing", *ASCE Journal of Structural Engineering, Vol.121(2), pp 161-173.*

Shen M. H. H. and Chu Y. C. (1992), "Vibrations of beams with a fatigue crack", *Computers and Structures, Vol. 45(1), pp 63-79.*

Shifrin E. I. and Ruotolo R. (1999), "Natural frequencies of a beam with an arbitrary number of cracks", *Journal of Sound and Vibration, Vol. 222 (3), pp 409-423.*

Soh C. K., Chiew S. P. and Dong Y. X. (2002), "Concrete-steel bond under repeated loading", *Magazine of Concrete Research, Vol. 54(1), pp 35-43.*

Sohn H, Czarnecki J. A. and Farrar C. R. (2000), "Structural health monitoring using statistical process control", *ASCE Journal of Structural Engineering, Vol. 126(11), pp 1356-1363.*

Sohn H. and Farrar C. R. (2000), "Damage diagnosis using statistical process control", *Proceedings of 7th International Conference in Recent Advance in Structural Dynamics, Southampton, UK.*

Staszewski W. J. and Chance J. E. (1997), "Identification of nonlinear systems using wavelets – experimental study", *Proceedings of the 15th International Modal Analysis Conference, Orlando, Florida, USA, pp 1012-1016.*

Storer D. M. and Tomlinson G. R. (1993), "Recent developments on the measurement and interpretation of higher order transfer functions from

nonlinear structures", *Mechanical Systems and Signal Processing, Vol. 7(2), pp 173-189.*

Sundara Raja Iyengar K. T. and Raviraj S. (2001), "Analytical study of fracture in concrete beams using blunt crack model", *ASCE Journal of Engineering Mechanics, Vol. 127(8), pp 828-834.*

Tan C. M., Owen J. S. & Choo B. S. (2001) "Nonlinear system identification of cracked reinforced concrete beams", *Proceedings of The COST F3 Conference of Structural System Identification, vol. 1, pp 281-291, Kassel, Germany, 5th September 2001.*

Tan C. M., Owen J. S. and Choo B. S. (2000), "The nonlinear vibrations of RC beams with distributed cracks", *Proceedings of The 4th International Conference on Modern Practice in Stress and Vibration Analysis, pp 273-284, Nottingham, UK, September, 2000.*

Thomson W. J. (1943), "Vibration of slender bars with discontinuities in stiffness", *Journal of Applied Mechanics, Vol. 17, pp 203-207.*

Thyagarajan S. K., Schulz M. J., Pai P. F. and Chung J. (1998), "Detecting structural damage using frequency response functions", *Journal of Sound and Vibration, Vol. 210(1), pp 162-170.*

Tomlinson G. R. (1988), "Linear or nonlinear – that is the question", *Proceedings on the 19th International Seminar on Modal Analysis, September 1988, Lueven, Belgium.*

Tsyfansky S. L. and Beresnevich V. I. (2000), "Nonlinear vibration method for detection of fatigue cracks in aircraft wings", *Journal of Sound and Vibration, Vol. 236(1), pp 49-60.*

Ulfkjær J. P., Krenk S. and Brincker R. (1995), "Analytical model for fictitious crack propagation in concrete beams", *ASCE Journal of Engineering Mechanics, Vol. 121(1), pp 7-15.*

Uzgider Z., Sanli A. K. and Piroglu F. and Caglayan D. B. (1993), "Identification of railway bridges using locomotive-induced vibrations", *Bridge Management 2, edited by J. E. Harding, Parke G. A. R. and Ryall M. J., Thomas Telford, London, pp 833-841.*

Van Den Abeele K. and De Visscher J. (2000), "Damage assessment in reinforced concrete using spectral and temporal nonlinear vibration techniques", *Cement and Concrete Research, Vol. 30, pp 1453-1464.*

Vanhoenacker K., Schoukens J., Guillaume P. and Vanlanduit S. (2000), "The use of multisine excitation to characterise damage in structures", *Proceedings of 25th International Seminar on Modal Analysis, Leuven, Belgium.*

Vanlanduit S., Guillaume P, Schoukens J. and Parloo E. (2000), "Linear and nonlinear damage detection using a scanning laser vibrometer", *Proceedings of 4th International Conference on Vibration Measurements by Laser Techniques: Advance and Applications, pp. 453-466.*

Vintzeleou E. N. and Tassios T. P. (1987), "Behaviour of dowels under cyclic deformations", *ACI Structural Journal, Technical paper No. 84-S3, pp. 18-30.*

Wang, Z. (2002), "The vibration behaviour of pre-stressed concrete beams", *First Year PhD Report, School of Civil Engineering, University of Nottingham, UK.*

Ward H. S. (1984), "Traffic generated vibrations and bridge integrity", *Journal of Engineering Structures, Vol.110(10), pp 2487-2498.*

Waters T. P. and Lieven N. A. J. (1996), "Reducing noise amplification effects in the updating of finite element models using measured frequency response functions", *Proceedings of 2nd International Conference of Structural Dynamic Modelling: Test, Analysis and Correlation, NAFEMS, pp. 25-40, Cumbria, UK.*

Wells Jr., 1994, "Recent advances in wavelet technology", *Reports to Computational Mathematics Laboratory, Department of Mathematics, Rice University, Houston, Texas, USA.*

Wenzel H. and Pichler D. (1998), "Detection of damages in prestressed concrete bridges by monitoring of the dynamic characteristic", *Articles of the Austrian Concrete Association, Vol. 32, p.p. 21-24.*

Worden K. (1989), "Parametric and non-parametric identification of non-linearity in structural dynamics", *PhD thesis, Heriot-Watt University, Edinburgh, UK.*

Worden K. (1998), "Random vibrations of a multi degree of freedom nonlinear system", *Proceedings of the 16th International Modal Analysis Conference, Santa Barbara, USA, pp 711-717.*

Worden K. and Manson G. (1997), "Random vibration analysis of a nonlinear system", *Proceedings of the 15th International Modal Analysis Conference, Orlando, Florida, USA, pp 1003-1011.*

Worden K. and Tomlinson G. R. (2001), "Non-linearity in structural dynamics – detection, identification and modelling", *Institute of Physics Publishing, Bristol and Philadelphia.*

Yankelevsky D. Z. and Reinhardt H. W. (1989), "Uniaxial behaviour of concrete in cyclic tension", *ASCE Journal of Structural Engineering, Vol. 115(1), pp 166-182*

Zhang W. and Testa R. (1999), "Closure effects on fatigue crack detection", *ASCE Journal of Engineering Mechanics, pp 1125-1132.*

Zhang Z. and Aktan A. E. (1995), "The damage indices for constructed facilities", *Proceedings of 13th International Modal Analysis Conference, Nashville, USA, pp 1520 1529.*

APPENDIX A
FLEXURAL VIBRATION OF UNIFORM BEAMS

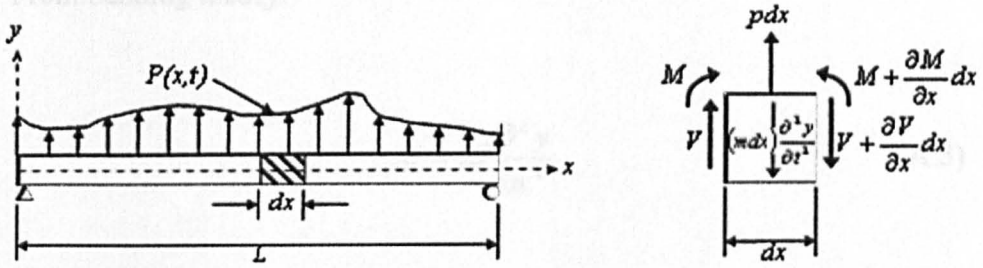

Figure A.1: Simple beam with distributed mass and load.

Consider in figure A.1 the free body diagram of a short segment of a beam, it is of length dx and is bounded by plane faces that are perpendicular to its axis. The forces and moments which are act on the element are also shown in the figure: they are the shear forces V and $V + (V/x)\,dx$; the bending moments M and $M + (M/x)\,dx$; the lateral load $p\,dx$; and the inertia force $(m\,dx)\ {}^2y/dt^2$. In this notation m is the mass per unit length and $p = p(x,t)$ is the load per unit length. Partial derivatives are used to express acceleration and variations of shear and moment because these quantities are functions of two variables, position x along the beam and time t. If the deflection of the beam is

small, as the theory assumes, the inclination of the beam segment from the unloaded position is also small. Under these circumstances, the equation of motion perpendicular to the x axis of the deflected beam obtained by equating to zero the sum of the forces in the free body diagram of figure A.1 is

$$V - \left(V + \frac{\partial V}{\partial x} dx \right) + p(x,t)dx - m dx \frac{\partial^2 y}{\partial t^2} = 0 \qquad \text{(A.1)}$$

which, upon simplification, becomes

$$\frac{\partial V}{\partial x} + m \frac{\partial^2 y}{\partial t^2} = p(x,t) \qquad \text{(A.2)}$$

From bending theory:

$$M = EI \frac{\partial^2 y}{\partial x^2} \qquad \text{(A.3)}$$

and

$$V = \frac{\partial M}{\partial x} \qquad \text{(A.4)}$$

where E is Young's modulus of elasticity and I is the moment of inertia of the cross sectional area with respect the neutral axis through the centroid. For a uniform beam, the combination of equation A.3 and A.4 results in

$$V = EI \frac{\partial^3 y}{\partial x^3} \qquad \text{(A.5)}$$

and

$$EI\frac{\partial^4 y}{\partial x^4}+m\frac{\partial^2 y}{\partial t^2}=p(x,t) \tag{A.6}$$

Equation A.6 is a forth order partial different equation with two variables. The standard way of solving these equations is by separation of variables. In this case, it is assumed that the solution may be expressed as the product of a function of position $\Phi(x)$ and a function of time $f(t)$:

$$y(x,t)=\Phi(x)f(t) \tag{A.7}$$

For free vibration, i.e. $p(x,t)=0$, equation A.6 can be rewritten as

$$EIf(t)\frac{d^4\Phi(x)}{dx^4}+m\Phi(x)\frac{d^2 f(t)}{dt^2}=0 \tag{A.8}$$

and rearranged:

$$\frac{EI}{m}\frac{\Phi^{IV}(x)}{\Phi(x)}=-\frac{\ddot{f}(t)}{f(t)} \tag{A.9}$$

For equation A.9 to exist, each side of the equation must equal to a same constant value. By designating the constant to be ω^2, the following equations can be written:

$$\Phi^{IV}(x)-a^4\Phi(x)=0 \tag{A.10}$$

and

$$\ddot{f}(t)+\omega^2 f(t)=0 \tag{A.11}$$

where

$$a^4 = \frac{m\omega^2}{EI} \tag{A.12}$$

By defining $C=(aL)^2$, ω can be conveniently expressed as

$$\omega = C\sqrt{\frac{EI}{mL^4}} \tag{A.13}$$

Equation A.11 is in the same form as that describes a free vibration of an undamped single degree of freedom system and therefore can be written as

$$f(t) = A\cos(\omega t) + B\sin(\omega t) \tag{A.14}$$

where A and B are constants of integration. By substituting $\Phi(x) = Ce^{sx}$, equation A.10 can be solved as

$$(s^4 - a^4)Ce^{sx} = 0 \tag{A.15}$$

For a nontrivial solution,

$$s^4 - a^4 = 0 \tag{A.16}$$

The roots of A.16 are

$$s_1 = a, \quad s_2 = -a, \quad s_3 = ai, \quad s_4 = -ai \tag{A.17}$$

General solution of equation A.10 can be obtained by substituting the roots into equation A.15 and by the superposition of these four possible solutions,

$$\Phi(x) = C_1 e^{ax} + C_2 e^{-ax} + C_3 e^{iax} + C_4 e^{-iax} \tag{A.18}$$

or in trigonometric and hyperbolic terms,

$$\Phi(x) = A\sin(ax) + B\cos(ax) + C\sinh(ax) + D\cosh(ax) \tag{A.19}$$

where C_1, C_2, C_3, C_4, A, B, C and D are constants of integration. The unknown constants in equation A.19 can be determined from the boundary conditions of the beam. For free-free boundary conditions, bending moment, M, and shear force, V, are zero at both ends. By applying the boundary conditions, equation A.19 can be written as

$$\begin{aligned} (\sinh(aL) - \sin(aL))A + (\cosh(aL) - \cos(aL))B = 0 \\ (\cosh(aL) - \cos(aL))A + (\sinh(aL) + \sin(aL))B = 0 \end{aligned} \tag{A.20}$$

and by equating the determinant of the unknown coefficient A and B to zero, the frequency equation for free-free beam can be derived as,

$$\cos(aL)\cdot\cosh(aL) - 1 = 0 \tag{A.21}$$

The first four natural frequencies, obtained by substituting the roots of equation A.21 into equation A.13 are presented in table 4.1. The corresponding normal modes are can also be obtained as

$$\Phi_n(x) = \cosh(a_n x) + \cos(a_n x) - \sigma_n(\sinh(a_n x) + \sin(a_n x)) \tag{A.22}$$

where

$$\sigma_n = \frac{\cosh(a_n L) - \cos(a_n L)}{\sinh(a_n L) - \sin(a_n L)} \tag{A.23}$$

It is similar for forced vibration case. Starting from equation A.6, which describes the flexural dynamic behaviour of a beam element, the general solution can be expressed by the summation of the products of the normal modes $\Phi_n(x)$ multiplied by weighing factors $u_n(t)$, to be determined, as shown,

$$y(x,t) = \sum_{n=1}^{\infty} \Phi_n(x) u_n(t) \tag{A.24}$$

By substituting this into equation A.6,

$$EI \sum_n \Phi_n^{IV}(x) u_n(t) = p(x,t) - \overline{m} \sum_n \Phi_n(x) \ddot{u}_n(t) \tag{A.25}$$

The normal modes satisfy equation A.10 and can be written as,

$$EI \Phi_n^{IV}(x) = \overline{m} \omega_n^2 \Phi_n(x) \tag{A.26}$$

Combining equation A.25 and A.26, multiplying both sides by $\Phi_m(x)dx$ and integrating between *0* and *L* give

$$\omega_m^2 \ddot{u}_m(t) \int_0^L \overline{m} \Phi_m^2(x) dx = \int_0^L \phi_m(x) p(x,t) dx - \ddot{u}_m(t) \int_0^L \overline{m} \Phi_m^2(x) dx \tag{A.27}$$

Using the orthogonality property, equation A.27 can be rewritten as

$$M_n\ddot{u}_n(t)+\omega_n^2 M_n u_n(t)=F_n(t) \tag{A.28}$$

and by introducing a damping term

$$M_n\ddot{u}_n(t)+C_n\dot{u}_n(t)+K_n u_n(t)=F_n(t) \tag{A.29}$$

where

$$M_n=\int_0^L \overline{m}\Phi_n^2(x)dx \tag{A.30}$$

$$C_n=2\xi_n\omega_n\int_0^L \overline{m}\Phi_n^2(x)dx \tag{A.31}$$

$$K_n=\omega^2\int_0^L \overline{m}\Phi_n^2(x)dx \tag{A.32}$$

$$F_n(t)=\int_0^L \Phi_n(x)p(x,t)dx \tag{A.33}$$

APPENDIX B
RUNGE-KUTTA METHODS

The range of differential equations that can be solved by analytical methods is relatively restricted. In such cases, where a differential equation and known boundary conditions are given, an approximate solution is often obtainable by the application of numerical methods. Runge-Kutta methods are arguably the most popular class of numerical methods for higher-order differential equations. This is not only because using the Runge-Kutta methods give a great degree of accuracy but also the numerical routines tend to be reasonably computationally efficient.

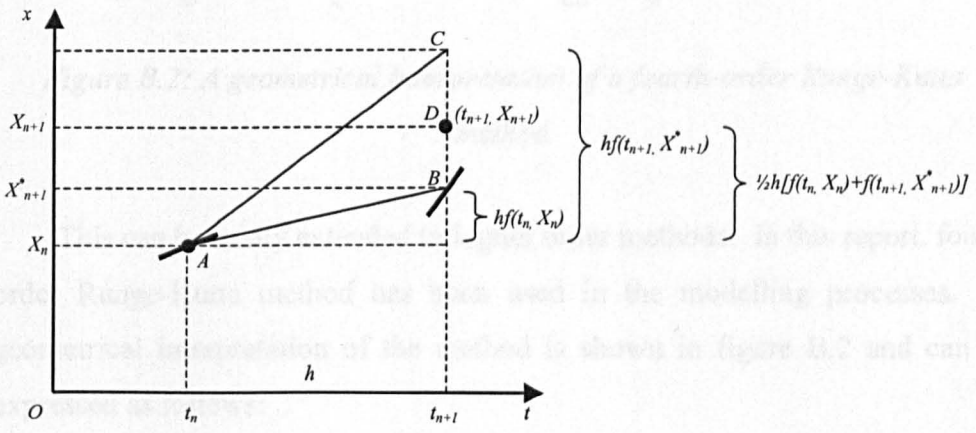

Figure B.1: A geometrical interpretation of a second-order Runge-Kutta method

Runge-Kutta methods are best described using geometrical interpretations. Figure B.1 shows a geometrical interpretation of second order Runge-Kutta method. Starting from the point (t_n, X_n) (point A in the figure) the predicted value X^*_{n+1} is calculated. The line AB has gradient $f(t_n, X_n)$, so the ordinate of the point B is the predicted value X^*_{n+1}. The line AC in the diagram has gradient $f(t_{n+1}, X^*_{n+1})$, the gradient of the direction field of the equation at point B, so point C has ordinate $X_n + hf(t_{n+1}, X^*_{n+1})$. The midpoint of the line BC (point D) has ordinate $X_n + \frac{1}{2}h(f(t_n, X_n) + f(t_{n+1}, X^*_{n+1}))$, which is the value found from second order Runge-Kutta method. In other words, the method can be viewed as the process of calculating the gradient of the direction field of the equation at points A and B and then assuming that the average gradient of the solution over the interval (t_n, t_{n+1}) is reasonably well estimated by the average of the gradients at these two points.

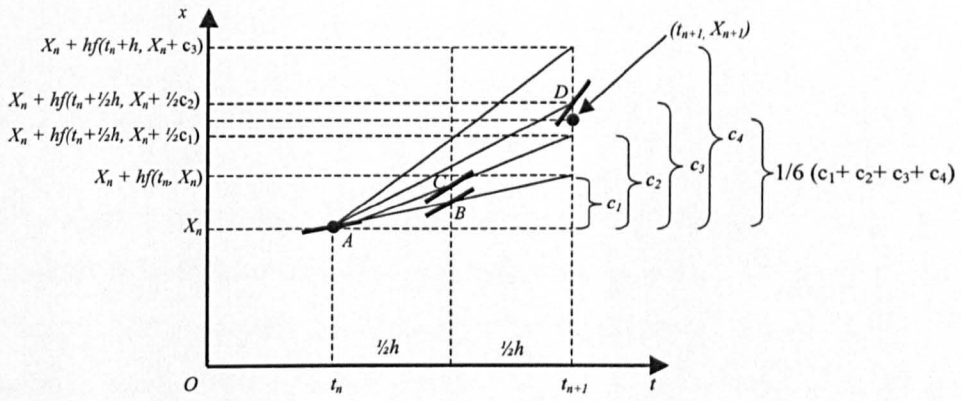

Figure B.2: A geometrical interpretation of a fourth-order Runge-Kutta method

This can be easily extended to higher order methods. In this report, fourth order Runge-Kutta method has been used in the modelling processes. A geometrical interpretation of the method is shown in figure B.2 and can be expressed as follows:

$$c_1 = hf(t_n, X_n) \tag{B.1}$$

$$c_2 = hf\left(t_n + \tfrac{1}{2}h, X_n + \tfrac{1}{2}c_1\right) \tag{B.2}$$

$$c_3 = hf\left(t_n + \tfrac{1}{2}h, X_n + \tfrac{1}{2}c_2\right) \tag{B.3}$$

$$c_4 = hf\left(t_n + h, X_n + c_3\right) \tag{B.4}$$

$$X_{n+1} = X_n + \tfrac{1}{6}\left(c_1 + 2c_2 + 2c_3 + c_4\right) \tag{B.5}$$

APPENDIX C

FOURIER TRANSFORMS

C.1 FOURIER SERIES

Fourier series have been used extensively in signal processing as it can convert time history data into the frequency domain. It bases on Fourier's finding that a periodic function may be expressed as the summation of an infinite number of sine and cosine terms. For a periodic function, the Fourier series may be written as

$$\begin{aligned} F(t) = a_0 + a_1\cos\bar{\omega}t + a_2\cos 2\bar{\omega}t + a_3\cos 3\bar{\omega}t + \ldots a_n\cos n\bar{\omega}t + \ldots \\ + b_1\sin\bar{\omega}t + b_2\sin 2\bar{\omega}t + b_3\sin 3\bar{\omega}t + \ldots b_n\sin n\bar{\omega}t + \ldots \end{aligned} \quad \text{(C.1)}$$

or

$$F(t) = a_0 + \sum_{n=1}^{\infty}\{a_n\cos n\bar{\omega}t + b_n\sin n\bar{\omega}t\} \quad \text{(C.2)}$$

where $\overline{\omega} = 2\pi/T$ is the frequency and T is the period of the function. The evaluation of the coefficients a_o, a_n and b_n for a given function $F(t)$ is determined from the following expressions:

$$a_0 = \frac{1}{T}\int_{t_1}^{t_1+T} F(t)dt \tag{C.3}$$

$$a_n = \frac{2}{T}\int_{t_1}^{t_1+T} F(t)\cos n\overline{\omega}t\,dt \tag{C.4}$$

$$b_n = \frac{2}{T}\int_{t_1}^{t_1+T} F(t)\sin n\overline{\omega}t\,dt \tag{C.5}$$

where t_i in the limits of the integrals may be any value of time, but is usually equal to either $T/2$ or zero. The constant a_0 represents the average of the periodic function $F(t)$.

C.2 DISCRETE FOURIER TRANSFORM (DFT)

When the periodic function $F(t)$ is supplied only at N equally spaced time intervals ($\Delta t = T/N$) $t_0, t_1, t_2, \ldots, t_{N-1}$, where $t_j = j\Delta t$, the integrals in equations C.3, C.4 and C.5 may be replaced approximately by the summations

$$a_n = \frac{1}{T}\sum_{j=0}^{N-1} F(t_j)\cos n\overline{\omega}t_j\Delta t \tag{C.6}$$

$$b_n = \frac{1}{T}\sum_{j=0}^{N-1} F(t_j)\sin n\overline{\omega}t_j\Delta t, \quad n = 0,1,2,\ldots \tag{C.7}$$

where $\overline{\omega} = 2\pi/T$. The above definitions for the Fourier coefficients have been slightly altered by omitting the factor 2 in the expressions for a_n and b_n. In this case equation C.2 is then written as

$$F(t_i) = 2\sum_{n=1}^{\infty}\{a_n \cos n\overline{\omega}t + b_n \sin n\overline{\omega}t\} \tag{C.8}$$

By using complex notations and appropriate substitutions, equations C.6 and C.7 can be rewritten as

$$C_n = \frac{1}{N}\sum_{n=0}^{N-1} C_n e^{2\pi i\left(nj/N\right)} \tag{C.9}$$

which is the formal definition of the discrete Fourier transform of a series $\{F(t_j)\}, j = 0, 1, 2, ..., N\text{-}1$ (Paz, 1997).

C.3 FAST FOURIER TRANSFORM (FFT)

Fast Fourier Transform is a numerical technique that is efficient for computer determination of the response in the frequency domain. It can be seen that equation C.9 can be represented, except for sign in the exponent by the exponential function as

$$A(j) = \sum_{n=0}^{N-1} A^{(0)}(n) W_N^{jn} \tag{C.10}$$

where

$$W_N = e^{2\pi i/N} \tag{C.11}$$

The evaluation of the sum is most efficient if the number of time increments N into which the period T is divided is a power of *2*, as in this case, the integers j and n can be expressed in binary form.